NASA CR-112310
CW-WR-73-028

DESIGN OF THERMAL PROTECTION SYSTEM FOR 8-FOOT HTST COMBUSTOR

by

S. Moskowitz

CURTISS-WRIGHT CORPORATION
WOOD-RIDGE, NEW JERSEY 07075

prepared for

NATIONAL AERONAUTICS AND SPACE ADMINISTRATION

NASA LANGLEY RESEARCH CENTER

Contract NAS 1-11714

FOREWORD

This report was prepared by the Power Systems Division of Curtiss-Wright, Wood-Ridge, New Jersey, to describe the studies conducted under Contract NAS 1-11714 for the design of a thermal protection system for the high pressure combustor for the NASA Langley Research Center 8-foot high temperature structures tunnel combustor. The program guidance provided by Mr. J. Karns and Dr. M. Anderson of the NASA Langley Research Center is gratefully acknowledged.

Major technical contributions toward the program were provided by Messrs. R. Cole, A. Defeo and M. Kulina of Curtiss-Wright, and their efforts are gratefully acknowledged.

Page Intentionally Left Blank

TABLE OF CONTENTS

TABLE OF CONTENTS (Continued)

LIST OF ILLUSTRATIONS

LIST OF ILLUSTRATIONS (Continued)

LIST OF TABLES

DESIGN OF THERMAL PROTECTION SYSTEM

FOR 8-FOOT HTST COMBUSTOR

S. Moskowitz
Curtiss-Wright Corporation

SUMMARY

The combustor in the 8-Foot High Temperature Structures Tunnel at the NASA-Langley Research Center has encountered cracking over a period of 50-250 tunnel tests within a limited range of the required operating envelope. A program was conducted which analyzed the failed combustor liner hardware and determined that the mechanism of failure was vibratory fatigue. A vibration damper system using wave springs located axially between the liner T-bar and the liner support was designed as an intermediate solution to extend the life of the current two-pass regenerative air-cooled liner design but within an envelope limited by

(a) 1800° F metal temperature at gas conditions of 4000° R in the low pressure region

(b) By buckling instability at the cold flow high pressure conditions

Several new liner designs were evaluated for feasibility to operate over the complete operating envelope. The designs included:

(a) Regenerative air-cooled ring-stiffened liner to resist a buckling failure mode at cold flow high pressure

(b) Regenerative air-cooled omega-shaped segment liner similar to turbojet afterburner designs

(c) Water-cooled nickel shell liner

(d) Water-cooled nickel tube liner

The effects of liner wall thickness, cooling air passage height, stiffener ring geometry, reflective coatings, and liner material selection were investigated for these designs. Preliminary layout design arrangements including the external water-cooling system requirements, weight estimates, installation requirements and preliminary estimates of manufacturing costs were prepared for the most promising configurations. A state-of-the-art review of thermal barrier coatings and an evaluation of reflective coatings for the gas-side surface of air-cooled liners were also performed.

Based on these studies, the two-pass regenerative type air-cooled omega-shaped segment liner and the water-cooled nickel sheet liner with circumferential water grooves were considered most suitable for the 8-foot HTST facility and capable of operating over the required operating envelope.

INTRODUCTION

The Langley Research Center's 8-foot High Temperature Structures Tunnel (HTST) is a facility used for testing large scale structural models and thermal protection systems applicable to hypersonic vehicles. The general arrangement of the HTST facility is presented in Figure A-1 (Appendis A). The facility is a large hypersonic blow-down tunnel which uses methane-air products of combustion as a test medium.

The energy level of the test gas is provided by burning methane gas in air in a high pressure combustor. The resulting combustion gases are expanded through an axisymmetric nozzle with an exit diameter of 8-feet into an open jet test section. Downstream of the test section the flow passes through a supersonic diffuser and is pumped by a single stage air ejector through a subsonic diffuser to the atmosphere.

The facility was designed to operate within an operating envelope as shown in Figure 1, with gas conditions up to 4000° F and 4000 psia. A description of the combustor operating procedure is presented in Appendix A.

The present high pressure combustor design arrangement is presented in Figure A-2. The outer housing or barrel pressure vessel is protected from the combustion gases by a double-pass regenerative-type thermal protection system. High pressure air supplied from a bank of 6000 psi bottles adjacent to the facility enters the outer housing through two inlet flanges located at the upstream station. The air flows downstream in the annular passage created by the outer housing and the cylindrical combustor liner support. The air returns upstream in the annular passage created by the cylindrical combustor liner support and the combustor liner. The air enters the combustor liner ID and flows downstream for the combustion process.

Fuel is introduced under separate control through two large axial tubes supplying a network of concentric fuel distributor rings in a plane about 11.33 feet from the upstream closure end of the outer housing.

A separate system of air film cooling and convective water cooling is used to cool the nozzle throat and the exhaust nozzle and is also shown in Figure A-2.

In the present design arrangement, the service life of the combustor liner has been less than 250 tunnel runs. Axial cracking has occurred in the liner

downstream of the fuel distributor rings. Where the crack progressed through the entire wall thickness, a burnout of the liner has occurred. The liner failures have required one of the following:

(a) Crack repair by welding

(b) Removal of the burnout sections and replacement by welding of an insert patch

(c) Replacement of the entire liner

As a result of this problem, NASA formulated a multi-phase program directed toward the redesign of the thermal protection system which would provide a life expectancy at least 1500 tunnel runs. Phase I incorporated the analytical studies and preliminary design of alternate systems to the extent that fabrication and installation requirements may be evaluated and preliminary manufacturing costs may be estimated. Subsequent phases are planned which involve the detailed design and experimental validation of one or more promising design concepts directed toward the selection of a final design and subsequent fabrication and testing of the design.

This report presents the results of the Phase I program.

The program's major objectives are summarized as follows:

(a) Identify the failure mode of the present combustion liner through metallurgical analysis of the failed hardware and analytical study of the thermal and stress conditions

(b) Establish a thermal computer model for liner temperature predictions which correlates with measured thermocouple data obtained from recent tunnel tests

(c) Evaluate the operating limitations of the present liner

(d) Study the feasibility of several design concepts for the liner

(e) Prepare preliminary analysis and design layouts of promising liner concepts

(f) Evaluate the cost, fabricability, installation requirements, etc. of the promising liner designs

DEFINITION OF SYMBOLS

A	heat transfer surface area, sq ft
C_p	specific heat at constant pressure, Btu/lb-^oF
D_h	hydraulic diameter, ft
D_i	wetted perimeter or inside diameter, ft
E	modulus of elasticity, psi
h	heat transfer coefficient, Btu/hr-sq ft-^oF
k	thermal conductivity, Btu/hr-ft-^oF
p	pressure, psia
Pr	Prandtl Number
q	heat flow, Btu/hr
Re	Reynolds Number
S	stress, psi
T	temperature, ^oF or ^oR
V	velocity, ft/sec
α	coefficient of thermal expansion, in/in-^oF
Δ	difference in or change in
ρ	density, lb/ft^3
γ	Poisson's Ratio
μ	viscosity, lb/sec-ft

Subscripts:

a	air-side	w	wall
b	bulk flow	∞	fully developed flow
c	convective		
g	gas-side		
l	water-side		

FAILURE ANALYSIS OF PRESENT LINER

The present liner design arrangement shown in Figure 2 consists of a 3/16 inch thick Inconel 600 cylinder with a smooth 36 inch ID and an OD surface with axial fins to promote cooling. The fins have a height of 3/16 inch, a width of 1/16 inch, a pitch of about 1/4 inch and run axially for the full length of the liner. The liner is cantilevered from a bolt attachment to the exhaust approach section at the combustor exit station. The liner has 32 axial T-bars equally spaced around the OD which are guided for the length of the liner in channels on the liner support. The liner support is a 1/2 inch thick AISI 304 cylinder with 39-3/8 inch ID and a 14 foot length. The liner support is cantilevered from a bolt attachment to the outer housing at 11.33 feet upstream of the fuel distributor rings. The support has 16 equally spaced axial T-bars which are guided in channels on the ID of the barrel or outer housing. The laminated outer housing is made of ASTM A20-56 with 44.5 inch ID, an average thickness of 4.5 inches and a length of 30 feet.

The failure history of the present liner design indicates that preferential cracking occurs along the T-bar weld attachment in the vicinity of the 7 o'clock location (viewed from upstream) at approximately one to three feet downstream of the fuel distributor rings. This location was also noted to have the maximum air-side metal temperature of 1170° F measured on the liner during tests at gas conditions of 3300° R and 600 psia. These gas conditions are substantially below the limits of the required operating envelope and do not represent the severest conditions for the liner. The liner has also been tested at other conditions including gas temperature up to 3640° R and pressures up to 3360 psia which resulted in lower liner temperatures.

Since the cracked liner section from the 7 o'clock location was no longer available, another cracked section located at approximately 1 o'clock was selected for metallurgical failure analysis. Figure 3 shows the liner section which was analyzed.

Visual and binocular examination of this liner segment revealed many axial cracks along the welds which attach the T-bars to the OD of the liner. A typical crack is shown in Figure 4. Figure 5 presents the fracture surface of the crack shown in the previous figure. The crack has progressed almost completely through the wall of the liner. The arrows indicate the location of multiple fatigue nuclei.

Further examination of the segment after grit blasting and etching the OD surface revealed, as shown in Figure 6, short axial cracks in the roots of the fin grooves adjacent to the T-bar welds. Figure 7 presents the fracture surface of some of the cracks shown in the previous figure. The arrows indicate the location of the multiple fatigue nuclei.

Figures 8 and 9 present the metallographic examination of the fracture surface adjacent to a T-bar weld. Fracture examination revealed the transgranular nature of the T-bar and the fin root cracks. Both types are typical of cracks produced by high cycles and high mechanical loads. The multiple

nuclei found in the fracture surfaces also are indicative of extremely high stresses. Both types of cracks progressed radially through the wall.

Metallographic examination of sections through the cracks revealed no metallurgical discrepancies that would have contributed to the failures.

Based on the results of this examination, the following were concluded:

(a) The cracks are not attributed to low cycle thermal fatigue

(b) The cracks are attributed to a vibratory fatigue mechanism

(c) Extremely high stresses are responsible for the fatigue cracking; these stresses may have occurred either during the high temperature portion of the test cycle or during cold flow operation prior to combustor ignition.

A small number of welds attaching the T-bars to the liner exhibited cracks due to improper fit-up of mating surfaces or lack of weld fusion. This type of crack is presented in Figure 10. However, the improper condition for welding was not associated or contributory to the fatigue failures described above.

A summary of the crack locations observed on several liners of similar design is presented in Figure 11. Design configuration I provided a cold nominal radial clearance of 0.390 inch above the liner T-bars. Configuration II provided a clearance of 0.140 inch. In either configuration drawing tolerances may produce a clearance reduction of 0.140 inch. During operation up to 4000° R gas temperature, thermal expansion between the liner and the support would result in additional clearance reduction of up to 0.294 inch. Therefore, an interference fit will occur for configuration II at temperature,and may occur under adverse drawing tolerances for configuration I.

It was observed that cracks occurred with a greater frequency in liner configuration II where radial interference readily occurs between the liner T-bars and the liner support during the test. The metallurgical failure analysis was performed on liner configuration I since configuration II was being used during this study.

Except for the 11 o'clock location, the crack summary reveals a pattern of liner cracking at the angular locations of the fuel distributor ring support spokes. The distributor is cantilevered from the fuel supply pipes. The spokes rest on metal pads welded to the I.D. of the liner. These pads had been added after the liner showed the effects of severe pounding from the spokes. The crack summary indicates the possibility of the cylindrical liner vibrating in a 6-mode pattern forced by the six radial support spokes of the fuel distributor rings.

The crack at the 11 o'clock location in liner configuration II occurs in the vicinity of the butt weld which was provided to form the cylinder from rolled plate.

DESIGN STUDIES

The study of liner design concepts was directed toward satisfying the following requirements:

(a) Maximum gas temperature = 4000° R

(b) Maximum gas pressure = 4000 psia

(c) Minimum service life = 1500 tunnel tests

(d) No erosion which creates foreign object damage to the test model

(e) Envelope limitations:

Maximum OD = 42 inches

Minimum ID = 36 inches

Maximum length = 23 feet

Recognizing that the failures of the present combustor have occurred within a restricted operating envelope of the facility, it was considered necessary to evaluate the new designs for other potential failure modes which may occur at the higher operating gas conditions. Consequently, the following design criteria were recognized in evaluating feasibility and applicability of new liner concepts:

(a) Minimum low cycle fatigue life = 1500 cycles as predicted by Manson's method

(b) Maximum liner temperature = 1850° F

(c) Critical buckling pressure = 2.5 x actual pressure load for hot flow operation

(d) Critical buckling pressure = 1.5 x actual pressure load for cold flow operation

(e) Minimum vibratory fatigue life $\approx$ 1500 tunnel tests (approximately 75 hours)

(f) Pressure stress $<$ 80% of yield strength

The selection of a maximum liner temperature was based on the oxidation characteristics, the severely reduced material properties, and the limited properties data available in the high temperature range.

A significant increase in thermal gradient across the liner wall thickness at the high gas temperature and pressure conditions was expected for the air-cooled liner designs. Therefore, the low cycle fatigue criteria were necessary.

The critical buckling criteria were established as a result of the large pressure load imposed on the liner resulting from the high gas pressure differential between the cooling air passage on the outer surface of the liner and the main gas chamber on the inside of the liner. The higher factor for hot flow conditions was selected for conservatism.

The following major combustor design concepts were studied:

A. Air-Cooled Designs

(1) Cylindrical liner formed by thin-sheet omega shaped segments with double-pass regenerative type cooling

(2) Cylindrical liner shell incorporating circumferential OD stiffener rings with double-pass regenerative type cooling

(3) Reflective coated cylindrical liner with double-pass regenerative type cooling

(4) Rework of present liner to incorporate a vibration damping system for extending the liner life within the current operating envelope limited by the metal temperature criterion

B. Water-Cooled Designs

(1) Liner shell and water jacket incorporating circumferential grooves which form the water flow passages

(2) Jacket shell and liner incorporating circumferential grooves which form the water flow passages

(3) Tubular liner formed by circumferential tube segments

During the preliminary design effort, studies were conducted to determine the effects of:

(a) Liner wall thickness

(b) Cooling air passage height

(c) Stifferner ring geometry

(d) Reflective coatings

(e) Liner materials

Design options were selected from these studies to complete the preliminary design arrangements. These studies and the preliminary design arrangements are discussed in the following sections.

Analyses of Present Air-Cooled Liner

Thermal Analysis Method and Results.- The accuracy of predicting the combustor liner temperature distribution depends on appropriate evaluation of the heat transfer coefficients on the air-side and gas-side surfaces of the liner. On the gas-side, the convective heat transfer takes place in a turbulent-flow entry region, where the aerodynamic and thermal boundary layers develop simultaneously. The heat transfer process in this region is known to be strongly influenced by the entrance conditions and cannot be predicted analytically. It is necessary, therefore, to rely upon experimental data for accurate evaluation of the heat transfer coefficient. In addition, radiation from the high temperature gas performs a significant role in the overall heat transfer. Here again, experimental data must be used to verify the estimated radiative heat transfer coefficient because of the complex dependency of radiation on temperature, pressure and combustion products. On the air-side liner surface, the complex passage geometry due to the presence of supporting devices and fins also makes prediction of heat transfer coefficients difficult.

A simplified thermal model was developed from correlation with the available test data supplied by NASA from the present liner to facilitate consistent evaluation of the heat transfer coefficients of interest under different combustor operating conditions. The actual temperature field of the liner is three-dimensional, especially near the fuel distributor rings. For simplicity, the initial model reduced the three-dimensionality to an equivalent one-dimensional problem in which the liner temperature was assumed to be independent of the longitudinal and circumferential coordinates. The model was established to reproduce, as closely as possible, the maximum average wall temperatures measured along the liner OD surface between fins at a gas temperature of 3300° R and pressures of 603, 1514 and 2440 psia as presented by the test curves in Figures 13, 14 and 15.

The model was required to establish the heat transfer coefficients on both sides of the liner so that the calculated wall temperatures would agree with the measured temperatures. The three heat transfer coefficients of concern in the model included air-side convection, gas-side radiation and gas-side convection. Since radiation from the outer surface of the liner to the inner surface of the liner support is small as compared to the convective heat transfer, it was disregarded in the model. To put the model on a sound physical basis, the following approach widely used in the literature was adopted:

(a) Reference values of the three coefficients were first evaluated from the established empirical relations or physical laws for ideal conditions

(b) Next, a correction factor was introduced for each coefficient to account for deviation from the ideal situation

(c) These factors were then evaluated from the test data

Since the test data did not permit direct evaluation of the correction factors, iterations were performed to determine the three unknowns using the test curves.

The results of this modelling technique suggested that radiation from the hot gas may be assumed to be independent of pressure in the range from 600 to 4000 psia and that the gas emissivity is approximately 0.64. This is in reasonable agreement with the rather limited reference data available (Reference 6-1, 6-2, and 6-3) on gas emissivity at very high pressures. The gas-side convective heat transfer coefficient was adequately estimated using the relation

$$h_{cg} = 1.5\, h_{cg\,\infty}$$

where $h_{cg\,\infty}$ is the heat transfer coefficient for fully developed turbulent flow and can be calculated from the equation (Reference 4)

$$\frac{h_{cg\,\infty}}{V\,C_p} = 0.023\,(Re)^{-0.2}\,(Pr)^{-2/3}\left(\frac{\mu_b}{\mu_w}\right)^{0.14}$$

The convective heat transfer coefficient on the air-side was predicted with reasonable accuracy by the empirical equation (Reference 5)

$$\frac{h_{ca} D_h}{k} = 0.023\,(Re_{D_h})^{0.8}(Pr)^{0.4}$$

using the appropriate local hydraulic diameter (D_h) and air velocity. During the initial modelling for feasibility studies, the air-side cooling passage was treated as an annulus, recognizing the blockage of the T-bars and channel supports as a reduction of area but not as a reduction of hydraulic diameter, and the correction factor differed negligibly from unity. For subsequent more detailed analysis of the cooling passage formed between the 32 T-bars, it was necessary to reduce the velocity in the grooves between the 3/16 inch height fins to duplicate these results. This effectively applied a degraded correction factor to the finned liner surface. This effective reduction in velocity agreed well with the reduction which would be expected due to the higher frictional resistance to flow in the grooves than in the passage free stream.

Results of the application of this initial thermal model to the current air-cooled liner configuration and the excellent correlation with test results are shown in Table 1. Predictions of metal temperatures to the 4000 psia, 4000° R maximum operating condition are also presented. A comparison of the metal temperatures for the 1.5 and 1.0 inch cooling air passage heights indicates the possibility for modifying the existing (1.5 inch cooling passage height) liner design to achieve acceptable metal temperature levels. However, the thermal design problem is formidable since

(a) the temperature gradient across the 3/16 inch liner wall is very high, and

TABLE 1.- COMPARISON OF PREDICTED AND MEASURED WALL TEMPERATURES ON PRESENT AIR-COOLED LINER

Gas Pressure, psia	Gas temp, ^{o}F	Cooling passage height, in.	Wall ΔT, ^{o}F	Predicted gas-side surface temp, ^{o}F	Predicted air-side surface temp, ^{o}F	Measured air-side surface temp, ^{o}F	Reference Figure
603	3300	1.5	190	1362	1172	1170	12
1514	3300	1.5	307	1222	915	890	13
2440	3300	1.5	400	1215	815	810	14
4000	4000	1.5	558	1746	1186	-	-
4000	4000	1.0	622	1542	920	-	-
4000	4460	1.5	637	2049	1412	-	-
4000	4460	1.0	716	1808	1092	-	-

"Page missing from available version"

page 12 missing

For many of the parametric studies undertaken during this investigation, it was found that the maximum thermal stress could be essentially evaluated by the relation

$$S = \frac{E\ \alpha\ (\Delta T)}{2(1-\gamma)}$$

The technique outlined in Reference 6 for low cycle fatigue life predictions was used for the liner analyses. In establishing the total strain range or equivalent stress range, the highest stress, either tension or compression, is determined and the material properties at the location of highest stress are utilized. The highest stress in the liner is a compressive stress on the inside of the liner where the stress due to the radial thermal gradient adds to the mechanical stress due to the pressure loading. This is also the location of highest metal temperature. The number of cycles to failure was obtained from life curves established by the techniques in Reference 6. The life estimates specified for the combustor designs used a value of 1/5 of Manson's upper bound data. The fatigue life predictions by this method will be more conservative than the life prediction of the analysis covering the original air-cooled liner design (Reference 7). That analyses had used an earlier technique (Reference 8) which yields life predictions approximately equal to Manson's upper bound data.

The results of the stress analysis of the present liner configuration for the operating conditions encountered by the liner prior to cracking show that the failure that occurred within about 50-250 cycles is not caused by thermal cycling. A summary of stresses is shown in Table 2.

TABLE 2.- PRESENT AIR-COOLED LINER STRESS ANALYSIS SUMMARY

	Condition run	Complete envelope
Maximum temperature	3640° R	4000° R
Maximum pressure	3360 psia	4000 psia
Pressure (hoop) stress	< 1300 psi	1300 psi
Average thermal stress		
Axial	21,225 psi @ 200° F	21,225 psi @ 200° F
Radial	17,700 psi @ 1085° F (Δt = 107° F)	82,000 psi @ 1738° F (Δt = 555° F)
Minimum low-cycle fatigue life	5000 cycles	2400 cycles
Buckling criteria	Unstable	Unstable
Low temp. factor of safety	0.79	0.79
High temp. factor of safety	1.24	0.88
Maximum gas-side liner temp.	1362° F	> 2000° F

The table shows that some of the design criteria established for this study are violated for the conditions run as well as for the complete envelope.

The table also reveals that the liner may exhibit buckling instability since the minimum value for buckling criteria (critical Δp/actual Δp) of 1.5 at the cold conditions and 2.5 at the hot conditions is not achieved. There is some supporting evidence that buckling has occurred at least once on the present liner design during tunnel testing.

The pressure load is small and results in an acceptable hoop stress.

The longitudinal temperature distribution, as obtained from the shell computer program, results in a peak stress 12 inches upstream of the fuel distributor rings. The stresses are as follows:

Wall Location	Longitudinal stress	Hoop stress
Inside	-7,752 psi	-21,225 psi
Outside	+7,752 psi	-16,574 psi

The metal temperature at this location is just over 200° F and the stresses are acceptable. In the area of the highest metal temperature and highest radial thermal gradient (one foot downstream of the fuel distributor rings), the axial thermal gradient results in a stress of less than 2000 psi and is not considered a significant factor at the location of highest thermal stress.

The temperature distribution through the liner wall was used to calculate the nominal thermal stress around the cylinder. In addition, the gradients in the vicinity of the T-bar were used to calculate additional stresses due to the effect of the T-bar stiffness.

The thermal gradients across the 3/16 inch liner thickness vary with the gas pressure conditions being run. The following table compares the thermal stress for the conditions existing during combustor operation at 3300° R gas temperature:

Pressure, psia	Wall ΔT, °F	Gas-side liner temp., °F	Stress, psi
603	190	1362	30,600
1514	307	1222	50,500
2440	400	1215	65,700

Since the stresses are above the yield strength of the Inconel 600 material at temperature, repeated application of the load will result in a finite life. From the low cycle fatigue data, the predicted number of cycles to failure is approximately 20,000.

The thermal distribution in the vicinity of the T-bar results in a peak longitudinal stress on the outer wall of the liner at the intersection with the T-bar. For the most severe condition run, the maximum thermal stress is 128,500 psi at a metal temperature of 815° F. For this condition, the predicted low cycle fatigue life is approximately 5000 cycles. For the complete operating envelope, a life of 2400 cycles at the liner wall ID is predicted.

The above life predictions for the maximum operating conditions run on the failed liners support the conclusion from the metallurgical analysis of the hardware that vibratory fatigue rather than thermal fatigue was responsible for the failure.

In addition to buckling, the criterion for liner temperature limit is exceeded within the operating envelope, as shown by an analysis at 4000° R and 600 psia gas conditions for the present configuration. Therefore, it was concluded that, although the predicted low cycle fatigue life criteria are satisfied, the present liner design is unsatisfactory for other reasons.

Present Air-Cooled Liner With Dampers

Consideration was given toward resolving the vibration problem on the present air-cooled liner since this could extend the useful liner life for current test operations especially if curtailment of selective regions of the operating envelope could be tolerated.

A vibration analysis was performed on the liner in order to evaluate the natural frequency characteristics and possible damping arrangements.

The basic natural frequencies of the liner and liner support are shown in the following table and Figure 15:

Nodes	Liner	Liner Support
4	11.9 cps	31.4 cps
6	33.6 cps	89.0 cps
8	64.8 cps	170.4 cps

In order to investigate the vibratory stresses associated with the various modes, the natural frequency data are plotted as a function of the number of nodes (points of zero deflection) and the associated nodal span. The figure illustrates that for a six-node pattern of liner vibration, the nodal span is 18.8 inches while for 32 nodes, one located at each T-bar, the nodal span is only 3.5 inches. Since a fatigue failure did occur, it can be assumed that the vibratory stress must have reached $\pm$50,000 psi, the endurance

strength of the material. For this analysis, the effect of steady-state stress due to pressure and thermal gradients is neglected which would lower the vibratory stress required to fail the liner. Figure 16 shows the amount of motion of the liner required to cause ±50,000 psi stress. The concentrated load at the center of the individual nodal span is also shown. This load is a static equivalent load and does not include any dynamic effects. For example, if the liner vibrates at 290 cps, it would correspond to a 16-node vibratory notion of the liner. For this condition the nodal span is 7.0 inches long and the maximum vibratory motion of the liner to cause a fatigue failure would be ±0.062 inch. A static force of 405 pounds is required to deflect the liner to that value. Assuming a magnification factor of 10, the exciting force would be 1/10 of that shown.

The dynamic or resonance effect on the load values is also shown on Figure 16. To estimate the damping required to control the vibration, it was assumed that a radial force at every other nodal span is required. This curve shows the total force required around the circumference. For the example noted above, the 16-node mode would require 335 pounds distributed around the liner to eliminate the vibration. This could be accomplished by applying 42 pounds force at eight locations. Since this is the force required to eliminate the vibration, a smaller force would be sufficient to reduce the vibratory stresses to acceptable values.

The force can be applied by utilizing a wave spring running the length of the liner to provide a satisfactory damping arrangement. The force can be applied either radially inward or outward without changing its effectiveness. Such an arrangement would change the vibration characteristics of the liner, depending upon the radial stiffness of the springs. This change in frequency is not considered detrimental.

Since the current liner is not failing from thermal effects and with 32 T-bar supports it appears to be structurally satisfactory for the static loads imposed, a design to incorporate a vibration damping device in the T-bar channels was provided. Figure 17 presents the preliminary design layout of the existing air-cooled liner with a wave spring type damper. A double thickness wave spring is located over the liner T-bars and is captured within the channels on the liner support. The Inconel X750 material spring is 0.05 inch thick, 1.20 inches wide with a free height of 1.13 inches and a pitch of 6.125 inches. The spring is attached to the liner support by two rivets at the downstream end. The wave spring may have a free length of over 12 feet; however, the free length may be made up of more than one spring for ease of fabrication.

To incorporate the wave spring damper in the present combustor, the combustor must be reworked to provide a space above the T-bars of 0.540 ±0.125 inch. This is accomplished by grinding the existing weld and removing the T-bar. The thickness of the T-bar flange is machined to 0.126 ±0.015 inch and then refixtured on the liner to 19.147 ±0.031 inch radius and rewelded. A preliminary estimate of the cost for reworking the present liner to incorporate the wave spring dampers is $12,000.

The axial force required to install 16 springs equally located between the liner and the liner support assemblies is 1950 lbs. The shear stress on the rivets attaching the wave spring to the liner support is 2200 psi.

At operating conditions the height over the T-bar will be 0.380 $\pm$0.12 inch and the total spring deflection is 0.750 inch. Under normal conditions, the double thickness spring compressed within this height provides a force of 40 lbs every six inches axially along the T-bar. The stress in the spring is approximately 70,000 psi. Inco X750 material has a minimum yield strength of 115,000 psi at room temperature.

Definitive information on the vibratory characteristics of the liner, which can be obtained by strain gauge instrumentation recordings, is required to select a specific damper design arrangement. Evidence from a composite history of liner cracks points to a six-node mode pattern of liner vibration caused by six radial supports for the fuel distributor rings. The wave spring damping arrangement at five or seven T-bar locations may be able to satisfy this six-node mode requirement. A wide range of damping forces may be generated by changing the spring rate values and the number of dampers around the liner.

In support of this design, a temperature distribution analysis was performed for a transverse section of the T-bar and liner. Operating pressures of 600 psia and 4000 psia were considered, both at 4000° R gas temperature. Coolant flow area and hydraulic diameter were estimated from the design layout, recognizing the changes made to the T-bar for insertion of the wave spring vibration damper. Upon examination of the actual shape of the coolant passage, it was decided to use a non-uniform velocity distribution in which the velocity in the regions between the liner OD and the T-bar support channel and along the web and above the T-section was reduced from free stream velocity because of the higher resistance to flow in these narrow sections. Because previous analysis in connection with the one-dimensional model had indicated that the fins were detrimental to thermal performance and they are not expected to contribute significantly to the structural integrity of the liner, a smooth outer skin was assumed for this analysis.

The temperature distribution for 4000 and 600 psia gas pressure is shown on Figures 18 and 19, respectively. At the higher pressure, the wall temperatures are not excessive for the material used but very high gradients approaching 700° F in the 3/16 inch thickness are indicated. At the lower pressure condition, wall temperatures exceed reasonable operating limits even for a material such as Hastelloy X. Consequently, the modified liner requires a restricted operating envelope. The modified liner will be satisfactory for high pressure operation, although an improved material may be required to obtain adequate cyclic life, but the maximum gas temperature will be limited at low gas pressures unless a suitable reflective coating can be applied.

Figures 20 and 21 present the transient temperature histories for selected points for a step change in gas temperature from ambient to 4000° R at 4000 psia and 600 psia, respectively. These figures indicate that the maximum temperature and the maximum temperature gradient across the liner will occur at the stabilized or steady-state condition.

Parametric Studies

Liner Wall Thickness & Cooling Air Velocity.- Examination of the test results and analysis using the one-dimensional model revealed that there are two fundamental thermal problems in regeneratively air-cooled configurations. At the lower end of the operating pressure range, radiant heat input to the liner from the hot gas may amount to 70 percent of the total heat flux while on the air-side the radiant component of the heat rejected from the liner to the air and the liner support is negligibly small. As a result, liner temperatures are high at low pressure and tend to exceed the useful operating limits of the material. High pressure operation greatly increases the convective heat transfer coefficient on both sides of the liner such that the radiant heat transfer coefficient which remains about the same as pressure changes, accounts for only 30 percent of the total heat flux. While this is favorable for cooling and results in generally lower liner temperatures, the substantially increased heat flux generates the second problem, that of high temperature gradients within the liner material causing high thermal stresses and resulting in low cyclic life.

In order to form a base for the structural analysis of liner design modifications, a parametric study was conducted at 4000° R gas temperature using simple cylindrical liners of various thickness and having different cooling side velocities as represented by a range of cooling air annular passage heights. Results of this analysis, as listed in Table 3 reveal the two types of thermal problems mentioned and also show that material thickness and air velocity (in terms of passage height) are very strong parameters in their effects on both the gas-side temperature and the wall temperature gradient.

The results of the parametric study presented in the table reveal the following:

(a) The liner temperature increases with decreasing gas pressure

(b) The temperature gradient increases with increasing gas pressure

(c) Reducing the cooling passage height results in reducing the liner temperature and increasing the gradient

(d) Reducing the wall thickness results in reducing the liner temperature and the gradient

The thermal benefits associated with the configuration using the smallest cooling air passage height may not be fully realized because the increased air velocity causes an increased pressure drop in the coolant passage annulus. The pressure drop associated with the three cooling passage heights studies are shown in Figure 22. The increased pressure drop, as the passage height is reduced, results in a proportionately increased structural loading of the liner. The maximum structural loading occurs at the cold flow conditions.

TABLE 3.- EFFECT OF AIR-COOLED LINER THICKNESS AND COOLING AIR VELOCITY AT 4000° R

Gas pressure, psia	Cooling passage height, in.	Liner thickness, in.	Wall ΔT, °F	Gas-side liner temperature, °F
4000	1.5	0.188	555	1738
4000	1.0	0.188	653	1561
4000	0.75	0.188	718	1464
4000	1.5	0.094	299	1579
4000	1.0	0.094	361	1354
4000	0.75	0.094	398	1217
4000	1.5	0.078	253	1550
4000	1.0	0.078	304	1313
4000	0.75	0.078	338	1174
2000	1.5	0.188	363	1791
2000	1.0	0.188	450	1569
2000	0.75	0.188	504	1437
600	1.5	0.188	166	2154
600	1.0	0.188	219	1874
600	0.75	0.188	263	1695
600	1.5	0.094	85	2118
600	1.0	0.094	114	1816
600	0.75	0.094	135	1617

Wall Thickness.- The thermal analysis of the present air-cooled liner indicates that for a given combustion environment, as the liner wall thickness is decreased both the thermal gradients in the liner and the maximum metal temperatures decrease. These advantages are offset somewhat by the fact that the pressure stresses increase and the liner is more likely to buckle. The combined effect of the thermal and pressure conditions on the low cycle fatigue strength of the liner is shown on Figure 23. In addition to the effect of wall thickness, the effect of increasing the cooling air passage height around the liner is presented. The figure shows that changing the cooling air passage height has little effect on the life of the liner. The change in wall thickness has a significant effect. Reducing the wall thickness from 0.188 inch to 0.125 inch will double the life of the liner.

As the cooling air pressure is reduced from 4000 to 600 psia, the liner thermal gradients decrease but the maximum metal temperatures increase. The cycles to failure predicted for the 0.188 inch thick liner operating at 4000° R gas temperature is shown in Table 4.

TABLE 4.- AIR-COOLED COMBUSTOR LIFE PREDICTIONS AT 4000° R GAS TEMPERATURE

Cooling passage height, in.	Gas-side liner temp, °F	Wall ΔT, °F	Cycles to failure
2000 psia gas pressure			
1.50	1791	363	5800
1.00	1564	450	5200
0.75	1437	504	5600
4000 psia gas pressure			
1.50	1738	555	2400
1.00	1561	653	2400
0.75	1464	718	2200

The table shows that a reduction in the gradient has more influence in increasing low cycle fatigue life than the metal temperature rise has in decreasing life. This effect continues until the metal temperature exceeds the material design limit.

As the wall thickness decreases, the susceptability to buckling increases sharply. Figure 24 shows the critical buckling pressure as a function of liner thickness. This figure presents curves for a cylinder with both ends supported and for a cylinder with both ends free. The actual combustor liner for this investigation has only one end supported. Therefore, the applicable curve would fall between the two curves presented. The lower curve was utilized as a conservative approach. Buckling design criteria were formulated which established that the critical buckling pressure shall be 1.5 times the actual pressure for cold and 2.5 times for hot operating conditions.

Material Selection.- The two materials considered most suitable for the air-cooled liner are Inconel 600 and Hastelloy X. Based on Manson's low cycle fatigue criteria, Figures 25 and 26 present the low cycle fatigue life for these materials. This was used in a parametric study of the effectiveness of the two materials in a high stress and high temperature environment. Figure 27 compares the materials for the thermal environment that would cause a

fatigue failure at 1500 cycles. The curves relate the stress due to thermal gradients to the maximum temperature of the material. From this comparison, it can be shown that for a given material temperature below 1630° F, Hastelloy X will take a larger thermal gradient than Inconel 600 before failure occurs. Similarly for a given thermal gradient above 825° F, Hastelloy X can satisfactorily operate at higher metal temperatures than Inconel 600. Figure 28 shows the cycles to failure for a thermal gradient of 800° F and 1000° F as a function of liner temperature for both materials.

From this study, it was concluded that in the range of thermal gradients and metal temperatures expected for an air-cooled liner, Hastelloy X has superior low cycle fatigue strength characteristics and therefore, is the preferred material for a new liner design.

Emissitivity.- Since the basic low pressure problem is that of excessive radiant heat input from the gas-stream, a one-dimensional analysis was made in which the emissivity of the gas-side liner surface was changed. The results presented in Table 5 are for an annular flow model with a 1.5 inch cooling passage height and a 0.188 inch wall thickness at 4000° R gas temperature.

TABLE 5.- EFFECTS OF EMISSITIVITY ON AIR-COOLED LINER TEMPERATURES

Surface type	Emissivity	Wall Δ T, °F	Gas-side liner temp., °F
600 psia gas pressure			
Oxidized	0.8	166	2154
Newly Machined	0.4	154	2013
High Reflectivity	0.2	147	1936
4000 psia gas pressure			
Oxidized	0.8	555	1738
Newly Machined	0.4	532	1671
High Reflectivity	0.2	520	1637

The table indicates that a reduction in wall temperature of about 140° F at 600 psia may be obtained by maintaining a surface reflectivity equivalent to the initial machined condition. Further improvement is available with highly reflective coatings as offered by the noble metals. At the higher pressure of 4000 psia, the temperature effect is not so pronounced but some reduction in the thermal gradient is obtained because of the reduced heat flux.

A discussion of reflective coatings is presented in a later section of the report.

Air-Cooled Ring-Stiffened Liner

The limitations in the operating envelope for the air-cooled liner similar to the present configuration occur at gas conditions of low pressure and high temperature due to excessive liner temperatures. Table 3 compares the liner temperature predictions for a range of cooling passage heights at the gas condition of 4000° R and 600 psia.

For a wall thickness of 0.188 inch, the liner temperatures are excessive at 1.5 and 1.0 inch passage heights. The smaller cooling passage height of 0.75 inch results in a reduced and acceptable liner temperature but at the same time causes an increased pressure differential across the liner wall. This higher pressure load imposes a severe liner buckling condition. For a liner of 0.094 inch thickness, the temperature associated with a 1.0 inch passage height is acceptable. However, the reduced wall thickness has increased the buckling susceptability.

Table 6 shows the results of a buckling analysis at gas conditions of 4000° R and 4000 psia for two liner configurations:

(1) The cylindrical liner with both ends free

(2) The cylindrical liner both ends supported

This table shows that to satisfy the buckling criteria the cooling air passage height and the liner thickness should be maximized which is contrary to the thermal criteria.

A second approach to reduce the liner temperature is to decrease the liner thickness. The table also shows that reducing the liner thickness in half will decrease the maximum liner temperatures about 200° F but will increase the buckling susceptibility. Since the effectiveness of the T-bars in controlling liner buckling cannot readily be determined, it was decided to study the use of cylindrical stiffener rings on the liner to preclude buckling. A parametric study was made to establish the height, width and spacing of rings for a liner that would meet the buckling criteria.

Each configuration was evaluated with regard to the design criteria at the following gas conditions:

Condition no.	Gas pressure, psia	Gas temp., ^{o}R
1	4000	4000
2	4000	3300
3	4000	2500
4	2000	460
5	600	4000

TABLE 6.- AIR-COOLED LINER CRITICAL BUCKLING PRESSURE COMPARISON AT 4000° R & 4000 PSIA GAS CONDITIONS

Cooling passage height, inch	Wall thickness, inch	Wall temp., ^{o}F		Critical Δp, psi		Actual Δp, psi
		Inside	Outside	Free end	Supported	
1.5	0.078	1550	1297	0.522	2.03	7.5
	0.094	1579	1280	0.885	4.17	7.5
	0.188	1738	1183	6.630	22.00	7.5
1.0	0.078	1313	1009	0.550	2.14	20.0
	0.094	1354	993	0.942	4.43	20.0
	0.188	1561	908	7.140	23.70	20.0
0.75	0.078	1174	836	0.562	2.19	45.5
	0.094	1217	819	0.962	4.53	45.5
	0.188	1464	746	7.250	24.00	45.5

Table 7 presents the results of the parametric stress study using the thermal predictions for a one-dimensional model of the ribbed liner without OD surface fins. Only configuration G satisfies the buckling criteria and has the potential for satisfying the liner temperature limit. Although configurations A and B satisfy the buckling criteria, they would operate at excessive liner temperatures at condition 5. The other configurations do not satisfy the 1.5 factor of safety for buckling at the maximum gas pressure (2000 psia) in the cold flow operating envelope.

TABLE 7.- PARAMETRIC STRESS STUDY OF RING-STIFFENED AIR-COOLED LINER

Config.	Cooling passage height, inch	Wall thickness, inch	Ring width, inch	Ring height, inch	Ring pitch, inch	No. of rings	Critical condition
A	1.5	0.188	0.093	0.188	3.0	57	Temp. > 1800° F @ Condition 5
B	1.5	0.188	0.375	0.188	6.0	29	Temp. > 1800° F @ Condition 5
C	1.5	0.093	0.375	0.188	2.75	62	F.S. < 1.5 @ Condition 4 F.S. < 2.5 @ Condition 3 Temp. > 1800° F @ Condition 5
D	1.125	0.125	0.375	0.250	5.0	35	F.S. < 1.5 @ Condition 4 F.S. < 2.5 @ Conditions 1,2,3
E	1.125	0.125	0.375	0.250	3.0	57	F.S. < 1.5 @ Condition 4 F.S. < 2.5 @ Conditions 1,2,3
F	1.125	0.125	0.375	0.312	3.0	57	F.S. < 1.5 @ Condition 4 F.S. < 2.5 @ Condition 3
G	1.125	0.125	0.375	0.312	2.75	62	None

F.S. = Buckling factor of safety

Table 8 presents the results of the buckling pressure analysis for the air-cooled ribbed liner described as configuration G. The buckling factors of safety for each of the operating conditions studied satisfy the criteria. Furthermore, the predicted low cycle fatigue life of this liner is in excess of 8000 cycles.

TABLE 8.- AIR-COOLED RIBBED LINER CONFIGURATION G
BUCKLING PRESSURE ANALYSIS

Operating condition	Gas pressure, psia	Gas temp., ^{o}F	Air-side temp., ^{o}F	Buckling Critical Δp, psi	Actual Δp, psi	Buckling factor of safety	Cycles to failure
1	4000	4000	1500	55.3	15.5	3.56	8000
2	4000	3300	1140	62.5	17.05	3.66	-
3	4000	2500	845	66.9	26.05	2.52	-
4	2000	460	60	74.6	49.2	1.54	-
5	600	4000	1797	50.5	2.32	21.7	13,400

Figure 29 presents the arrangement of the ring stiffened liner incorporating 62 circumferential ribs machined to the geometry and pitch described above for configuration G. The liner is fabricated from Hastelloy X and incorporates 32 equally-spaced axial T-bars welded to the OD of the liner similar to the present liner configuration. The T-bars are locally notched to straddle the circumferential stiffening ribs and are not welded to these ribs. The existing liner support may be used without rework if the cooling passage height remains unchanged. The following attachments will be the same as the present combustor arrangement:

(a) Liner to the downstream exhaust approach section

(b) Liner support to the outer housing at the upstream end.

The preceding heat transfer and stress parametric studies indicated that the most effective method for obtaining lower wall temperatures and lower temperature gradients in the liner is to reduce liner thickness; also circumferential ribs spaced at frequent intervals would provide buckling strength considerably improved over the simple cylindrical shell design and would permit substantial reduction of liner thickness. Therefore, a thermal analysis was performed on one of the ring stiffened liner designs resulting from the stress study. In this analysis, determination of the heat transfer

coefficients on the air side was the major problem since there is very little information in the literature on heat transfer from surfaces having ribs or fins perpendicular to the flow direction. However, several reports (References 9 to 12) dealing with recent work on gas-cooled reactors were found, and although the reported experiments were at much lower Reynolds numbers than exist in this case, there was sufficient information to estimate the axial distribution of the convective heat transfer coefficient and to approximate the average increase in its value over that of a smooth surface.

The temperature distributions for the ribbed liner at both 600 psia and 4000 psia operating gas pressures are presented in Figure 30 for the following configuration:

Rib height	=	0.4 inch
Rib width	=	0.4 inch
Liner wall thickness	=	0.10 inch
Rib pitch (axial)	=	3.0 inches
Cooling passage height	=	1.5 inches

Although the average liner temperatures are lower, as expected, the low velocity in the wake of the ribs results in local temperatures that are excessive at the lower gas pressure condition. Radial temperature gradients are generally low except in the rib where the high velocity over the OD of the rib produces very low temperatures. The large axial gradients noted in the figure which do not exist in the smooth liner without ribs (except near the fuel distribution rings) also add to the general thermal stress problem. However, the use of a reflective coating on the gas-side surface of the liner may reduce wall temperatures and gradients sufficiently so that the structural advantages of the ribbed design may be utilized.

Transient response of this liner was calculated for the simplified one-step sequence consisting of instantaneous application of the maximum gas temperature of 4000° R at each of the two pressure conditions, 600 and 4000 psia. Figures 31 and 32 present the temperature history at four liner locations selected to reveal the maximum wall temperature gradient and the maximum local temperature. The figures show that the maximum temperature and the maximum gradient occur at the stabilized or steady-state condition. Also, no unexpected increase in gradient due to the axial distribution of temperature occurs during the transient.

Air-Cooled Omega Segmented Liner

A type of liner design which is used for high temperature combustors and as turbojet afterburners consists of an assembly of axially parallel segments formed in an omega-shaped cross-section such that the liner supports are integral with the inner wall. Attachment of the supports to the housing is by an axial C-shaped clip or clamping device. Advantages of this design with regard to heat transfer are that thinner material can be used without structural problems and the coolant stream is not seriously obstructed by liner supports or brackets since there is no requirement to provide clearance for large radial growth.

Figure 33 presents the preliminary design layout of the omega liner configuration using two-pass regenerative air cooling. The liner is composed of 36 omega-shaped segments welded to each other at the OD to form a full 360° liner. The welds are longitudinal and are positioned in the cold and low stressed region of the liner. The segments are formed from 12 feet long and 0.125 inch thick sheet stock of Hastelloy X material. The segments are butt-welded together on a drum fixture and the welds are dressed flush on the OD surface of the segments.

The omega shape was selected since it has been successful in afterburner liners in aircraft turbojet engines and is known to successfully accommodate circumferential thermal growth. A cold gap of about 0.060 inch between segments is provided for circumferential expansion. The gap at operating conditions is less than 0.018 inches. The downstream end of the liner is welded to an end closure seal plate which incorporates a 72 lug radial spline centering flange. The end closure is shaped to receive the 36 omega-shaped segments and is welded completely around the periphery, thus forming a leak-proof construction.

The portion of the liner upstream of the combustion zone is welded to an ID sleeve and an end closure plate. This end plate is shaped to seal the area between segments which would otherwise present a leakage path for the combustor air as it discharges from the cooling passage to the main stream flow path. The sleeve not only closes the gap between segments at the cold end but also serves as the cylindrical surface for supporting the fuel distributor.

The liner support (Drawing LC-704750) is reworked at the forward end to provide an external flange for mounting to the rear face of the intake closure cover (Drawing H-47241-1-3). The ring attachment flange which is welded to the ID of the outer housing (Drawing 47241) upstream of the fuel distribution rings is removed. The aft-face of the liner support is reworked to provide a flange which incorporates an OD seal, for mounting a 72 lug centering ring which receives the liner. A ring attached by 72 screws, traps the liner and liner support assembly through the thermal expansion centering device. The aft flange is welded to the liner support at the 16 T-bar locations by an airfoil-shaped strut which also forms the necessary air passage for the air to flow between the inner wall of the liner support and the cooling air-side wall of the liner segments.

The omega liner is longitudinally held in position by 36 C-clips which are attached to the inner wall of the liner support. These clips restrain the liner from buckling under the differential pressure between the cooling air passage and the main gas chamber. During manufacturing of the assembly, the liner is used as the fixture for positioning and tack-welding the C-clips, thus facilitating subsequent assembly of the liner and liner support.

The entire combustor liner assembly weighing 2561 lb is centilevered from the upstream closure plate and is centered and supported by the exhaust nozzle inlet approach section.

The liner and liner support assembly is attached to the closure cover by thirty-two 1/2 inch diameter bolts.

An L-shaped ring is welded to the OD of the high pressure combustor nozzle approach section (Drawing LE 516488) at the forward end. This ring incorporates a generous chamfer and a cylindrical pilot for receiving the aft-end of the liner and support assembly. This arrangement facilitates installation.

A Viton-A seal is provided on the OD of the aft-end of the liner and support assembly to preclude leakage of air from entering the combustion chamber at the inlet face of the high pressure combustor nozzle approach section. An axial gap is also provided at this location to accommodate the rearward thermal expansion of the liner support. The thermal expansion of the liner in this configuration is forward.

A preliminary estimate of cost for tooling and fabrication of the omega liner is $90,000.

The initial thermal analysis of this configuration using a modification of the one-dimensional model showed that the maximum gas-side wall temperature at 600 psia operation is 1830° F and the maximum gradient through the wall is 502° F at 4000 psia. A more detailed thermal analyses of this design at both 600 psia and 4000 psia provided the results shown in Figures 34 and 35, respectively. The thermal analyses revealed one problem area which must be solved in final design, namely, that a means of preventing ingress of hot gas into the attachment bulb section of the omega segment must be incorporated since there is essentially no cooling of that portion of the liner enclosed by the attachment clip. For the analyses shown it was assumed that the clearance between liner segments would be controlled to a dimension that leakage of hot gas into the region between segments would be cooled to an average temperature of 1560° F. Under the conditions assumed, the temperatures and thermal gradients at the mid-section of the segment in this design are the lowest of any of the air-cooled configurations. These values may be improved in this design by reflective gas-side surface coating of the segments as shown in Table 9 by the results of the one-dimensional model at 4000° R gas temperature.

TABLE 9. - EFFECT OF EMISSIVITY ON OMEGA LINER TEMPERATURE

Surface Type	Emissivity	Wall $\triangle T$, ° F	Gas-side liner temp., ° F
600 psia gas pressure			
Oxidized	0.8	165	1830
New Machined	0.4	150	1689
High Reflectivity	0.2	143	1613
4000 psia gas pressure			
Oxidized	0.8	502	1432
New Machined	0.4	478	1368
High Reflectivity	0.2	466	1337

The thermal analysis indicated two other areas for potential problems:

(a) The large thermal gradient along the leg of the bulb attachment section of the liner segment

(b) The local peak temperature at the radius between the liner ID and the leg of the bulb attachment

Both of these problems appear to have practical solutions which can be provided during a final design by the following:

(a) Extending the length of the C-clip to increase the coverage of the segment leg

(b) Increasing the radius between the liner ID and the leg of the bulb attachment to increase the ratio of air-side to gas-side local surface area

Transient temperature histories of the liner at the center of the segment and at the maximum temperature section of the omega liner are presented in Figures 36 and 37 for a step change in temperature from ambient to 4000° R at 600 and 4000 psia, respectively. The figures indicate that the maximum temperature level and the maximum wall temperature gradient occur when the steady-state condition is reached.

For the stress analysis, the omega-shaped segment liner was considered a frame member under a uniform pressure with ends pinned at the clip. A strain energy method was used to calculate the redundant force. The technique has been successfully used to analyze turbojet afterburners of similar configuration.

The results of the stress analysis at 4000° R and 4000 psi is summarized in Table 10 and shows that the maximum stress in the liner consists of a thermal stress of 66,000 psi due to a temperature differential of slightly over 500° F. The analysis was conducted at the location of maximum gradient; combining the thermal stress with a 2054 psi stress due to pressure results in a low cycle fatigue life of over 16,600 cycles for Hastelloy X material at a liner temperature of about 1450° F.

TABLE 10. - AIR-COOLED OMEGA LINER STRESS SUMMARY

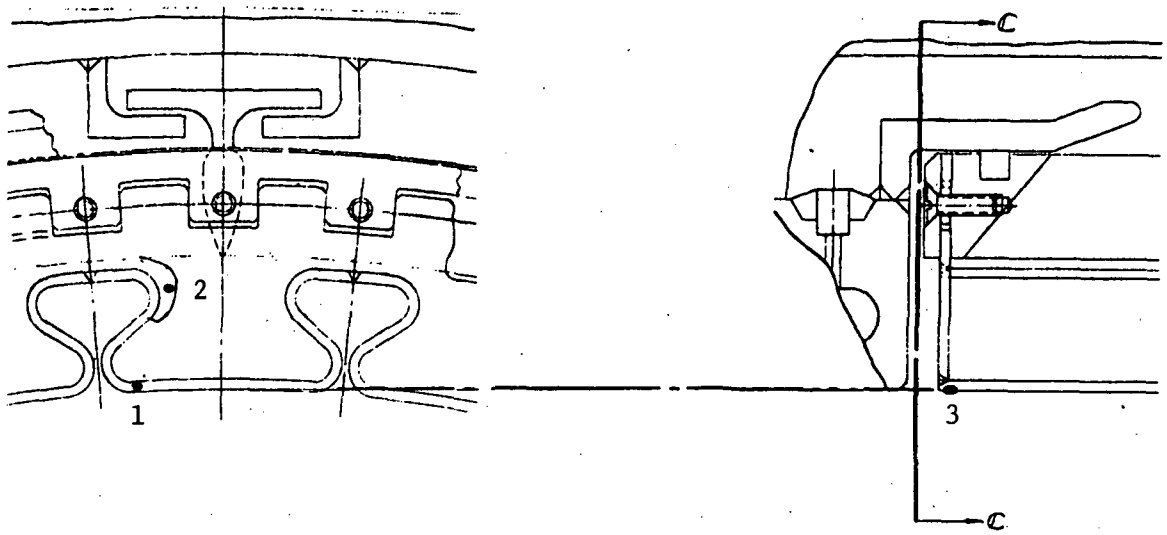

Location	Temp, ° F	Stress, psi	Stress type	Allow. stress, psi	Cycles
1	1430	2,050 66,000	Mechanical Thermal	26,100	11,600
2	800	780	Mechanical	34,100	∞
3	1180	35,600	Thermal	-	∞

The resulting stresses in the retaining clip are very small and will provide unlimited life.

The end plate attached to the liner at the downstream location was analyzed to determine the effect of the temperature gradients in the liner. The thermal stress will be 35,600 psi resulting in an acceptable low cycle fatigue life. The analysis also showed that buckling of the liner would not occur as a result of the restraint offered by the end seal plate.

Based on the results of the analyses, the omega liner satisfies all the design criteria with the possible exception of the material temperature limit. However, the liner temperatures are lowest among all the air-cooled liner designs studied. Furthermore, this design lends itself to local repair or replacement of individual segments, if necessary.

Water-Cooled Shell Liner

Thermal Analysis Methods and Results. - In the water-cooled thermal protection system, the flow of coolant and the heat transfer characteristics are independent of the gas flow. As a result, the low pressure problem experienced by regeneratively air-cooled systems does not exist and the maximum heat flux condition becomes the primary design consideration. The water-cooled system was therefore, analyzed for the 4000 psia operating condition and (because of an expressed desire by NASA to eventually operate at gas temperatures higher than in the contract specification) for 4460° R temperature.

Gas-side heat transfer coefficients were evaluated in the same manner as previously discussed for the air-cooled systems. The water-side heat transfer coefficient was predicted by the equation (Reference 13)

$$\frac{h_l D_h}{k} = 0.023 \left(\frac{pVD_h}{\mu_b}\right)^{0.8} \left(Pr\right)_b^{0.33}$$

This equation does not correct for possible sub-cooled nucleate boiling on the walls, which would increase the heat transfer.

In water-cooled systems having very high heat flux, the water-side wall temperatures are higher than the bulk boiling temperature of the liquid and a certain amount of nucleate boiling will occur. The problem in such systems is the selection of an operating water pressure and velocity high enough to prevent bulk boiling or the formation of large steam pockets on the walls, which might result in local burn-out. Bulk boiling can be easily avoided by raising water pressure such that the saturation temperature is above the coolant exit temperature at all times. The prevention of burn-out requires that the maximum possible heat flux from the gas is less than the critical heat flux; the latter is a function of water pressure, velocity and passage geometry. In the present analysis, Bernath's correlation for sub-cooled boiling was employed to predict the critical heat flux (References 14 and 15). According to this correlation, the critical heat flux may be predicted by

$$\left(\frac{q}{A}\right)_{crit} = h_{crit}\left(T_{w_{crit}} - T_b\right)$$

where

$$T_{w_{crit}} = 1.8\left[57 \ln P - 54\left(\frac{P}{P+15}\right) - \frac{V}{4}\right] + 32$$

$$h_{crit} = 10{,}890\left(\frac{D_h}{D_h - D_i}\right) + \frac{48V}{D_h^{0.6}}$$

The water flow conditions selected for this design were a flow velocity of 17 fps and minimum water pressure of 350 psia, correxponding to a saturation temperature of 432° F. These factors and the dimensions of the circumferential water grooves were the results of an iterative optimization procedure coordinating design, stress analysis and heat transfer requirements. During these studies, the possibility of using AISI 321 stainless steel instead of nickel as an economy measure was explored. The results at 4000 psia and 4460° R gas temperature, using the modified one-dimensional model, are shown in Table 11. This table presents the temperatures of the selected design configuration using 0.078 inch wall thickness for both nickel and stainless steel. The stainless steel was ruled out of further consideration because of high temperature gradients combined with high gas-side liner temperatures which resulted in inadequate cyclic life and excessive axial growth relative to the cool outer support jacket.

TABLE 11. - COMPARISON OF WATER-COOLED SHELL LINER TEMPERATURES FOR TWO MATERIALS

Material	Circumferential location	Wall ΔT, ° F	Gas-side Wall temp., ° F	Water-side wall temp., ° F	Water temp., ° F	Water ΔT, ° F
Nickel	Water inlet	293	686	393	100	189
	Water outlet	279	848	569	289	
Stainless steel	Water inlet	684	1045	361	100	168
	Water outlet	654	1174	520	268	

For ease of manufacturing, a configuration using nickel in sheet form with the grooves in the relatively free-machining steel jacket was initially considered. The dimensions of this configuration are shown on Figure 38. The expected temperature distribution at the water inlet station is shown in Figure 39. The figure indicates that the maximum temperature gradient in the

nickel sheet liner is 298° F and the gas-side wall temperature is 665° F at the center of the water groove, increasing to 791° F at the center of the web. At the corresponding locations at the hot end (outlet) of the water groove the maximum gradient is 284° F and the gas-side wall temperature is 827° F at the center of the water groove and 953° F at the center of the web.

For this configuration a two-step transient analysis was performed assuming the following:

(1) Instantaneous gas temperature rise representing combustor ignition from ambient to 4400° F at 600 psia

(2) After five seconds, a pressure increase from 600 to 4000 psia at constant gas temperature

Figure 40 shows that temperatures and temperature gradients increase with time, reaching maximum values at steady-state conditions.

Detailed structural analysis of the sheet liner with grooves in the support housing indicated that the configuration was not adequate and that a design with grooves in the nickel liner would offer significant structural advantages. The dimensions of the revised design are shown on Figure 41. The temperature distribution analysis of the revised design is presented in Figure 42. This figure shows a slightly lower temperature gradient (278° F) at the thinnest section, but a higher gradient (472° F) through the web. The gas-side wall temperature is 597° F at the thin section rising only to 628° F at the web. Figure 43 presents the temperatures at the water outlet end of the water groove. This figure shows a 274° F gradient at the thin section, a 468° F gradient at the web and wall temperatures from 769° F to 800° F.

The one-step transient analysis was performed and the liner temperature history is presented in Figure 44. The figure shows that steady-state operation is attained in less than three seconds with no unexpected variations in gradient. The maximum temperature level and the maximum gradient occur at the steady-state condition.

The Bernath correlation for sub-cooled boiling was applied to this configuration. The critical wall temperature using 350 psia minimum water pressure, is 532° F and the critical heat flux is 3.8×10^6 Btu/hr-sq.ft. Analysis of the wall temperature distribution in the water troove shows a maximum local heat flux at the center of the groove of 1.48×10^6 Btu/hr-sq.ft. which is low enough to assure safety even if the local heat transfer coefficient is substantially increased by sub-cooled boiling.

The final configuration of the water-cooled shell liner has 429 grooves or water passages. Using water at an initial temperature of 100° F and a 189° F bulk temperature rise, the total water flow is 192.6 lb/sec (1441 gpm). The total heat rejection rate for the liner is 1.32×10^8 Btu/hr if the entire liner is heated, but the actual rate will be somewhat reduced because the liner in the vicinity of the fuel distribution rings will not be subjected to the full heat flux. The water pressure drop in the grooves is estimated at 26 psi without inlet, exit and piping losses.

Mechanical Design. - A layout design of the water-cooled combustor assembly is presented in Figure 45. The design consists of a 321 stainless steel outer liner or jacket about 12 feet long and a nickel type A liner about 11.5 feet long. The liner is 0.25 inches thick across the web and has circumferential grooves machined on the OD. The grooves have a root radius of 0.1 inch and a height of 0.18 inches. The pitch of the circumferential grooves is 0.32 inch. The upstream face of the liner has a flange with an O-ring groove on its front face for mounting a high pressure leak detector sleeve. The leak detector sleeve pilots and seals on the ID of the jacket and bolts to the front face of the liner flange. The leak detector consists of two OD O-ring seal grooves with an annulus formed between the two Viton A O-ring seals.

The forward face of the exhaust nozzle approach section (Reference Drawing No. LE516488) is reworked by providing a bolting circle, an entering OD chamfer and an OD O-ring groove. Installation of a L-shape ring which has a large entering chamfer, an OD O-ring groove and a cylindrical surface for supporting the aft-end of the water-cooled combustor is provided at this section.

The outer jacket is fabricated from six cylindrical rolled sheets and six longitudinal U-shaped lower-half water manifolds. The six equally spaced half-manifolds are butt welded to the six cylindrical rolled sheets to form a cylinder. A 0.500 inch circumferential slot by 0.200 inch wide is machined in each manifold half with an axial pitch of 0.96 inch. A slot in #1 water inlet manifold corresponds with a slot in the same transverse plane in #1 water outlet manifold. The slot in #2 inlet manifold is displaced 0.32 inches in relation to the slot in #1 inlet manifold. The slot in #3 inlet manifold is displaced 0.64 inch in relation to #1 inlet manifold. Thus, each manifold feeds only one-third of the total number of water grooves in the liner. At each inlet manifold slot, the water divides so that the coolant travels 180° in each groove and exits in the outer manifold, 180° opposite to the water inlet manifold. The water inlet manifolds are located 120° apart and the water outlet manifolds are also located 120° apart. This configuration produces a more symmetrical circumferential temperature on the liner and the web between grooves proved to be a very effective heat transfer fin, thus reducing the thermal gradient in the liner.

The jacket is final machined on the ID, the forward and aft flanges and the ID aft pilot. The liner is then inserted into the jacket and circumferentially welded at the aft-end.

Half pipes about 11.5 feet long are welded to the lower-half of the water manifolds to form the six longitudinal manifolds. Six plugs are welded on the aft face of the water manifolds to seal the ends. The plugs are shaped so that no flow restriction occurs at the first water inlet and water outlet slot.

The existing attachment ring flange at the ID of the combustor outer housing assembly is machined-off. The water-cooled liner assembly is attached to the rear face of the intake closure cover by a cylindrical shell support with an OD of 40.875 inches and a length of 11.6 feet. The shell is perforated with 532 holes of 1.0 inch diameter, 28 circumferentially per row for 19 axial rows with a 5.0 inch pitch for admission of the combustor air. Local cut-outs are provided in this shell section for assembly of the water piping.

The three 120° circumferentially located water inlet pipes which are attached to the manifold are merged into one 4.0 inch pipe with a large radius three-quarter turn loop for pipe expansion. The 3.0 inch diameter pipes are bolted to the manifolds at the front face of the water-cooled combustor liner with 4 bolts. A Viton A O-ring face seal is provided at the bolting flange. The front face of the 4.0 inch water inlet pipe is bolted to the rear face of the intake closure by an 8-bolt flange connection using a flexitallic metal seal. The existing intake closure requires rework to provide for the two flanged water connections on the front and rear faces.

The water outlet pipe assembly is a mirror image of the water inlet pipe assembly and is attached in the same manner.

The installation procedure consists of assembling the water-cooled combustor, shell support, water inlet and outlet pipe assemblies, fuel distributor ring and pilot burner assemblies, etc. to the rear face of the intake closure and then installing the entire assembly into the combustor outer housing. The entering chamfer for the aft-pilot support is arranged so that even with the assembly resting on the bottom of the outer housing, it will enter the aft-end of the combustor assembly.

The estimated weight of the combustor assembly including liner and jacket (4620 lb), piping (882 lb) and perforated shell (2128 lb) totals 7630 lb. This excludes the intake closure and fuel distribution rings.

Electron-Beam Welded Alternate Design. - The use of a water-to-gas pressure differential controller for the water supply system of the above combustor design is necessary since the liner is susceptible to buckling if the following occurs:

(a) The water pressure exceeds the gas pressure during cold flow operation

(b) The water pressure occurs prior to initiating airflow through the combustor

Therefore, consideration was given to a means of electron-beam welding the liner to the jacket so that human or controller error could not result in liner failure due to buckling. A preliminary stress analysis indicated a requirement for attaching the liner and jacket by circumferential welds at an axial pitch of approximately 4.0 inches for the maximum condition of 500 psig water pressure in the liner and atmospheric pressure in the combustor.

The fabrication of the liner for the electron-beam welded configuration requires a different approach. Intimate contact is required between the liner and jacket prior to welding in order to avoid a condition where the beam cuts through the piece. Therefore, the nickel liner and stainless steel jacket will be machined to provide a diametral shrink fit. The jacket may be made in bands, the length of which will be determined on full-scale electron-beam welded samples to find shrinkage factor per weld (estimated to be approximately 0.005 inch) and to optimize band length for acceptable distortion. Since there are a very limited number of electron-beam welding vacuum chambers in this country that will accept a 12-foot long cylinder, the grooved liner will be

made in two or more equal lengths and the liner and jacket welded sub-assemblies will be joined with a circumferential bolting flange.

The jacket or outer shell bands are expanded by heating to 250° F with flexible electrical heating tape and after positioning on the liner, are allowed to shrink back during cooling to provide intimate contact with the liner. Proceeding from one end, the liner and jacket are circumferentially welded at about a 4-inch axial pitch. The circumferential weld pass is interrupted at each of the six water manifolds.

The welds are made from the OD through the outer shell into the liner web. The weld extends 0.060/0.080 inch into the web and has a 0.035/0.045 inch interface width. The weld is kept shallow in the web to minimize shrinkage and distortion. Since these are blind welds, excessive shrinkage could cause weld-to-web mismatch and excessive distortion could cause poor weld fill at the joint.

If a 360° circumferential weld pass is required to join jacket bands then, the manifold section of the jacket is chamfered to the nominal OD of the outer shell at the band ends. This permits weld penetration at the band joint during a complete circumferential weld pass. Subsequently, the chamfered manifold joints are filled with weld metal by the TIG process to seal these sections.

Based on this preliminary feasibility study, the electron-beam welded liner represents a significantly more difficult fabrication problem, than the water-cooled liner and jacket without welding.

A preliminary estimate of the cost for tooling and fabricating the water-cooled shell liner is $125,000. An additional cost of $20,000 is estimated to incorporate electron beam welded attachment of the liner ribs to the jacket.

Stress Analysis. - Two versions of the water-cooled shell and jacket liner were analyzed at the gas conditions of 4460° F and 4400 psia and the results are shown in Table 12.

The first configuration had a smooth nickel liner with water grooves on the ID of the jacket. The liner thickness for this design was increased from 0.078 to 0.125 inch in order to reduce the bending stress due to the gas pressure loading on the section spanning the water grooves from 29,400 psi to 12,000 psi, which is below the yield strength (16,000 psi) of nickel at the operating temperature of 800° F. The liner shear stress is 4530 psi at this location. The hoop stress due to the pressure loading in the unsupported area of the 0.125 inch liner is excessive (131,700 psi) and yielding would result.

The pressure load on the liner results in an axial friction force of 19,200 pounds at each web. It requires about 20 inches at each end of the liner to generate a sufficient axial force to prevent the liner from growing. The estimated temperature differential of 325° F between the liner and jacket causes a high thermal stress of 87,800 psi. The combined stress due to the pressure load and thermal gradients results in a low cycle fatigue life of less than 800 cycles.

TABLE 12. - WATER-COOLED LINER DESIGN STRESS SUMMARY COMPARISON

Configuration	Hoop stress, psi	Bending stress, psi	Thermal Stress		Axial restraint, psi	Buckling stability	stress, psi	Low-cycle fatigue, cycles
			Radial ΔT, psi	Axial ΔT, psi				
A. Grooves in Jacket	131,700	$\pm$12,000	-58,000	-	-87,800	Unstable	-150,600	1800
B. Grooves in Liner								
Web Section		-	-82,560	-	-63,830	Stable	-146,390	2600
Center of Passage	-	$\pm$2130	-47,500	27,000	-63,830	Stable	-86,460	12800

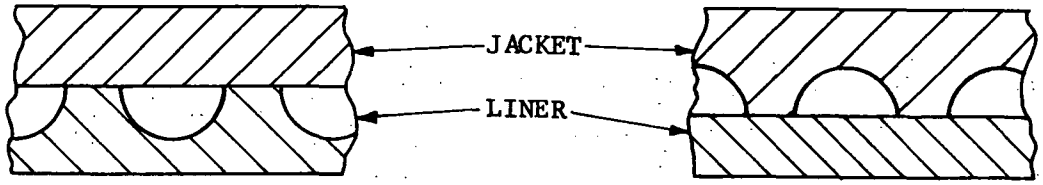

CONFIGURATION A CONFIGURATION B

On the basis of these stress results, a revised water-cooled liner, which incorporates a smooth jacket with water grooves in the nickel liner, was investigated. With the liner having an arch type support resisting the pressure loading, the maximum bending stress will be 2,130 psi at the section of minimum thickness (0.078 inches).

The thermal gradient and thermal stress in the arch area of the liner are as follows:

	Wall ΔT, ° F	Thermal stress, psi
Axial gradient	16	27,000
Radial gradient (minimum thickness)	264	47,500

Combining the thermal stress and pressure stress results in a total stress of 86,460 psi and a low cycle fatigue life of over 12,800 cycles. The prediction was based on the low cycle fatigue curve for nickel as shown on Figure 46.

The highest stress in the liner will occur in the thickest section (center of web) where the radial gradient results in a stress of 82,560 psi. An additional thermal stress will occur in this section since the liner cannot freely expand but is restricted by the cooler jacket. This restriction adds another 63,830 psi compressive stress at the inner wall surface. The predicted low cycle fatigue life is 2600 cycles.

Based on this study, the water-cooled liner is an attractive configuration for final design study since it offers the potential for the broadest operating envelope without violating any of the design criteria.

Water-Cooled Tube Liner

In many high temperature combustors and nozzles in the liquid-fueled rocket field, the thermal protection of the combustor wall is provided by circulating the liquid fuel through many small parallel tubes acting as a barrier between the hot gas and the shell structure. This type of design was investigated for the HTST combustor in order to evaluate alternates to the structural and manufacturing problems of the shell type liner.

Figure 47 presents the preliminary design layout of the water-cooled tube liner. The liner is formed into a cylinder by axially stacking together 678 half-circular tubular segments. Each tube has an OD of 0.375 inch and a wall thickness of 0.049 inch and is made from nickel type A material.

The construction of the liner support housing is similar to the jacket design of the shell liner. The support housing is fabricated from six rolled sheets and six longitudinal U-shaped lower-half water manifolds. The six equally spaced half-manifolds are butt welded to the six rolled sheets to form

a cylinder. Two 0.375 inch diameter holes on 0.455 inch centers are reamed in each manifold half with an axial spacing of 1.215 inches. Each hole incorporates an upper and lower groove with a height of 0.12 inch and a depth of 0.007 inch.

The pair of holes in the #1 water inlet manifold corresponds with the pair of holes in the same transverse plane in the #1 water outlet manifold. The pair of holes in the #2 and the #3 water inlet manifolds are displaced 0.405 inches and 0.810 inches, respectively, in relation to the holes in #1 manifold. Thus, each manifold feeds only one-third of the total number of tubes in the liner. At each pair of holes in the inlet manifold, the water divides so that the coolant travels 180° in each tube and exits in the outlet manifold 180° opposite to the inlet manifold. The water inlet manifolds are located 120° apart and the outlet manifolds are also located 120° apart.

The liner support housing is final machined on the ID, the front and rear flanges and the ID rear pilot. Subsequently, the ends of each tubular segment are inserted and expanded to a depth of 0.40 inch and welded in the reamed holes of the manifolds to form a leak-proof construction.

The half-pipes, about 11.5 feet long, are welded to the lower half of the manifolds to form the six longitudinal water manifolds. Plugs are welded to the rear face of the manifolds to seal the ends.

The outside radius of the 180° tube segment is 0.080 inch smaller than the inside radius of the liner support housing to provide for thermal expansion of the tube. The ends of the tube segments are formed with a 0.28 inch radius for an included angle of 75°.

Each tube is supported at 12 eaually spaced circumferential locations. The 0.50 inch wide supports for the tubes are made of nickel type A material machined into an omega shape so that the 0.375 inch tubes are snapped into positions with 0.08 inch clearance between the tube and the ID of the liner support housing. The supports are approximately 11.75 inches long for ease of manufacturing.

The perforated supporting shell, the water inlet and outlet pipe assemblies, etc. are the same as described for the water-cooled shell liner.

The reworks to the existing combustor housing inlet closure and exhaust nozzle approach section front face and the assembly and installation of the water-cooled combustor with nickel tubes into the combustor outer housing are the same as described in the section for the water-cooled shell liner design.

Table 13 presents the results of a one-dimensional thermal analysis of the tube liner configuration using a water velocity in the tubes of 17 fps and gas conditions of 4460° F and 4000 psia. Wall temperatures and temperature gradients are lower than those of the shell type liner because of the reduced wall thickness; but the total heat rejection increased because of the larger surface area exposed to the hot gas stream. Therefore, the water flow was increased by selection of an increased tube diameter to maintain the same water temperature rise.

TABLE 13. - WATER-COOLED TUBE LINER TEMPERATURES AT 4460° R AND 4000 PSIA

Circumferential location	Wall ΔT, ° F	Gas-side wall temp., ° F	Water wall temp., ° F	Water, ° F
Water Inlet	187	557	369	100
Water Outlet	172	717	539	282

The tube liner design using 678 half circular tubes has a total water flow of 289.6 lb/sec (2166 gpm). The total heat rejection rate was calculated to be 1.91×10^8 Btu/hr if all tubes are heated but will be somewhat lower because tubes in the vicinity of the fuel distributor rings will be cooler. Water pressure drop in the tubes is estimated at 16 psi, considerably reduced from the grooved liner design because of the larger water passage flow area.

Based on this study, the tube liner appears to be an approach with potential; however, this configuration requires a larger capacity external water cooling system and it represents a design which has little experience in direct fired pressure vessel applications.

External System for Water-Cooled Liner

The external system required for the water-cooled liner designs consists of two thermally coupled loops:

(1) The primary water loop for cooling of the combustor liner and heat transport

(2) A secondary water loop for heat rejection from the system

The primary water loop consists of a self contained system incorporating a circulating pump, storage tank, heat exchanger, pressure control system and fill system. The water is filtered and chemically treated to prevent accumulation of foreign material, scale formation and fouling of the heat exchanger and other components. The pressure control system is designed to maintain the combustor water cooling system pressure about 50 psi below gas pressure over the combustor operating range up to 500 psi to prevent liner buckling. For higher combustor pressures, the water cooling system is maintained at a nominal 500 psi to prevent the formulation of steam. The differential pressure is interlocked into the combustor fuel system so that shut-off or reduction of fuel flow is initiated if the gas-to-water differential pressure drops below a pre-selected value during operation other than the filling cycle.

The fill system includes a water level indicating device for the combustor, heat exchanger and storage tank. Each device is interlocked with the combustor fuel system to prevent fuel flow if a full condition for the component is not indicated.

The secondary water loop contains a cooling tower and pumping system which is thermally coupled to the heat exchanger in the primary loop. A flow switch in the pumping system is provided and interlocked into the fuel system.

An alternate and possibly less expensive system may be designed to use treated river water to absorb the heat load and return the heated water to the river. This alternate system has obvious ecological disadvantages and was not considered acceptable.

Selection of water system equipment was based on the following two operating conditions which for sizing studies represent the air facility's shortest and longest hot runs:

Gas temp., ° R	Gas press., psia	Heat load, Btu/hr	Test period, sec.
4000	4000	1.35×10^8	30
4000	2200	0.83×10^8	180

The maximum exit water temperature from the combustor for both conditions is 289° F, although slightly higher temperature can be tolerated for the lower heat load condition. To prevent the formation of steam at 289° F, a nominal operating pressure of 500 psi is used which is well above the saturation pressure.

Based on the above operating conditions, the heat exchanger and equipment sizing was established to satisfy the following maximum requirements:

	30 sec.	180 sec.
Heat load, Btu/hr	1.41×10^8	0.865×10^8
Inlet temperature, ° F	100	174
Exit temperature, ° F	289	289
Water flow, gpm	1500	1500
Pressure, psig	500	500

Several heat exchanger systems were investigated based upon heat rejection time between tests from four to twenty-four hours. They are described below.

Typical water systems are shown schematically in Figures 48 and 49. Initially water is drawn from a source for storage in the tank. A main pump circulates the water through the water jacket, heat exchanger and back to the tank. Valving is included to provide for either the filling or circulating functions. Float switches at the water jacket, heat exchanger and tank provide the interlocks to the fuel system. All float switches must indicate a full condition before the fuel system can be energized.

A differential pressure regulating system sensing tank pressure and combustor pressure modulates a control valve in a by-pass line to maintain the required differential. If the differential pressure does not fall within a pre-selected band, the fuel system is de-energized.

Since the tunnel test time is very short and the time between tests is relatively long, several combinations of system components and sizes are possible which satisfy the expected operating conditions. Table 14 presents several of the possible systems. Systems I and II appear to bracket potentially the most feasible and practical design features.

System I is a closed loop 500 psi system with a small water storage tank. The maximum load is absorbed by the heat exchanger and the cooling tower. Continuous testing at maximum heat load is possible but costly. The preliminary costs for this system are shown in Table 15.

Since several hours elapse between tests, this time may be used to circulate the hot water (stored in two 3000 gallon tanks) through a smaller heat exchanger utilizing a smaller cooling tower.

The heat exchanger and cooling tower size requirements for System II were studied to determine costs associated with fast or slow cooling periods between tests with the test sequences assumed as shown in Table 16.

For this study the water temperature prior to all first tests was 100° F for the heat exchanger and 85° F for the cooling tower. Figure 50 presents the heat exchanger and cooling tower requirements for cooling periods up to 24 hours in terms of initial equipment costs for test sequences 1, 3 and 4. For test sequence 2, two 3000 gallon storage tanks are of sufficient capacity to maintain low water temperature through mixing, to initiate the second test at moderate gas conditions without cooling the water between the test periods. Test sequence 3 is the controlling condition for sizing since it requires the largest heat exchanger and cooling tower.

The preliminary costs for System II which satisfies test sequence 3 and is sized for a 4-6 hour cooling period are also presented in Table 16. Thus, System II is shown as the more economic and practical arrangement.

The alternate systems (III through VI in Table 14) have major cost disadvantages as discussed below.

TABLE 14. - WATER COOLING SYSTEM ALTERNATES

System	Type	Primary water tank	Primary pressurization (500 psi)	Primary main pump (1440 gpm)	Primary heat rejection	Secondary water supply	Disadvantages
I	Closed	Small (500 gal)	Pump or Gas	100 psi	Large heat exchanger (1.3×10^8 Btu/hr 100° F Outlet)	Large	Heat exchanger and cooling tower costs
II	Closed	Large (6,000 gal)	Pump or Gas	100 psi	Small heat exchanger (6×10^4 Btu/hr 100° F Outlet)	Small	Tank cost
III	Closed	Small	Pump or Gas	100 psi	Moderate heat exchanger (1.3×10^8 Btu/hr 150° F Outlet)	Large	Heat exchanger and cooling tower costs
IV	Open (not recycled)	Small	None	500 psi	None	Moderate	Main pump cost, water outlet temperature, continuous water treatment
V	Open	Large	None	500 psi	Cooling tower (1.3×10^8 Btu/hr	None	Tank, cooling tower and main pump costs
VI	Closed	Small	None	500 psi	Condenser (1.3×10^8 Btu/hr 100° F outlet)	Large	Condenser, cooling tower and main pump costs

TABLE 15. - EXTERNAL WATER COOLING SYSTEM PRELIMINARY COST ESTIMATES

Item*	Description	System I $	System II $
1	Charge pump - 11 stage centrifugal (20 gpm/500 psi)	4,000	4,000
2	Check valve - swing type (20 gpm/500 psi)	50	50
3	Differential pressure regulating system	3,000	3,000
4	Reservoir** (500 psi)	2,000	23,000
5	Circulating pump (1500 gpm/100 psi p)	6,600	6,600
6	Ball valve - pneumatic actuator and solenoid (1500 gpm/500 psi)	1,000	1,000
7	Float switch - normally open	300	300
8	Solenoid valve (20 gpm/500 psi)	100	100
9	Pressure relief valve (600 psi)	300	300
10	Fill relief valve (20 gpm/25 psi)	25	25
11	Ball valve - pneumatic actuator and solenoid (20 gpm/500 psi)	200	200
12	Fill check valve (20 gpm/500 psi)	75	75
13	Heat exchanger***	40,000	3,000
14	Float switch - normally open	300	300
15	Water level switch	300	300
16	Vent valve	25	25
17	Solenoid valve (20 gpm/500 psi)	100	100
18	Solenoid valve (20 gpm/500 psi)	100	100
19	Cooling tower and pumping system	550,000	15,400
-	Filtration and water softening system	10,000	5,000
-	Chemical conditioning	2,500	1,500
-	Pipe, fittings, nuts, bolts, etc.	5,000	5,000
-	Miscellaneous	5,000	5,000
	Total material	$ 606,925	$ 76,675
-	Installation labor	115,000	45,000
	Grand total	$745,925	$119,675

* Reference Figures 48 and 49
** System I - 500 gallon tank
System II - two 3,000 gallon tank
*** Reference text for capacity

TABLE 16. - CONDITIONS FOR SIZING WATER SYSTEM COMPONENTS

Test Sequence	1st Test			2nd Test		
	Time, second	Gas temperature ° R	Gas pressure, psia	Time, second	Gas temperature ° R	Gas pressure, psia
1	30	4460	4000	30	4460	4000
2	30	4460	4000	180	4000	2200
3	180	4000	2200	30	4460	4000
4	180	4000	2200	180	4000	2200

(a) The main pump for System I or II is externally pressurized and requires a relatively low differential pressure; but all system components are designed for the maximum operating pressure of 500 psi. A high pressure main pump (shown for System IV, V and VI) may be considered but pump horsepower increases by a factor of seven and high voltage motor starting equipment is required.

(b) Heat exchangers in the circulating system operate at 500 psi to maintain the water in a superheated condition. If the heat exchanger is not in the circulating circuit, the tank must be pressurized to prevent violent boiling within the tank. In either case, a pressure control valve must be provided.

(c) If a condenser is considered as part of the high pressure pump system, a heat exchanger is still required to sub-cool the water from 212° F to 174° F or 100° F.

Consequently, these factors made the alternate systems unattractive.

Coatings Review

Thermal Barrier Coatings. - A brief state-of-the-art review of thermal barrier materials for possible application to the inside diameter of the combustor liner was performed. The review was based on available published technical literature and general industry experience. No specific testing to confirm the information was performed for this program.

The term thermal barrier refers to a temperature resistant, low conductivity, insulating material applied to a metallic structural component, such as a combustor liner, to reduce the heat flux to the component from a hot gas environment. The purpose of the barrier is to keep the temperature of the component at a level where the metal maintains its structural integrity to reduce the cooling requirement to the component.

Ceramic materials are an obvious choice for thermal barriers because of their low thermal conductivity; however, there have not been many successful service applications of ceramic thermal barriers, primarily due to the following:

(a) The poor thermal shock resistance of ceramic materials applied directly onto metal substrates

(b) The difficulty in obtaining a good bond between the ceramic material and the metal substrate

(c) The large difference in the coefficient of thermal expansion between ceramic materials and the structural metal substrates

These deficiencies usually result in failure of the thermal barrier by cracking at the ceramic surface and/or separation of the ceramic from the metal substrate.

Several methods have been attempted to overcome these difficulties.

One of these methods has been the utilization of a thermal sprayed high-bond-strength undercoat (such as nickel-aluminide), between the metal substrate and a thermal-sprayed ceramic top coating. Thermal-spraying is a group of processes wherein finely divided metallic or non-metallic materials are deposited in a molten or semi-molten condition to form a coating. The coating material may be in the form of powder, ceramic rod, wire, or molten materials.

Some advantage has also been gained by heating of the metal substrate during coating. This places the coating under a residual compressive stress at ambient temperature and reduces the tensile stress in the coating, due to the thermal expansion mismatch at elevated temperatures.

Another approach has been the use of a metallic honeycomb supported thick ceramic barrier. In this method, a metallic honeycomb reinforcing structure is brazed to the metal substrate. The honeycomb cells are filled with either a dense ceramic by hot mercury or with a low conductivity ceramic foam. The entire structure is then oversprayed with a dense ceramic coating for erosion protection.

A third approach has been the use of non-reinforced thermal-sprayed cermet coatings formed by mixing a ceramic material in varying proportions with a metallic material. The metal contributes bonding properties and thermal shock resistance, and the ceramic material contributes low thermal conductivity. Grading of the coating from a pure metal at the substrate surface to a pure ceramic at the gas stream surface, with varying proportion layers in between is most beneficial. In graded coatings, the thermal stresses from the thermal expansion mismatch are more evenly distributed throughout the coating, rather than being concentrated at the coating-substrate interface. This increases the resistance of the coating to cracking and spalling failures from thermal cycling.

TABLE 16. - CONDITIONS FOR SIZING WATER SYSTEM COMPONENTS

Test Sequence	1st Test			2nd Test		
	Time, second	Gas temperature ° R	Gas pressure, psia	Time, second	Gas temperature ° R	Gas pressure, psia
1	30	4460	4000	30	4460	4000
2	30	4460	4000	180	4000	2200
3	180	4000	2200	30	4460	4000
4	180	4000	2200	180	4000	2200

(a) The main pump for System I or II is externally pressurized and requires a relatively low differential pressure; but all system components are designed for the maximum operating pressure of 500 psi. A high pressure main pump (shown for System IV, V and VI) may be considered but pump horsepower increases by a factor of seven and high voltage motor starting equipment is required.

(b) Heat exchangers in the circulating system operate at 500 psi to maintain the water in a superheated condition. If the heat exchanger is not in the circulating circuit, the tank must be pressurized to prevent violent boiling within the tank. In either case, a pressure control valve must be provided.

(c) If a condenser is considered as part of the high pressure pump system, a heat exchanger is still required to sub-cool the water from 212° F to 174° F or 100° F.

Consequently, these factors made the alternate systems unattractive.

Coatings Review

Thermal Barrier Coatings. - A brief state-of-the-art review of thermal barrier materials for possible application to the inside diameter of the combustor liner was performed. The review was based on available published technical literature and general industry experience. No specific testing to confirm the information was performed for this program.

The term thermal barrier refers to a temperature resistant, low conductivity, insulating material applied to a metallic structural component, such as a combustor liner, to reduce the heat flux to the component from a hot gas environment. The purpose of the barrier is to keep the temperature of the component at a level where the metal maintains its structural integrity to reduce the cooling requirement to the component.

Ceramic materials are an obvious choice for thermal barriers because of their low thermal conductivity; however, there have not been many successful service applications of ceramic thermal barriers, primarily due to the following:

(a) The poor thermal shock resistance of ceramic materials applied directly onto metal substrates

(b) The difficulty in obtaining a good bond between the ceramic material and the metal substrate

(c) The large difference in the coefficient of thermal expansion between ceramic materials and the structural metal substrates

These deficiencies usually result in failure of the thermal barrier by cracking at the ceramic surface and/or separation of the ceramic from the metal substrate.

Several methods have been attempted to overcome these difficulties.

One of these methods has been the utilization of a thermal sprayed high-bond-strength undercoat (such as nickel-aluminide), between the metal substrate and a thermal-sprayed ceramic top coating. Thermal-spraying is a group of processes wherein finely divided metallic or non-metallic materials are deposited in a molten or semi-molten condition to form a coating. The coating material may be in the form of powder, ceramic rod, wire, or molten materials.

Some advantage has also been gained by heating of the metal substrate during coating. This places the coating under a residual compressive stress at ambient temperature and reduces the tensile stress in the coating, due to the thermal expansion mismatch at elevated temperatures.

Another approach has been the use of a metallic honeycomb supported thick ceramic barrier. In this method, a metallic honeycomb reinforcing structure is brazed to the metal substrate. The honeycomb cells are filled with either a dense ceramic by hot mercury or with a low conductivity ceramic foam. The entire structure is then oversprayed with a dense ceramic coating for erosion protection.

A third approach has been the use of non-reinforced thermal-sprayed cermet coatings formed by mixing a ceramic material in varying proportions with a metallic material. The metal contributes bonding properties and thermal shock resistance, and the ceramic material contributes low thermal conductivity. Grading of the coating from a pure metal at the substrate surface to a pure ceramic at the gas stream surface, with varying proportion layers in between is most beneficial. In graded coatings, the thermal stresses from the thermal expansion mismatch are more evenly distributed throughout the coating, rather than being concentrated at the coating-substrate interface. This increases the resistance of the coating to cracking and spalling failures from thermal cycling.

Because of its versatility, plasma spraying appears to be the most practical thermal-spray method for application of these coatings. Plasma spraying is a thermal-spraying process wherein a non-transferred constricted electric arc-gas mixture is utilized as the source of heat for heating or melting and propelling the cooling material to the workpiece.

Recent research on the latter two concepts (References 16, 17 and 18 has indicated that the plasma sprayed, graded cermet thermal barrier approach is superior to other methods of application of thermal barrier materials.

Graded thermal barrier coatings were applied as five or six equal thickness layers, starting with pure metal plasma sprayed on the substrate and grading to pure ceramic in the outer layer. The composition of the individual layers were as follows:

Layer	% Metal	% Ceramic
First	100	--
Second	75	25
Third	50	50
Fourth	25	25
Fifth	10	90
Sixth	--	100

For five layer coatings, the 10% metal - 90% ceramic layer is omitted. Three and four layer graded coatings have also been utilized in the industry (References 19 and 20) but test evaluations of these coatings have not been published. The compositions of such coatings are:

Layer Three Layer Coating	% Metal	% Ceramic
First	100	-
Second	50	50
Third	-	100

Layer Four Layer Coating	% Metal	% Ceramic
First	100	-
Second	65	35
Third	35	65
Fourth	-	100

Screening tests were conducted on the five ceramic materials, 1) alumina, 2) zirconia, 3) mullite, 4) spenel and 5) zircon and zirconia (ZrO_2) was selected as the best ceramic constituent based on thermal conductivity and thermal shock resistance. Three metal systems were studied, 1) nickel-alumide (Ni-5% Al), 2) nichrome (Ni-20% Cr) and 3) Hastelloy X (Ni-Cr-Mo alloy) and Hastelloy X was selected as the best system, although differences were marginal between Hastelloy X and nichrome.

The methods utilized in evaluating both the honeycomb reinforced 0.065 inch thick and the 0.030 inch thick non-reinforced plasma-sprayed thermal barrier materials and the test criteria for combustor liners were as follows:

(a) Thermal Shock - Barrier able to survive 100 thermal shocks of approximately 2500° F/sec at gas temperatures up to 2600° F

(b) No erosion through barrier for an exposure equivalent to 10 hours in a dusty environment (per MIL E 5007C)

(c) Ballistic Impact - 75% of thermal shock strength after impact

The results of the thermal shock tests on combustor liner specimens showed that no failures occurred in 100 tests at 3000° F for the Hastelloy graded to zirconia systems. The erosion tests showed this system satisfied the criteria by running 12.4 hours. The ballistic impact tests showed this system retained 100% of its thermal shock resistance after impact.

It has been generally found experimentally that the thermal conductivity follows the law of mixtures for graded cermet coatings.

The relationship between the reduction in heat flux as a percent of the heat flux for an unprotected surface vs the heat transfer coefficient is as follows:

Heat transfer coefficient Btu/hr-sq.ft.-° F	Reduction in heat flux %
100	10 - 14
200	17 - 25
300	23 - 33
400	28 - 39
500	32 - 45
1000	50 - 61
2000	63 - 77

It is obvious that the thermal barrier coatings are most useful where the heat transfer coefficients are high. For combustors, the reduction in heat flux is in the range of 20%.

In conclusion, industry experience indicates that the best thermal barrier material based on effectiveness, durability, and ease of application in a non-reinforced, plasma-sprayed cermet coating with the composition graded from 100% metal at the liner interface to 100% ceramic at the gas stream interface. Limited specimen testing indicates that zirconia is the best choice for the ceramic and either nichrome or Hastelloy X for the metal component in the cermet coating. However, the advantages of thermal barriers to reduce the heat flux diminishes in the applicable range of heat transfer coefficients for combustor liners.

Reflective Coatings. - The use of a reflective coating for temperature control was also considered for the air-cooled liner to maintain the operating temperature of the nickel-base superalloy at a level where material properties are suitable for the application.

Previously it was shown by thermal analysis that a highly reflective surface for the liner would result in a reduction in liner metal temperature of 200° F which in some designs is sufficient to satisfy the design criteria of 1850° F maximum liner temperature.

A reflective type, thermal control coating for the combustor should have the following properties:

(a) High reflectivity or low emissivity at the liner operating temperature

(b) High resistance to oxidation at operating temperatures to prevent degradation of the reflective properties with time at temperature

(c) Capability for application to the liner surface at reasonable cost

Candidate reflective coatings for the liner include rhodium, chromium, platinum, and gold. For the noble metals, a thickness of 0.1 mil is required for the liner surface. For chromium, a thickness of one mil is required.

The emissivity values for the candidate materials are as follows:

Rhodium	0.25
Chromium	0.34
Platinum	0.27 - 0.38
Gold	0.05 - 0.17

A review of the general characteristics of the candidate materials is presented below.

Rhodium is principally used where maintained high and uniform reflectivity is essential, and as such is a prime choice for a thermal control coating. The melting point of rhodium is 3591° F. It remains bright and untarnished during

atmospheric exposure and its general resistance to corrosion is exceptionally high. Rhodium is superficially oxidized in air at temperatures above about 1100° F but the oxide dissociates at about 2000° F in air.

The main characteristics of chromium on which rests the commercial use of chromium electrodeposits are:

(a) Appearance

(b) Resistance to corrosion and heat hardness

(c) Resistance to wear

(d) Low coefficient of friction and non-adhesion to certain materials

Factors which limit the use of chromium under certain conditions are brittleness resulting from lack of elasticity and a possible reduction in fatigue strength of the base metal. Continuous heating above 1200° F gives rise to oxidation. Oxidizing and reducing agents have little effect on chromium and it resists corrosion from most chemicals.

Platinum does not oxidize at any temperature up to its melting point, 3250° F, and is attacked by very few chemicals in liquid solutions. It should not, however, be treated in the presence of oxidizable materials. Metallic salts, particularly lead salts, carbon, sulfur, phosphorous, and the oxidizable compounds should not be heated in contact with platinum. The result of such treatment would be embrittlement of the platinum and alteration in other thermophysical properties.

Pure gold is not attacked by oxygen, sulfur or sulfur dioxide. Hydrogen has little effect on pure gold at elevated temperatures, however, chlorine will attack gold even at room temperature. Electroplated gold has wide applications as a coating to resist corrosion and tarnishing over a wide range of temperatures. However, it has a relatively low melting point of 1945° F for combustion applications.

The cost of plating with the noble metals is substantially affected by the problems associated with processing the cylindrical liner which is 3 feet in diameter and 12 feet long. The processing is made easier for the omega-shaped liner by plating the ID of the segments prior to butt welding the segments into the cylindrical liner. The processing problem takes on greater significance considering that the current market cost of the metals is $70 to $150 per ounce. Rhodium and platinum are roughly twice the cost of gold. It is estimated that the cost of plating the liner may be in the range of $50 per square foot.

Instrumentation Requirements for Tunnel Test

The instrumentation requirements for initial tunnel testing of the reworked or new combustor design studied are presented below. The data obtained can be useful in

(a) Verifying the analyses and life predictions

(b) Modifying the design to correct problems prior to testing at more severe conditions.

Stress & Vibration Data. - The prime purpose of strain gage instrumentation on the air-cooled liner is to establish the vibration characteristics of the liner. It is desirable to attach the strain gages in the area where cracks have been observed or are expected. As an alternate arrangement, strain gages on the inside surface upstream of the fuel rings is an expedient choice. About ten gages are to be installed around the circumference in order to establish the vibrational mode shape. Gages are to be oriented in a tengential direction and the dynamic responses of the gages are to be recorded on magnetic tape.

Pressure gages and microphone pickups are to be used to measure the internal dynamic environment of the combustor during a complete run. A compromise may be made as to location because of the severe temperature and pressure conditions existing. The major purpose of this instrumentation is to establish the exciting force that is causing the liner to vibrate.

This instrumentation can be used to detect changes in the excitation of the system or response of the liner as modifications to the configuration are made. The effectiveness of liner damping arrangements can be evaluated by the magnitude of the dynamic stress response. Other approaches to resolving the problem such as changing the liner's natural frequency or altering the excitation source, (i.e., fuel rings) may also be evaluated. The latter change may be verified by the pressure or microphone pickups.

The vibration characteristics of the omega liner will substantially differ from that of the current cylindrical shell liner or the ribbed liner. In order to establish the acceptability of the vibratory characteristics of the omega liner, strain gages are to be installed on the outer surface of the liner. At least three different segments shall be instrumented with the gages installed on each segment, two tangential near the corners of the channel and one axial at the center. The axially directed gages are to be repeated every six inches for a two-foot section downstream of the fuel rings. This instrumentation may be able to detect any serious vibration that may cause a fatigue problem.

Also, pressure and microphone pickups are to be employed to establish the dynamic pressure environment inside the combustion liner.

Although the water-cooled liner should have much more damping than the current air-cooled liner, it is advantageous to establish its vibratory stress characteristics throughout its expected operating range in a manner described for the air-cooled liner.

Thermal Data. - To confirm the heat transfer analysis of the regenerative air-cooled designs, temperature and pressure instrumentation shall be installed during initial operation, measuring the inner and outer surface temperatures at eight circumferential locations in five axial planes at about one foot axial spacing from the plane of the fuel distributor rings.

At two diametrally opposite locations at four feet from the fuel rings, additional outside surface thermocouples shall be installed to measure temperatures at five circumferential locations between

(a) Adjacent T-bar supports of the reworked present liner or the ribbed liner

(b) At corner and center points of one segment of the segmented omega liner

Cooling air temperature shall be measured at four circumferential locations at both ends of the liner. Static pressure taps shall be installed to measure pressure at the entrance and exit of the cooling passage at four circumferential locations and to measure hot gas-side pressure upstream and downstream of the fuel rings and at the exit of the liner.

Gas leakage into the bulb attachment region of the omega liner shall be measured at five segments at five axial planes at about one foot axial spacing from the fuel rings.

Use of temperature sensitive paints is also recommended for the air-side surface of the air-cooled liners to determine local regions of high circumferential and axial temperature gradients. This data, in addition to thermocouples at locations of maximum gradients expected, may be converted to stress to verify life predictions.

For the water-cooled shell liner, the inside wall temperature shall be measured as above, but at only two axial planes, two feet and four feet from the fuel rings because no appreciable gradient in axial temperature distribution is expected. Water temperature and pressure in and out of the three manifold pairs and system total water flow shall be measured. Static pressure measurements are not required since there is no pressure loading structural problem associated with airflow.

CONCLUDING REMARKS

Based on the preliminary design studies and the parametric thermal and stress analyses of the thermal protection system for the 8-foot HTST combustor, the following are recommended:

(1) Conduct a final design study of the two most promising liner concepts: (a) the water-cooled nickel shell liner with grooves and (b) the air-cooled omega shaped segment liner

(2) Conduct manufacturing evaluations to finalize the fabrication process, tooling concepts and electron-beam welding parameters for construction of the water-cooled liner and the air-cooled omega liner and to explore lower cost methods

(3) Conduct a final analysis of the external water-cooling system design to optimize the system costs, capacity and flexibility and to prepare detail specifications

(4) Continue the vibration analysis of the strain gage and microphone data measured on the present air-cooled liner to identify the mode shape of vibration and excitation sources (Appendix B)

(5) Complete the final design of the wave spring damper system to extend the useful life of the present air-cooled liner design

(6) Rework the present air-cooled liner (or fabricate a new liner without OD surface cooling fins) to incorporate the wave spring dampers and re-measure the vibratory characteristics of the liner

(7) Evaluate the application of reflective coatings for the air-cooled liners by testing specimens for significant characteristics after exposure to the combustor environment

REFERENCES

1. Hottel, H.C., and Sarafin, A.F., "Radiative Transfer," Chapter G, McGraw-Hill, 1967.
2. Lefebvre, A.H., and Herbert, M.V., "Heat Transfer Processes in Gas Turbine Combustors," Proceedings of the Institution of Mechanical Engineers, Vol. 174, No. 12, p. 463, 1960.
3. Ballal, D.R., and Lefebvre, A.H., "A Proposed Method for Calculating Film-Cooled Wall Temperatures in Gas Turbine Combustion Chambers," ASMG Paper 72-WA/HT-24, 1972.
4. McAdams, W.H., "Heat Transmission," Chapter 9, McGraw-Hill, 1954.
5. Knudsen, J.G., and Katz, D.L, "Fluid Dynamics and Heat Transfer," Chapter 14, McGraw-Hill, 1958.
6. Halford, G.R., and Manson, S.S., "Application of a Method of Estimating High Temperature Low Cycle Fatigue Behavior of Materials," Transactions of the ASM, Vol. 61, 1968.
7. "Design Report on the Combustor Unit for the NASA High Temperature Structural Dynamics Facility" ALCO Products Incorporated, 1961.
8. Coffin, L.F. Jr., "Thermal Stress and Thermal Stress Fatigue M.I.T. Summer Notes, 1958 "Behavior of Metals and Design Requirements for Elevated Temperatures."
9. Veda, T., and Harada, I., "Experiment of Heat Transfer on the Surfaces with Transverse Fins for Flow Direction," Bulletin of ASME, Vol. 7, No. 28, 1964, p. 759.
10. Karasev, E.K., "Investigation of the Hydrodynamics and Heat Transfer in a Channel with the Turbulizers on the Heat Transfer Surface," in "Heat and Mass Transfer," ed. by A.V. Lykov and B.M. Smolskii, NASA TT F-431, Vol. 1, p. 190, 1967.
11. Mantle, P.L., Freeman, A.R., and Watts, J., "Conductivity Effects on Ribbed Surface Heat Transfer," Int. J. Heat and Mass Transfer, Vol. 14 No. 11, p. 1825, 1971.
12. Kattchee, N., and Mackewicz, W., "Effects of Boundary Layer Turbulence Promoters on the Local Film Coefficients of ML-1 Fuel Elements," Nuclear Science and Engineering, Vol. 16, p. 31, 1963.
13. Hill, P.G., and Peterson, C.R., "Mechanics and Thermodynamics of Propulsion," Chapter 14, Addison-Wesley, 1965.
14. Bernath, L., "A Theory of Local-Boiling Burnout and its Application to Existing Data," Chemical Engineering Progress Symposium, Ser. 56, No. 30, p. 95, 1960.
15. Tong, L.S., "Boiling Heat Transfer and Two-Phase Flow," p. 156, Wiley, 1965.
16. Newman, R.L., Cross, K.R., Spicer, W.C., Sheels, H.D. and Driskell, T.D. ACS Paper 21-C-71F, Sept. 1971
17. Cavanagh, J.R., Cross, K.R., Newman, R.L. and Spicer, W.C., "The Graded Thermal Barrier - A New Approach for Turbine Engine Cooling," AIAA Paper No. 72-361 - April 1972.

18. Musyar, L.E., and Edenborough, N.B.,"Mechanical Properties of Thermal Barrier Materials Program," EDR 7510 and EDR 7622, Dept. of Navy Contract No. N00019-72-C-0418, July 1972, and Oct. 1972.
19. "Metco Cermets" - Metco Technical Data Bulletin 149A 5M 8/63 - Metco,Inc., Westbury, L.I.
20. Mogul, J., (Curtiss-Wright) and Meringolo, V. (Metco), Personal Communications, Dec., 1972.
21. Handbook of Physiochemical Properties of Elements.
22. Statement of Work - Design of Thermal Protection System for 8-Foot HTST Combustor, NASA-Langley Research Center, 1-13-2681 Exhibit A, March 24, 1972.

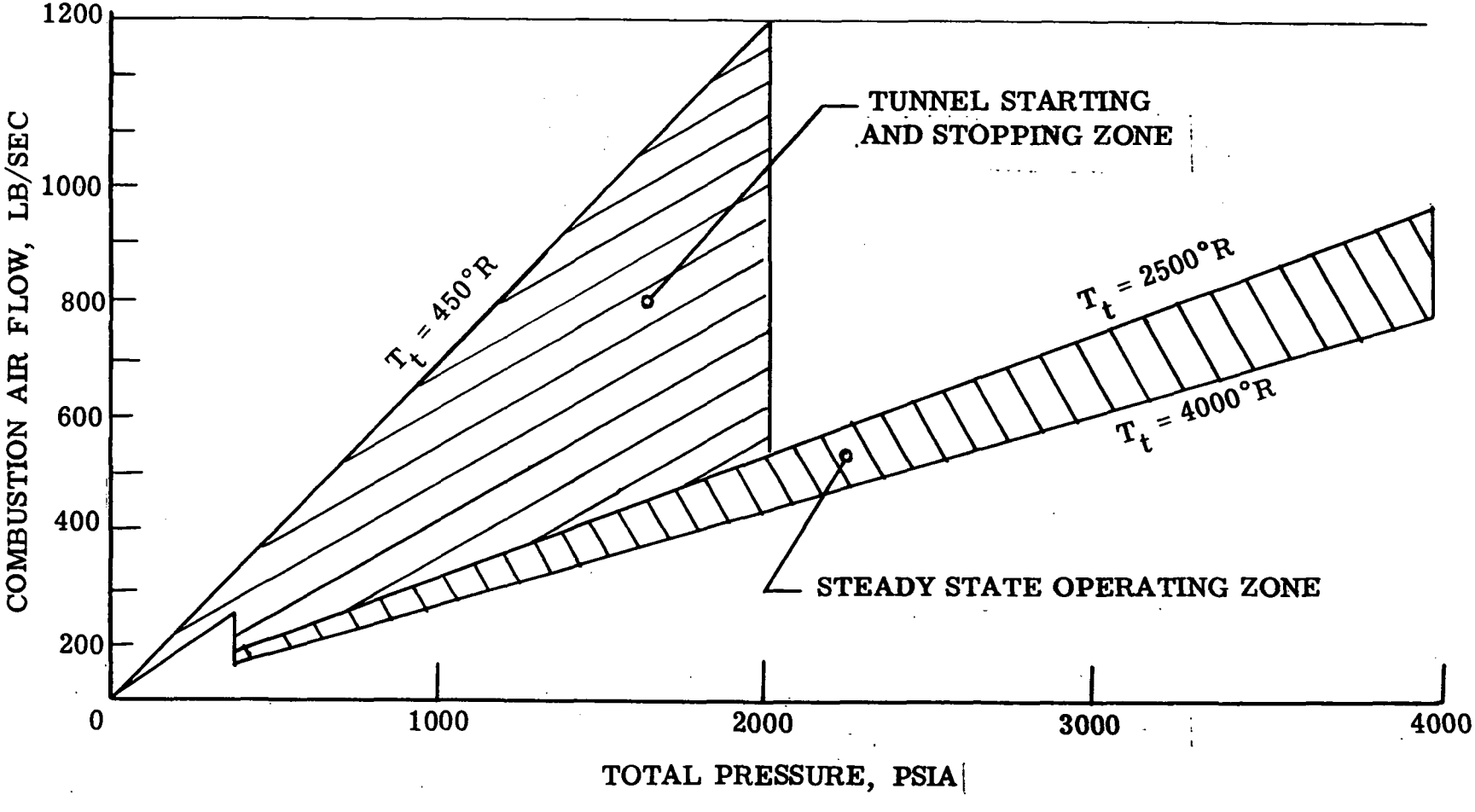

Figure 1. HTST Combustor Operating Envelope.

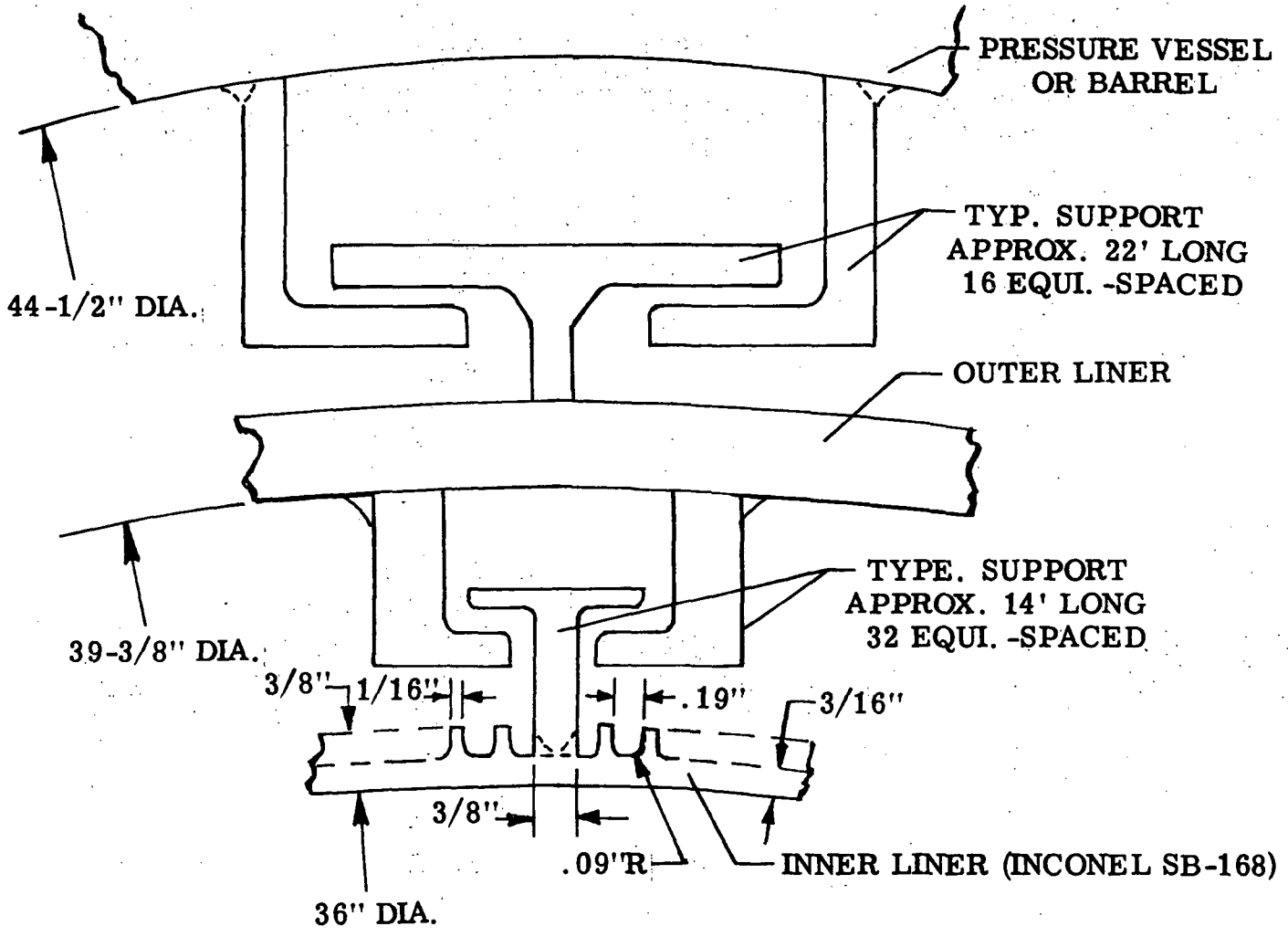

Figure 2. Liner Design Arrangement

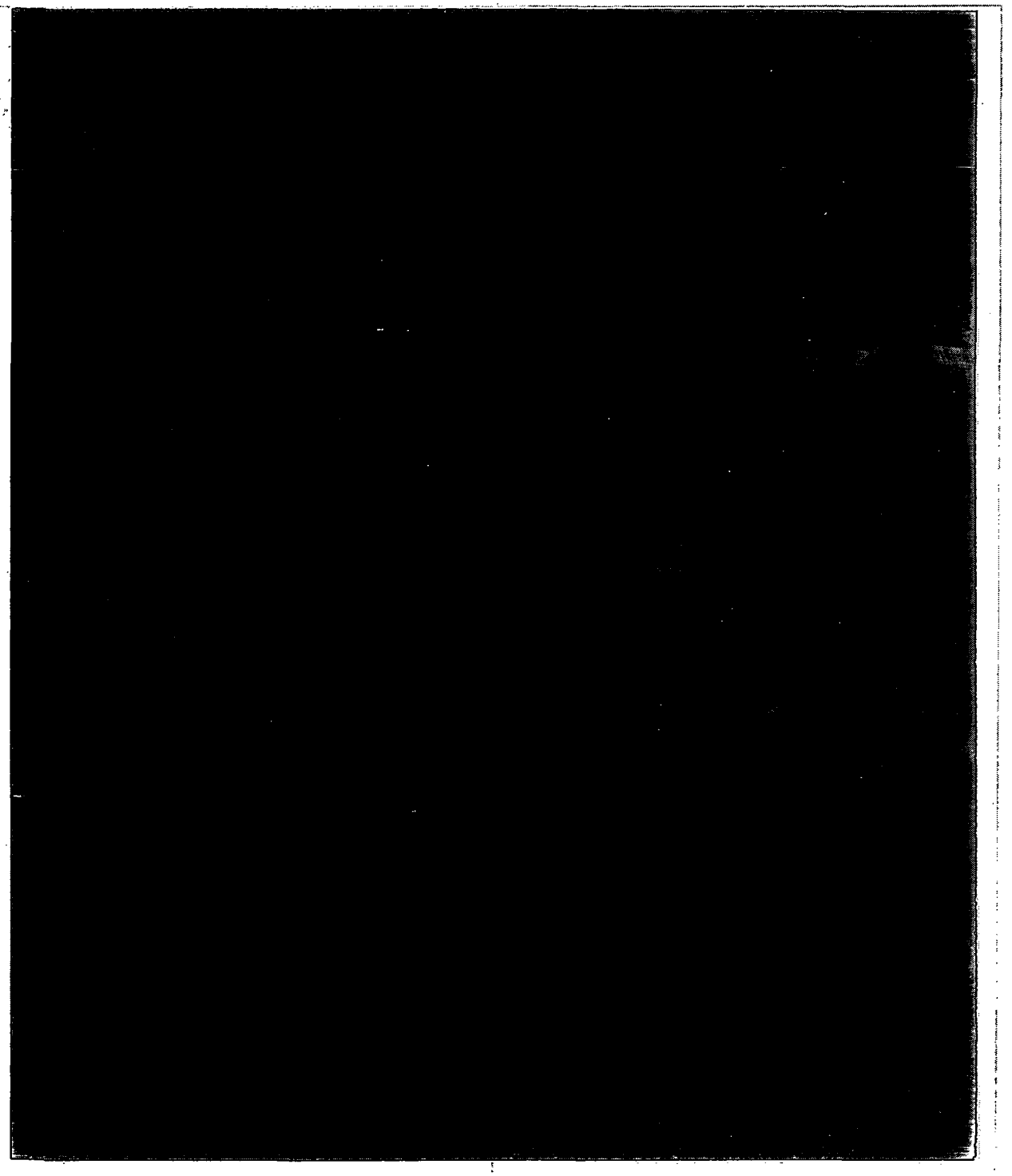

Figure 3. Liner Segment for Metallurgical Analysis.

Repro 1945-20A
7/69

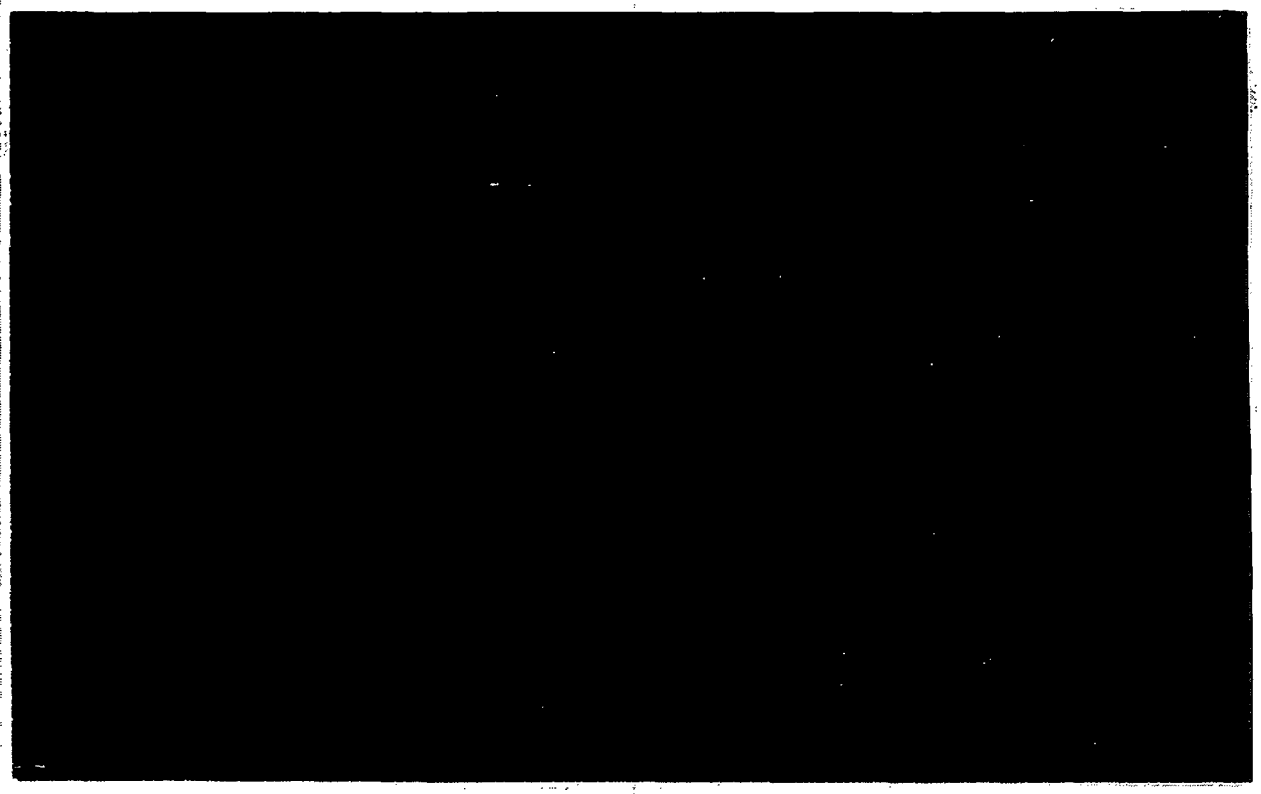

Mag. 3X

Figure 4. Typical Axial Crack (Arrow) Along a T-Bar Weld Bead.

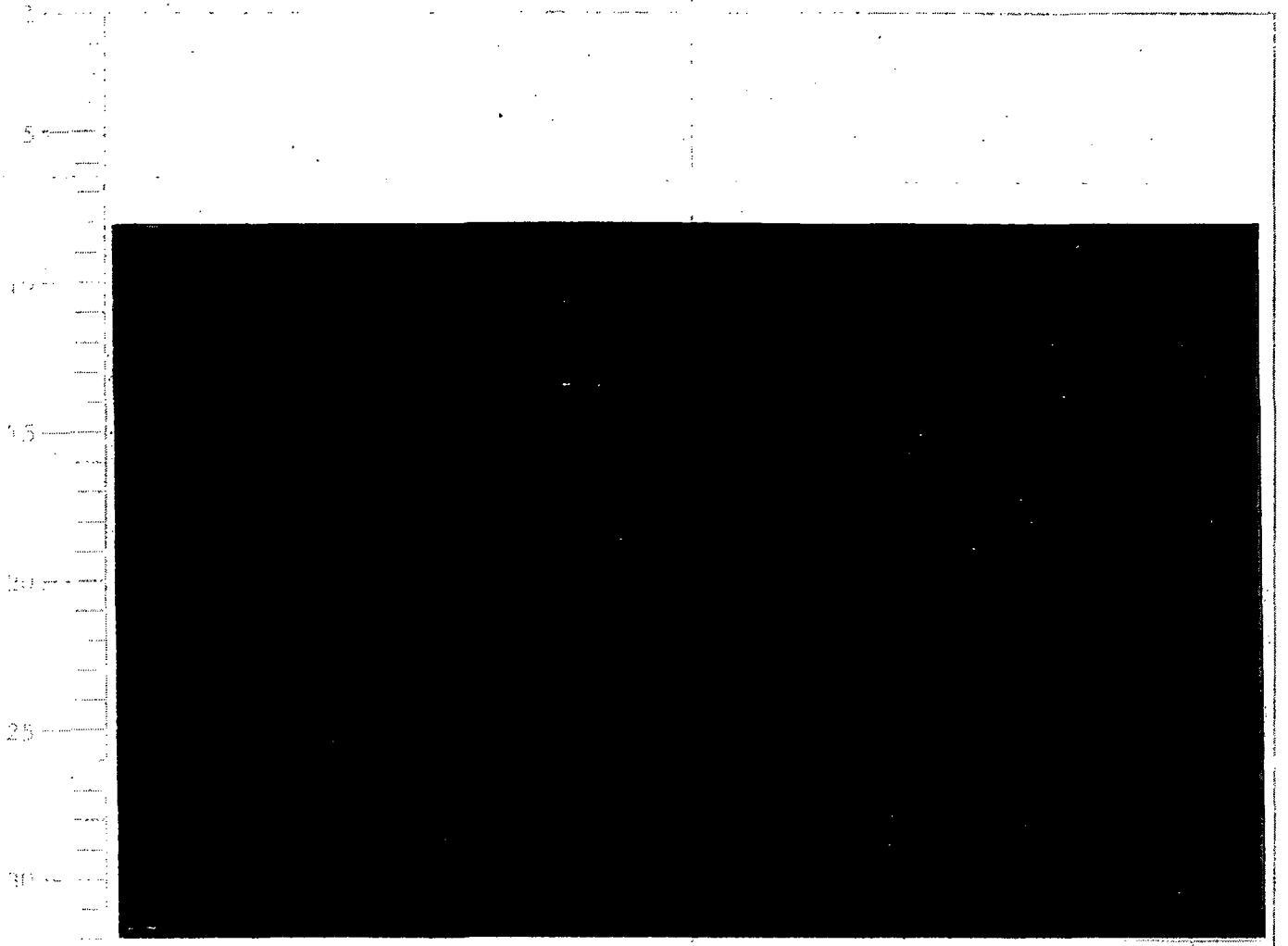

Mag. 5X

Figure 5. Fracture Surface of Crack Along T-Bar Weld.

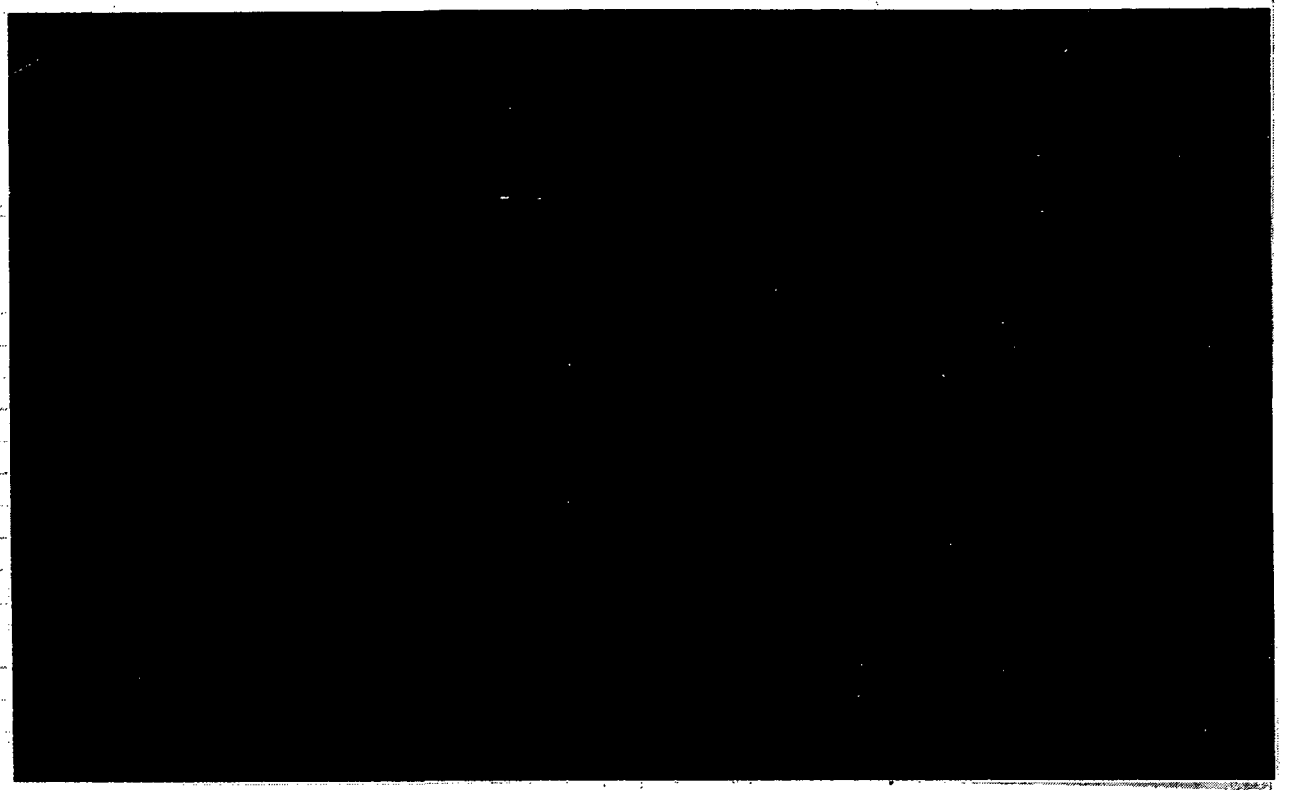

Mag. 5X

Figure 6. Cracking (Arrows) in the Roots of Fin Grooves.

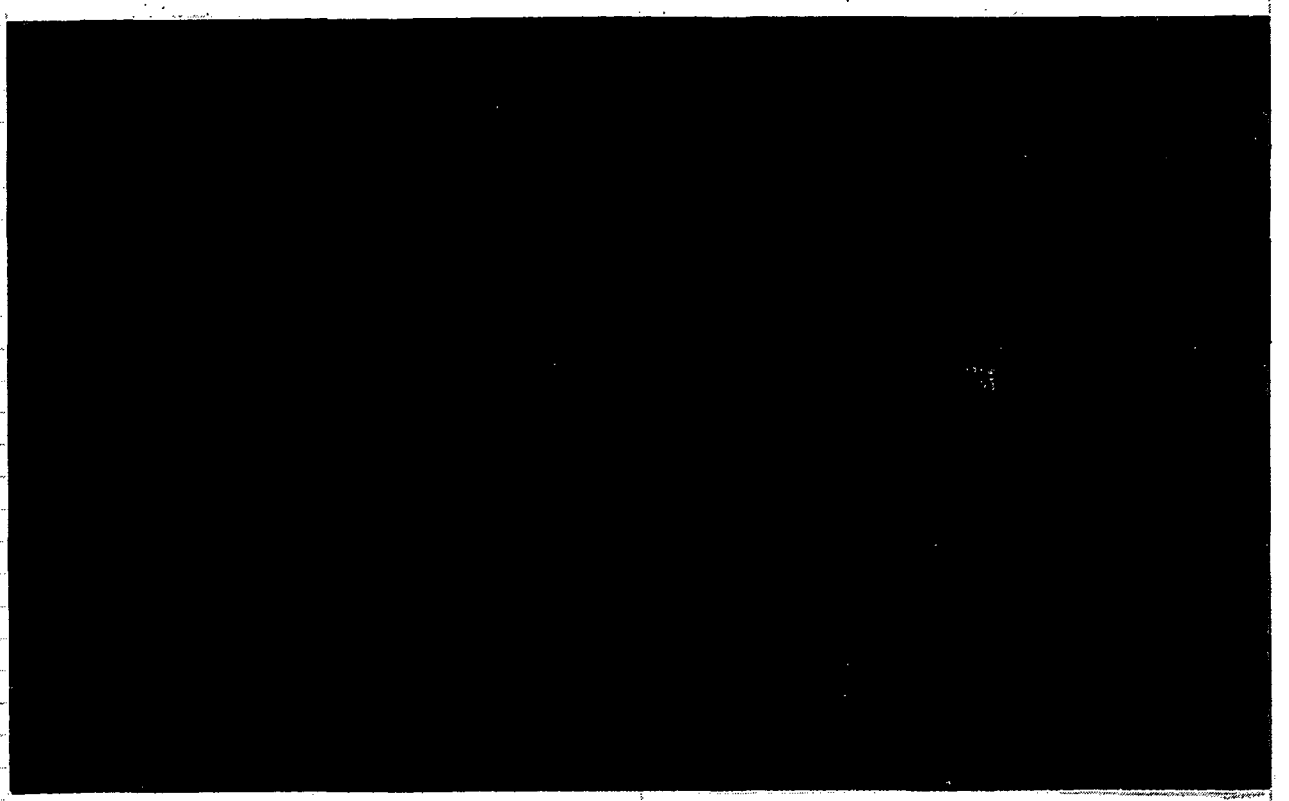

Mag. 3X

Figure 7. Fracture Surface of Cracks in Fin Groove.

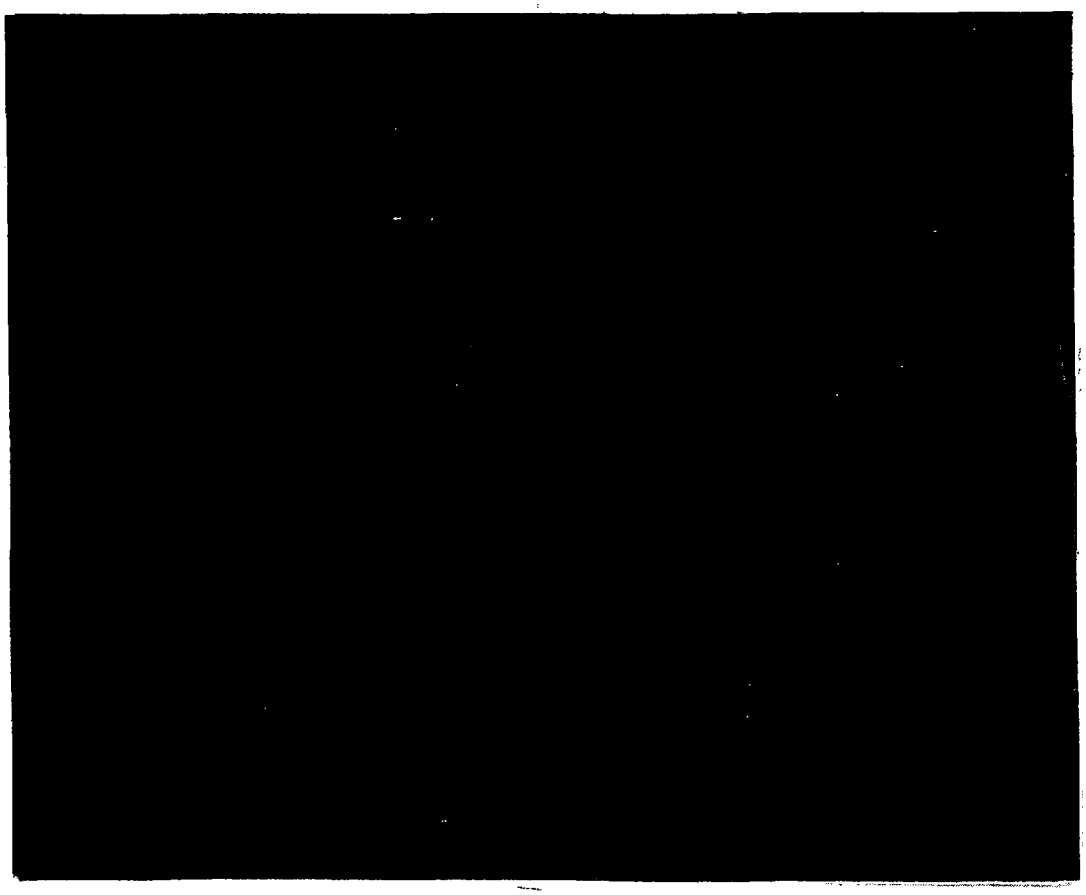

Figure 8. Fracture Surface Adjacent to T-Bar Weld.

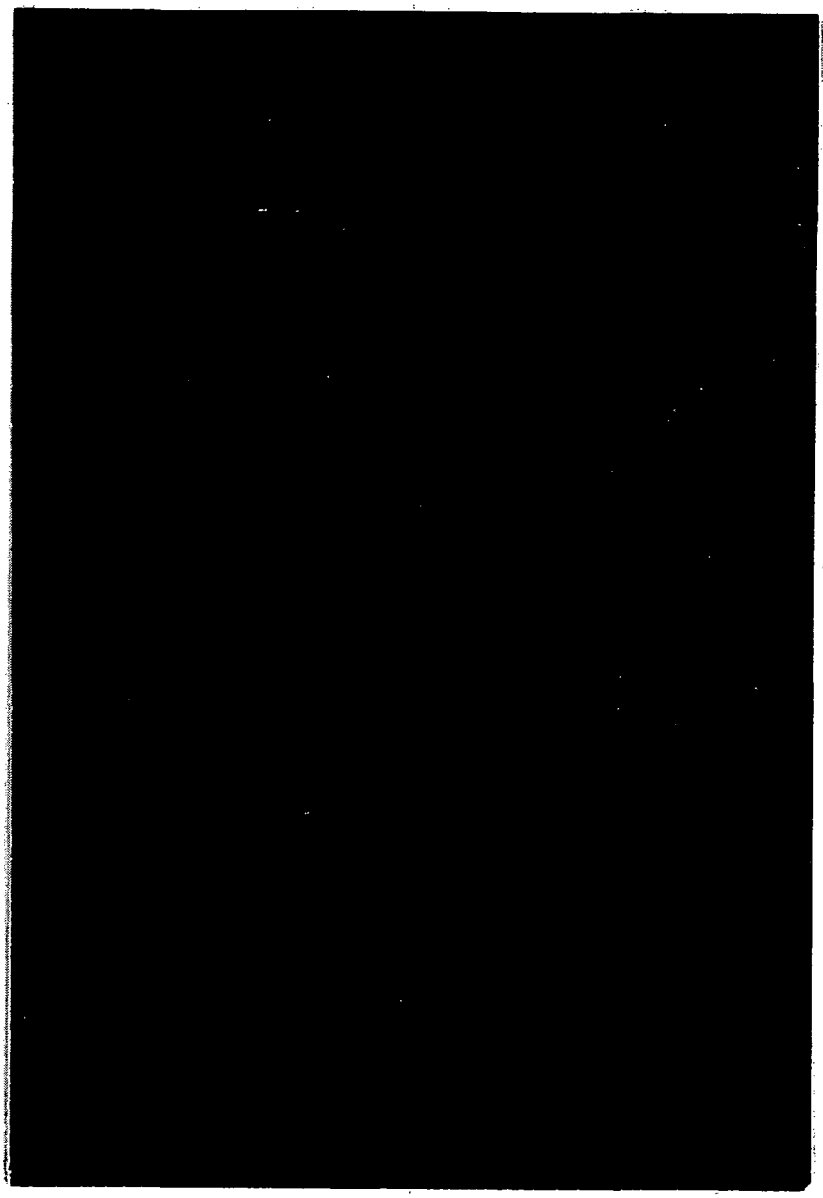

Mag. 50X

Figure 9. Fracture Surface Adjacent to T-Bar Weld.

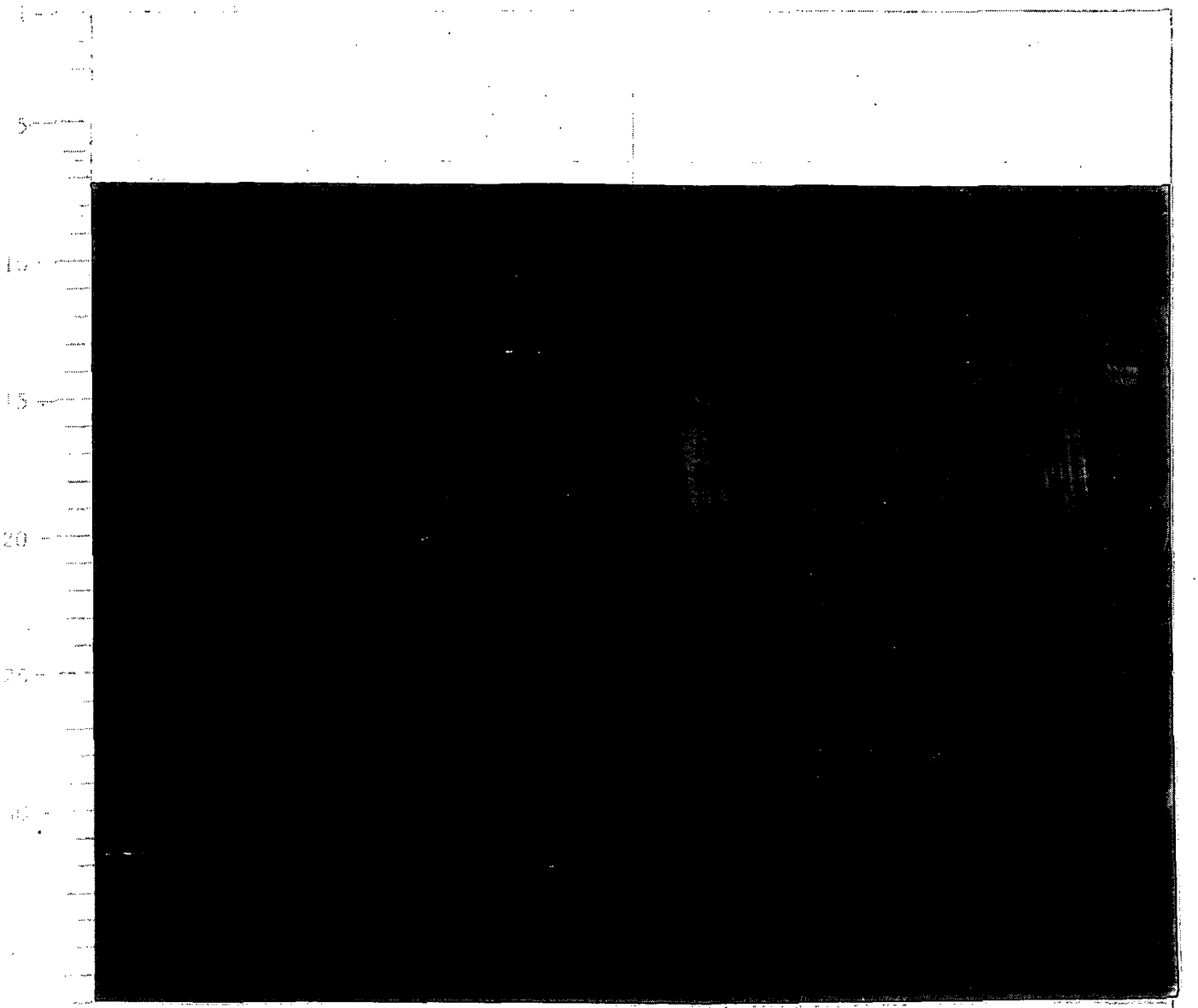

Figure 10. Crack (Arrow) Through a Poor Quality Weld Bead.

"Page missing from available version"

PAGE 66

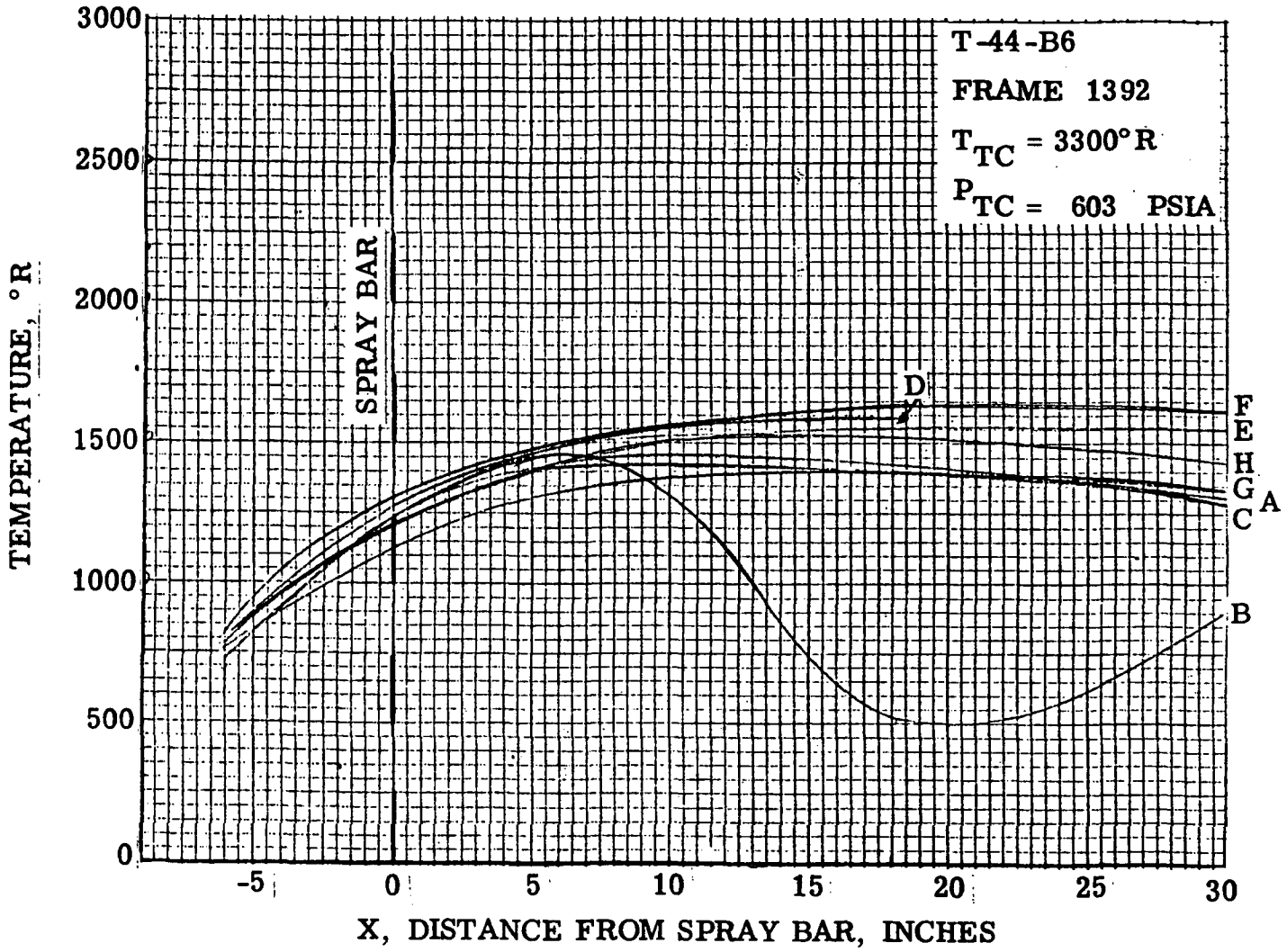

Figure 12. Test Temperatures Distribution at 603 Psia. (NASA Supplied Data)

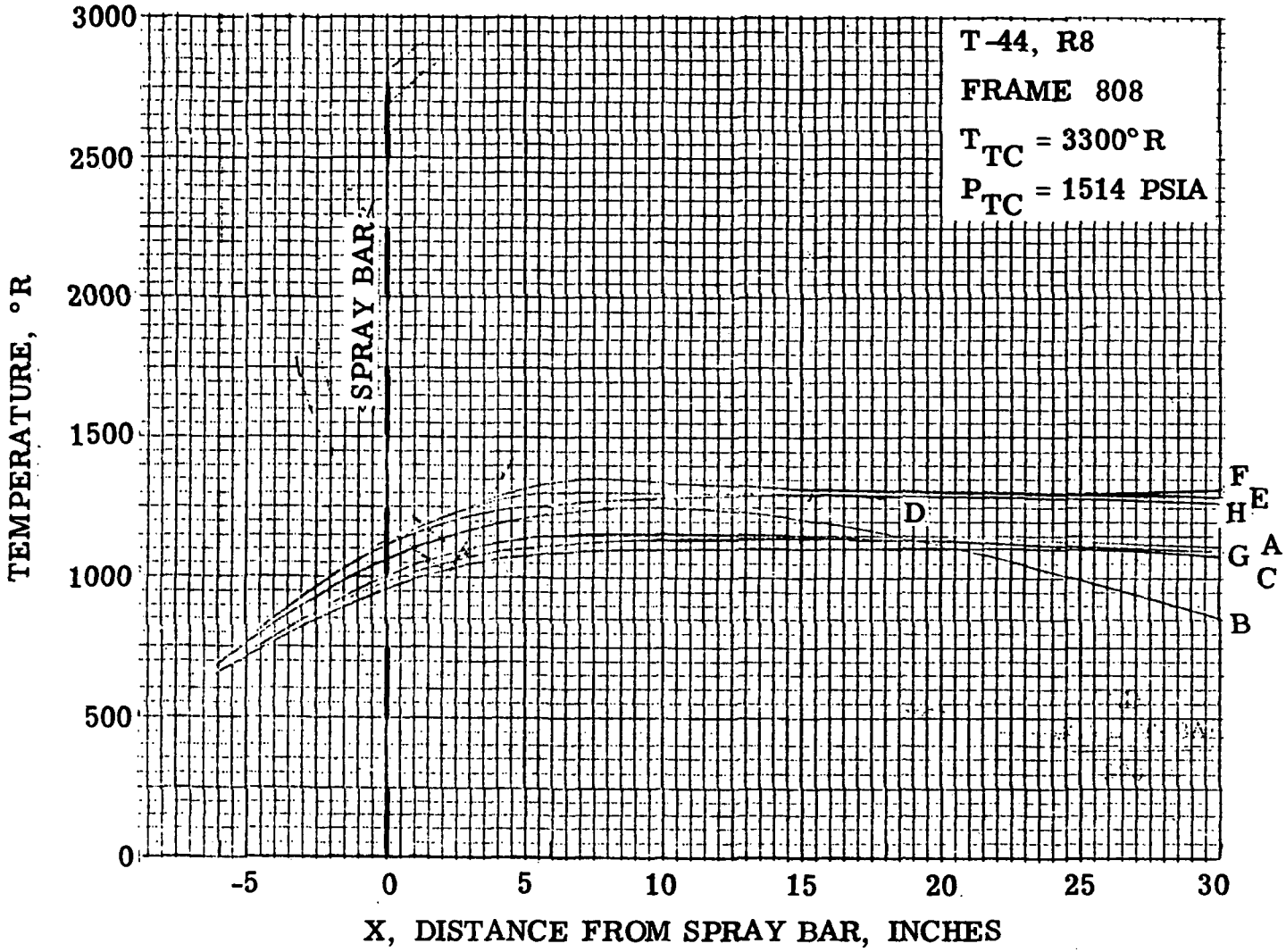

Figure 13. Test Temperatures Distribution at 1514 Psia. (NASA Supplied Data)

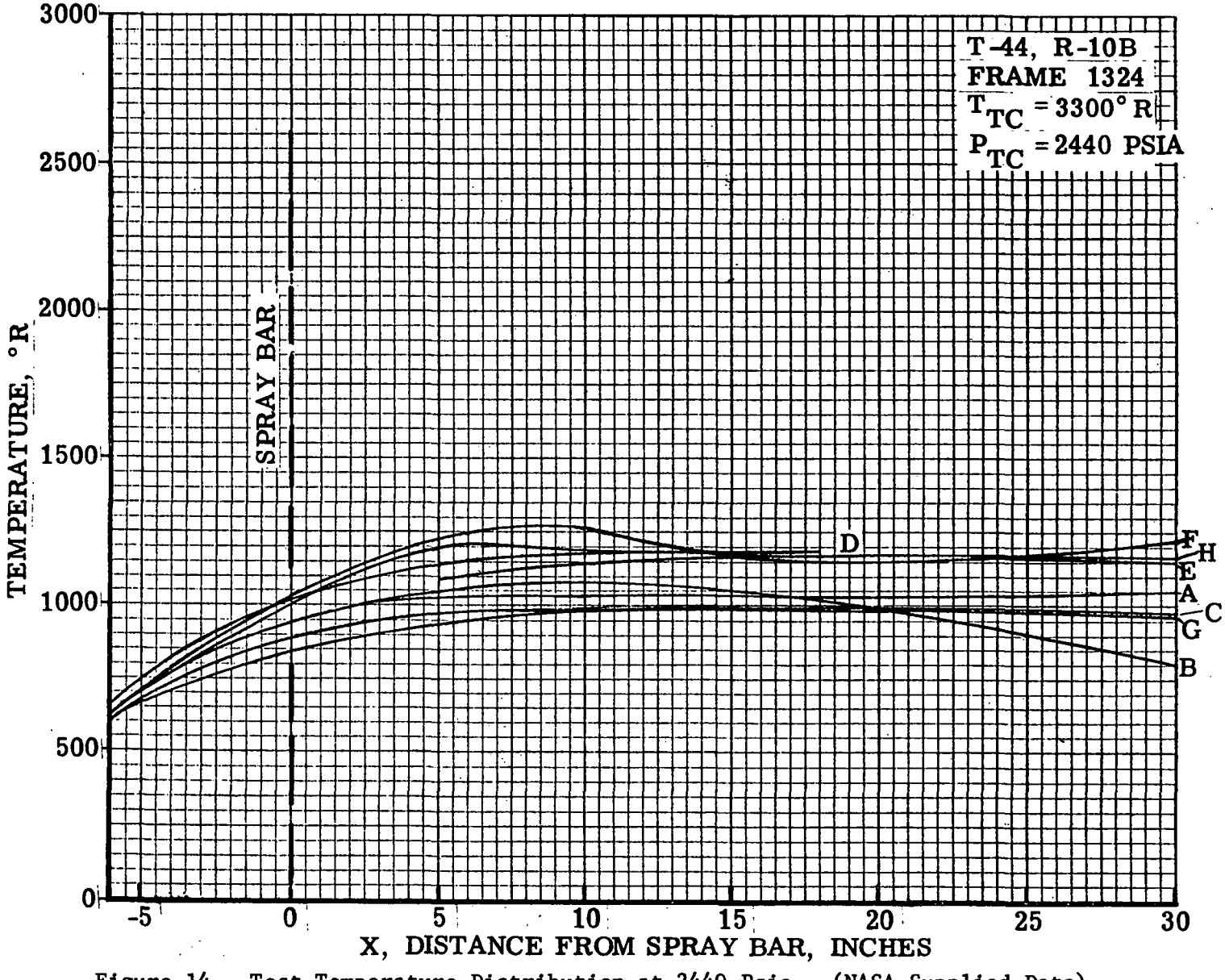

Figure 14. Test Temperature Distribution at 2440 Psia. (NASA Supplied Data)

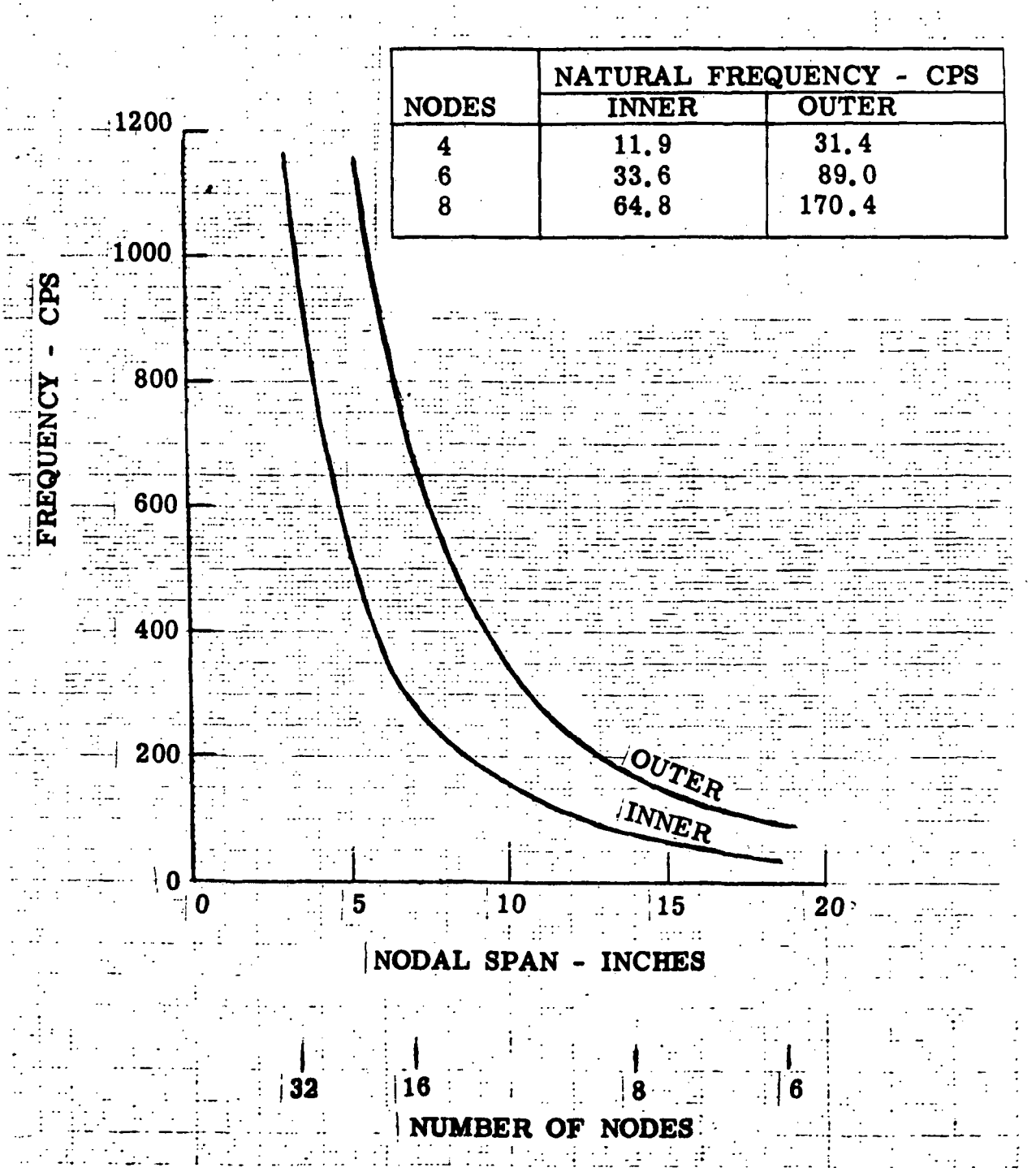

Figure 15. Natural Frequency of Air-Cooled Liners.

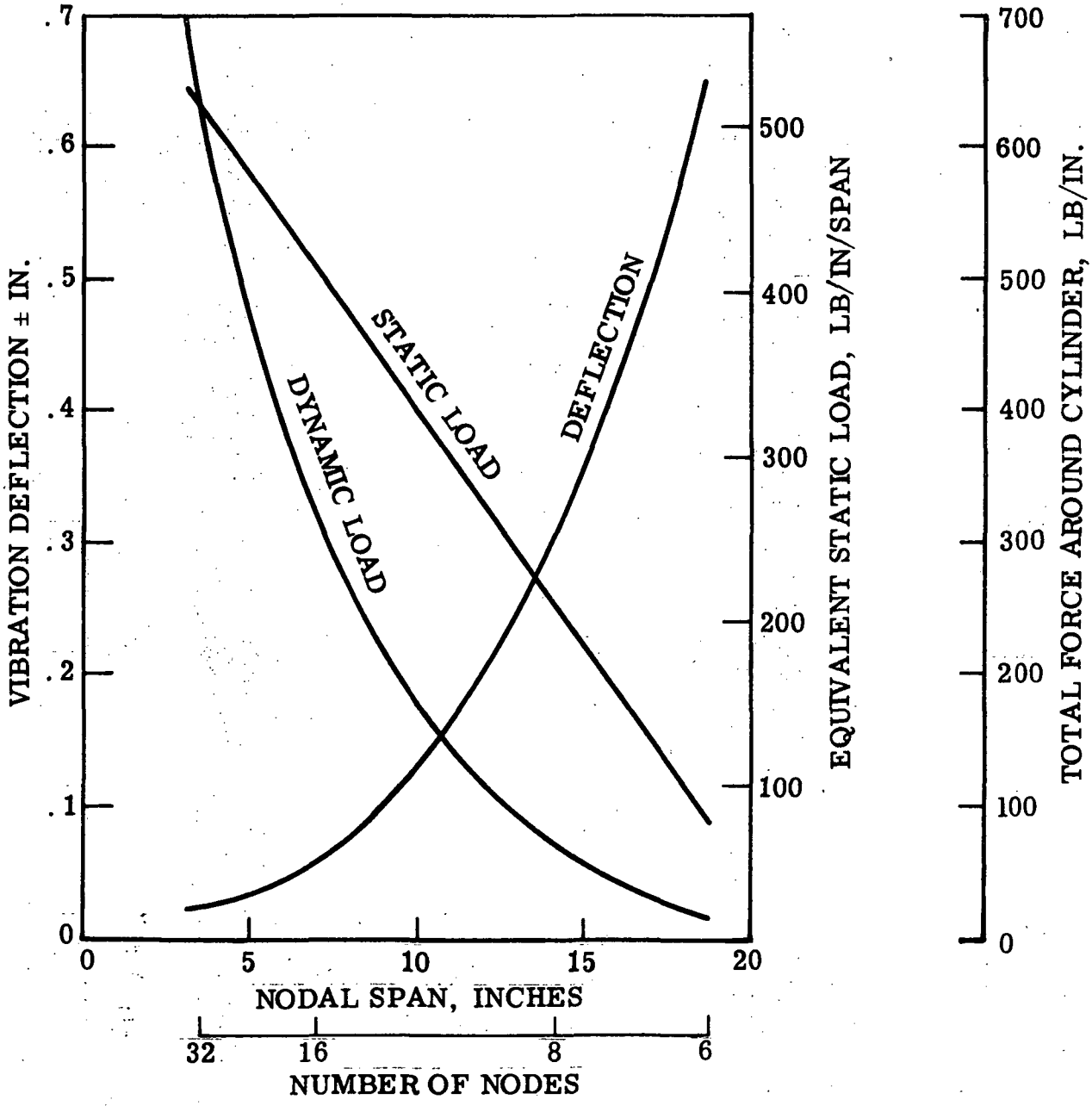

Figure 16. Vibratory Loading of Air-Cooled Liner.

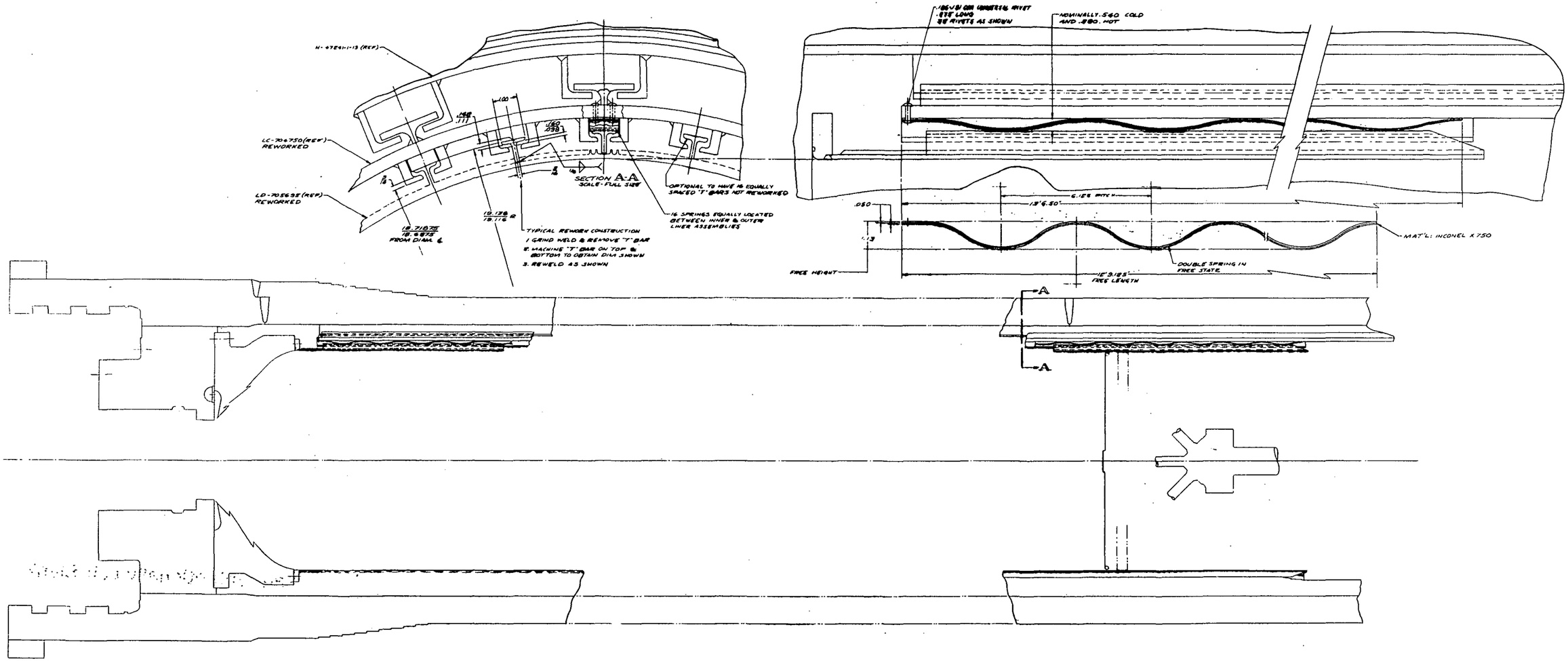

Figure 17. Air-Cooled T-Bar Liner with Wave Spring Vibration Dampers.

Page Intentionally Left Blank

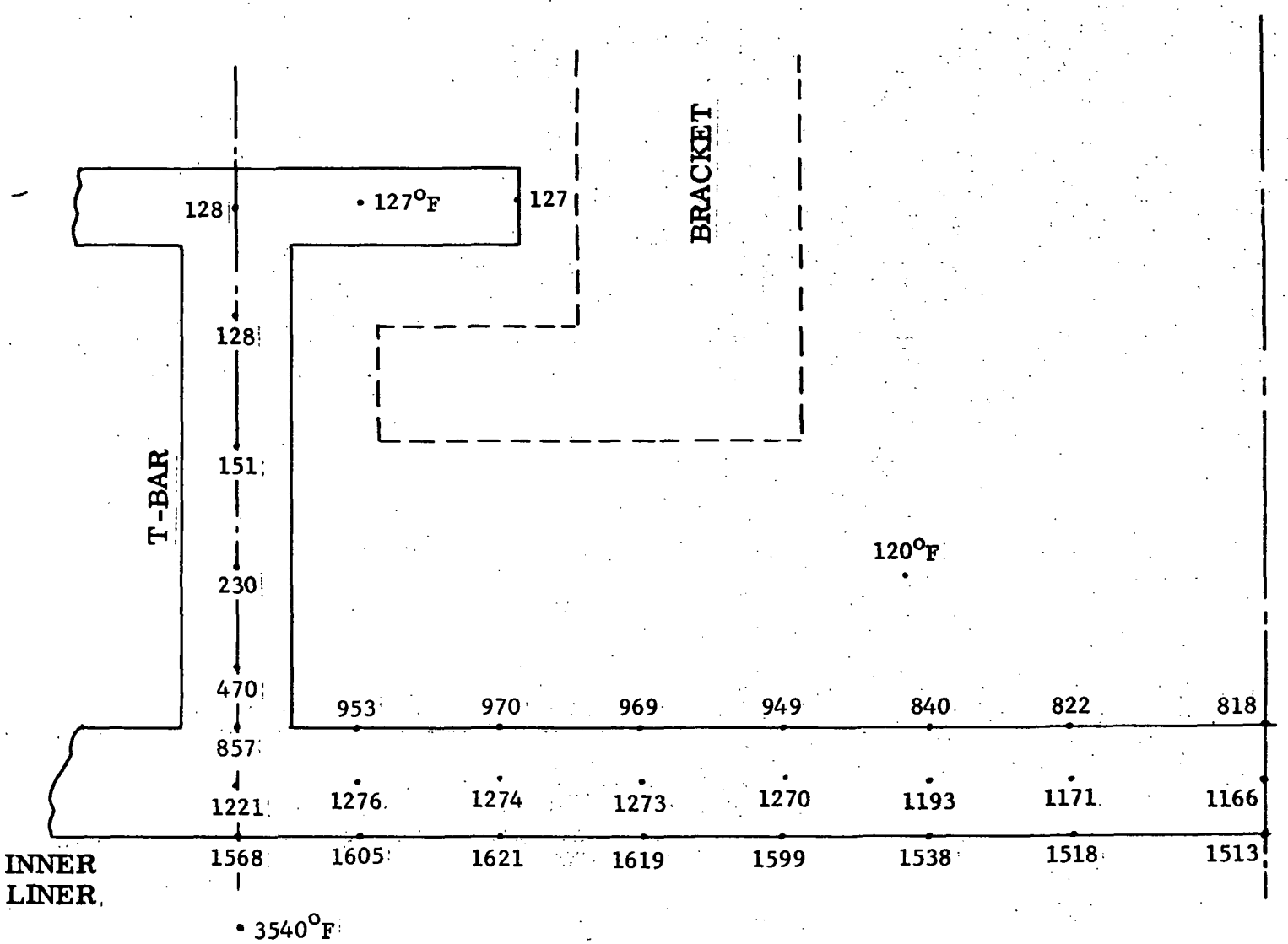

Figure 18. T-Bar Liner Temperature Distribution at 4000 Psia.

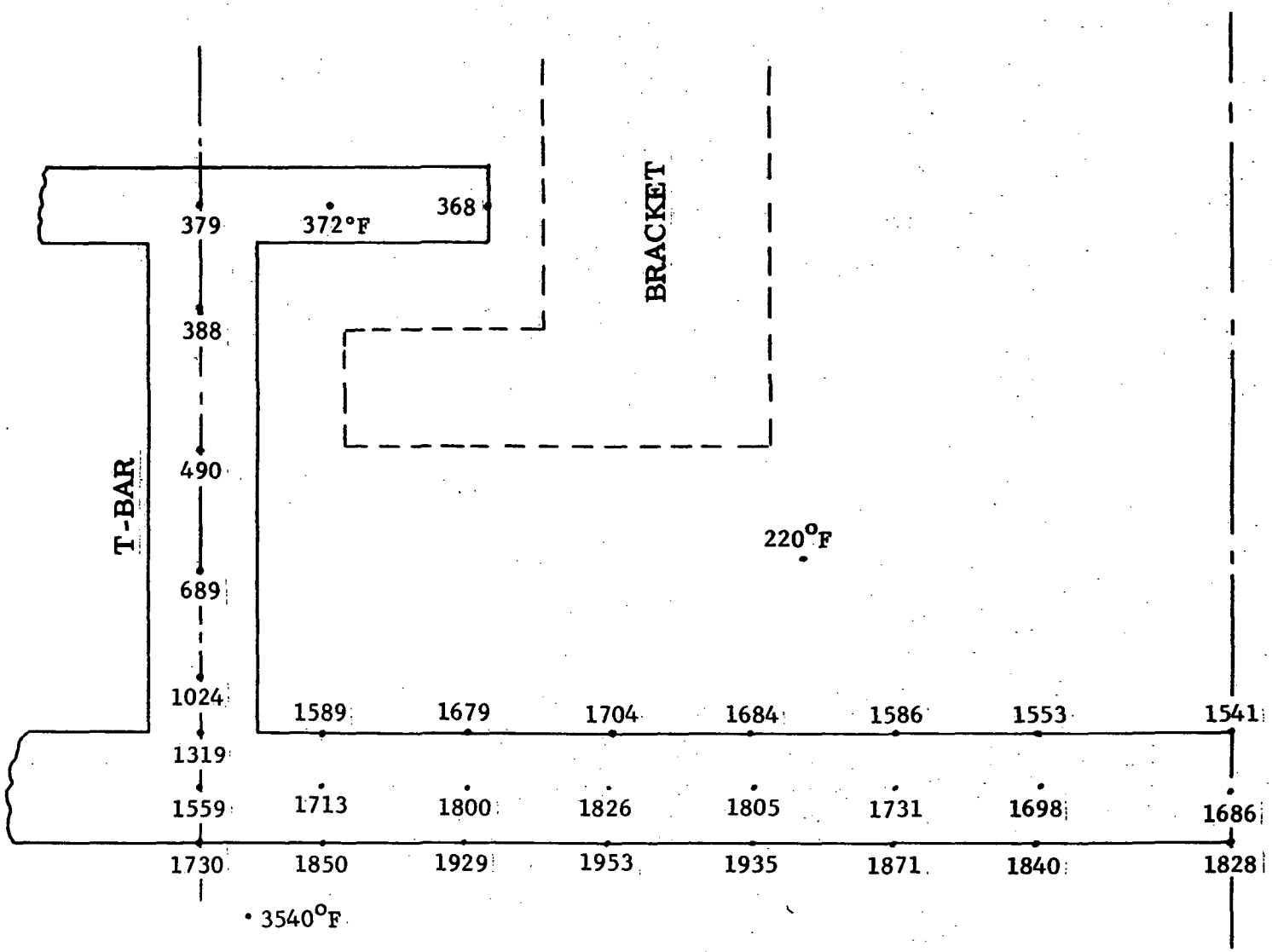

Figure 19. T-Bar Liner Temperature Distribution at 600 Psia.

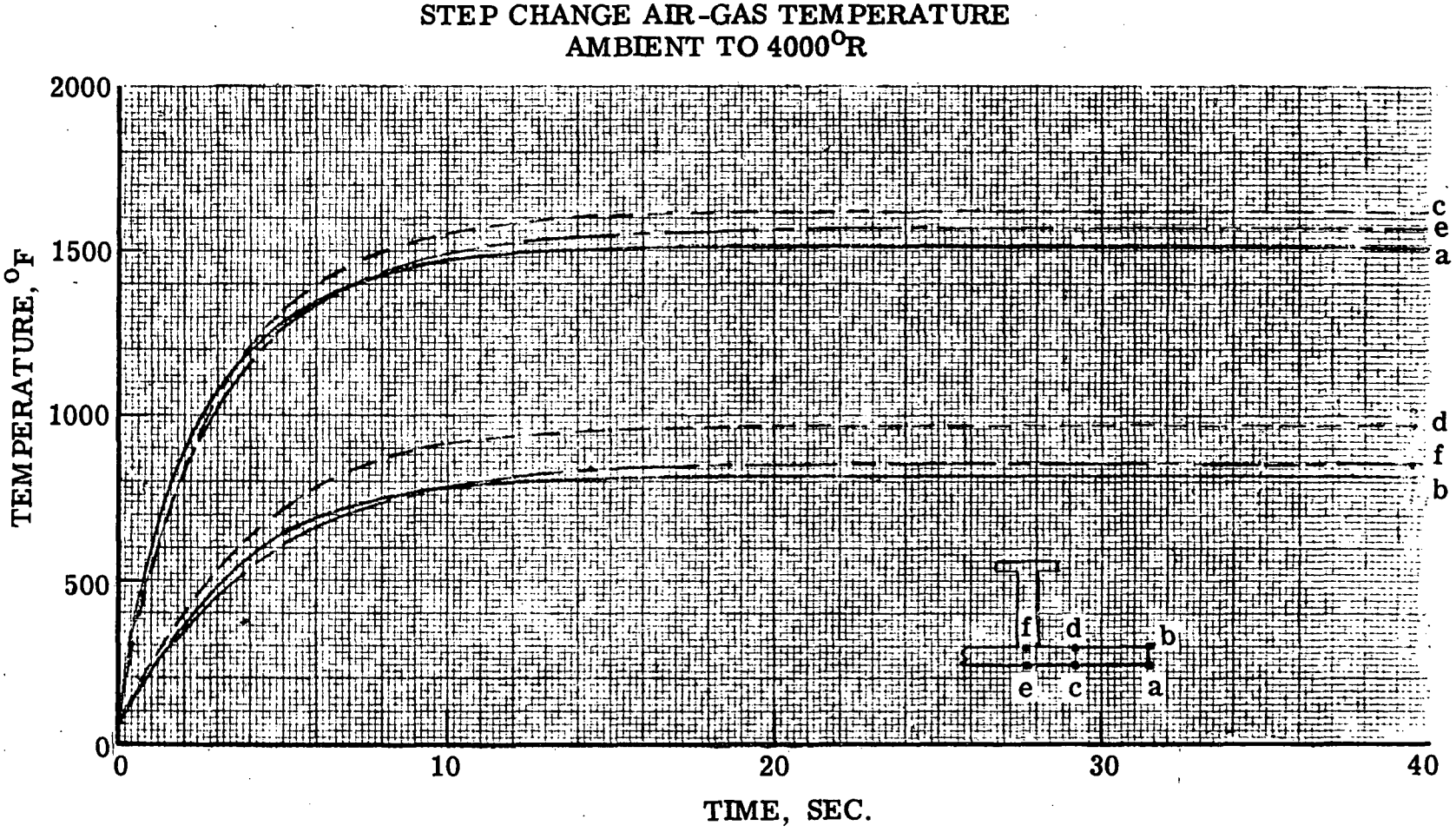

Figure 20. T-Bar Liner Transient Temperatures at 4000 psia.

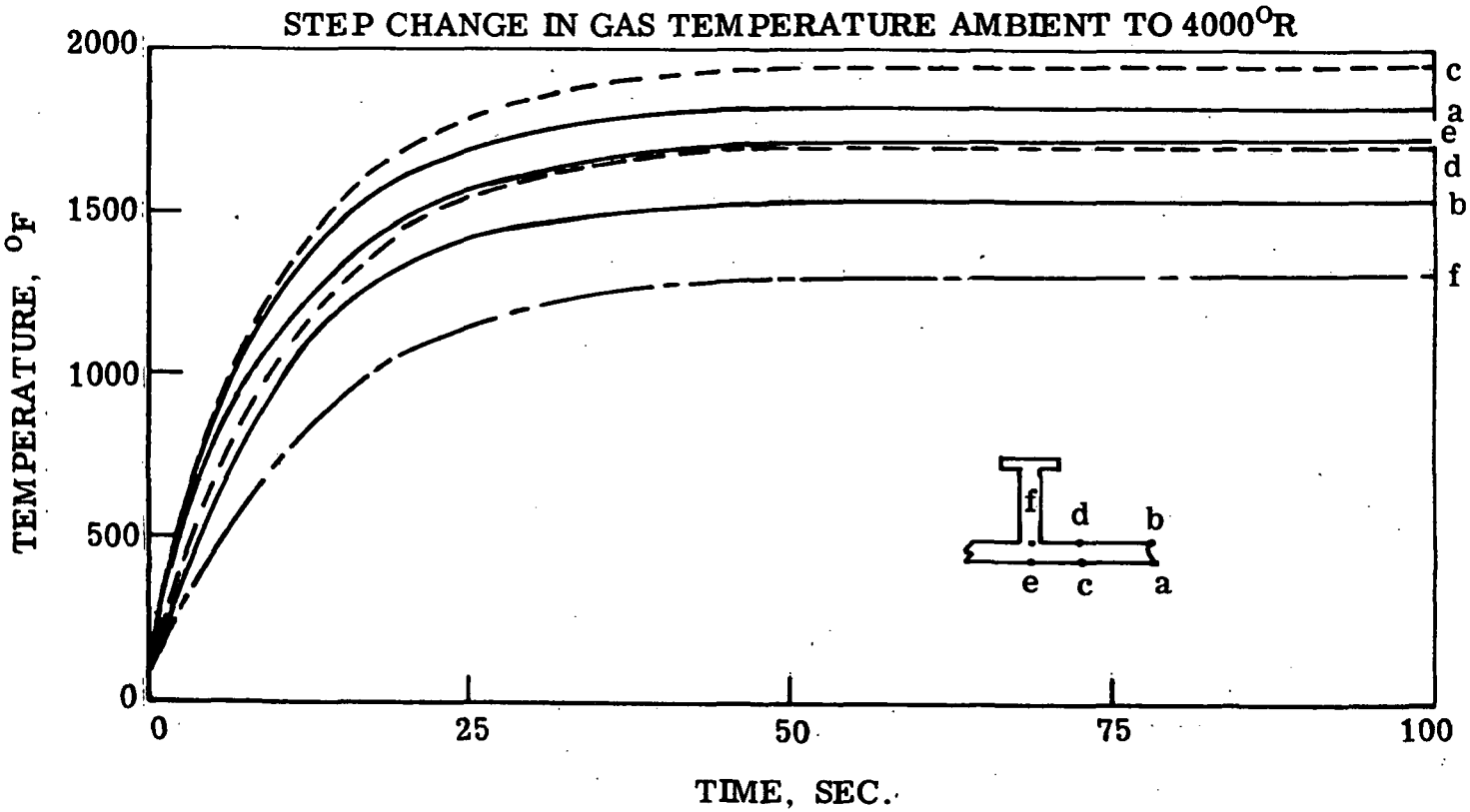

Figure 21. T-Bar Liner Transient Temperatures at 600 psia.

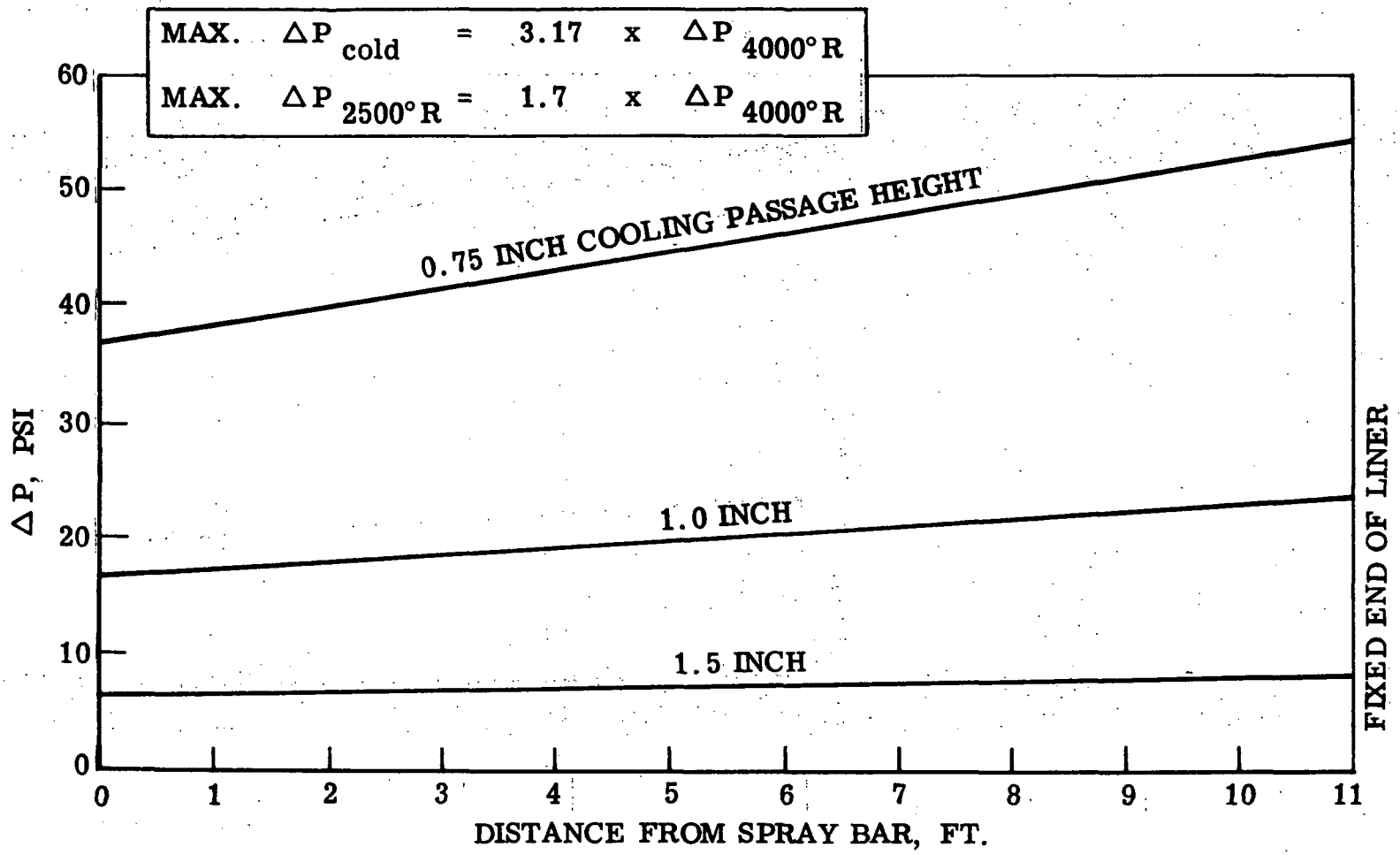

Figure 22. Effect of Cooling Passage Height on Pressure Differential Across the Liner at 4000 psia and 4000 ^{o}R

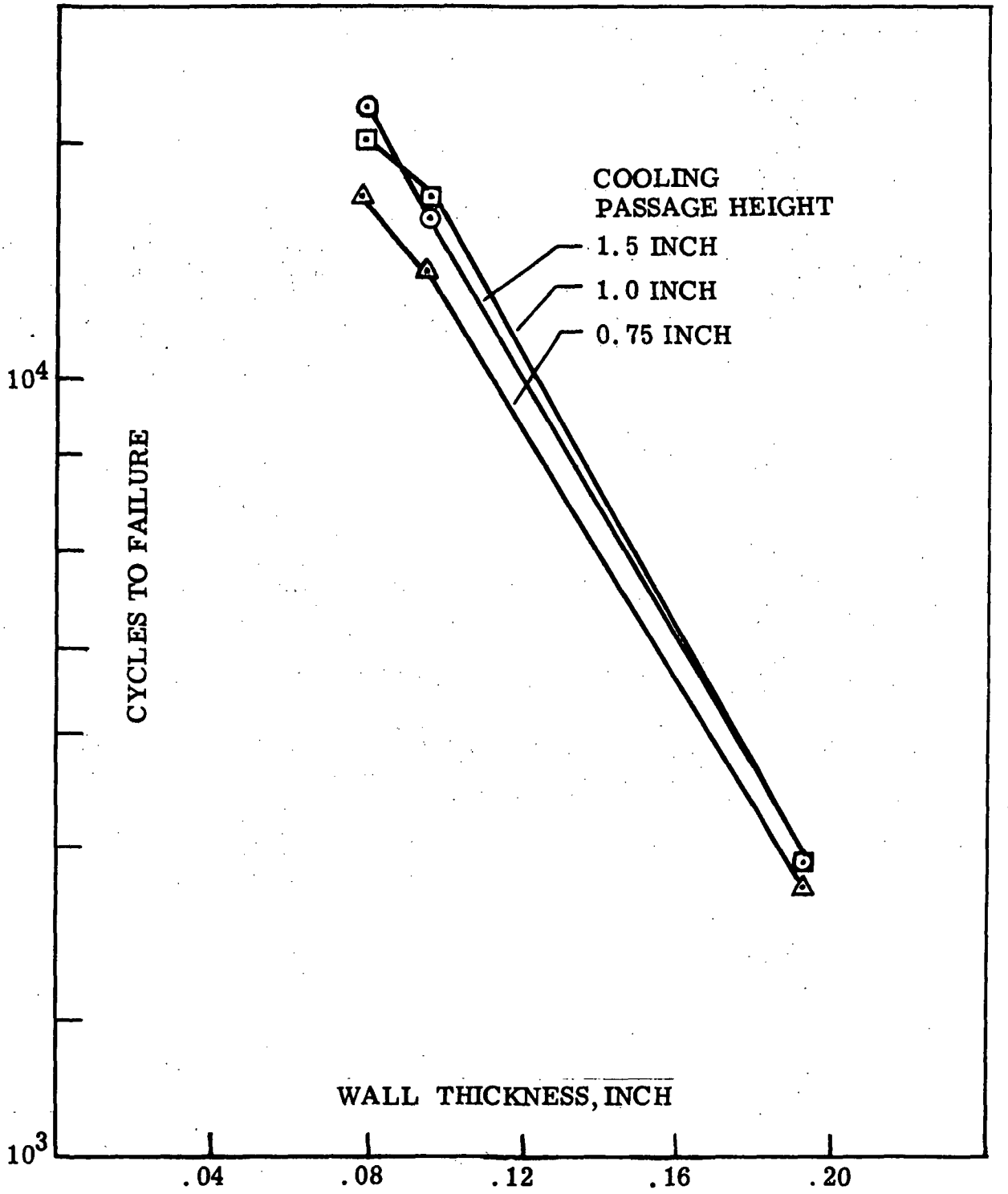

Figure 23. Effect of Air-Cooled Liner Wall Thickness on Low Cycle Fatigue.

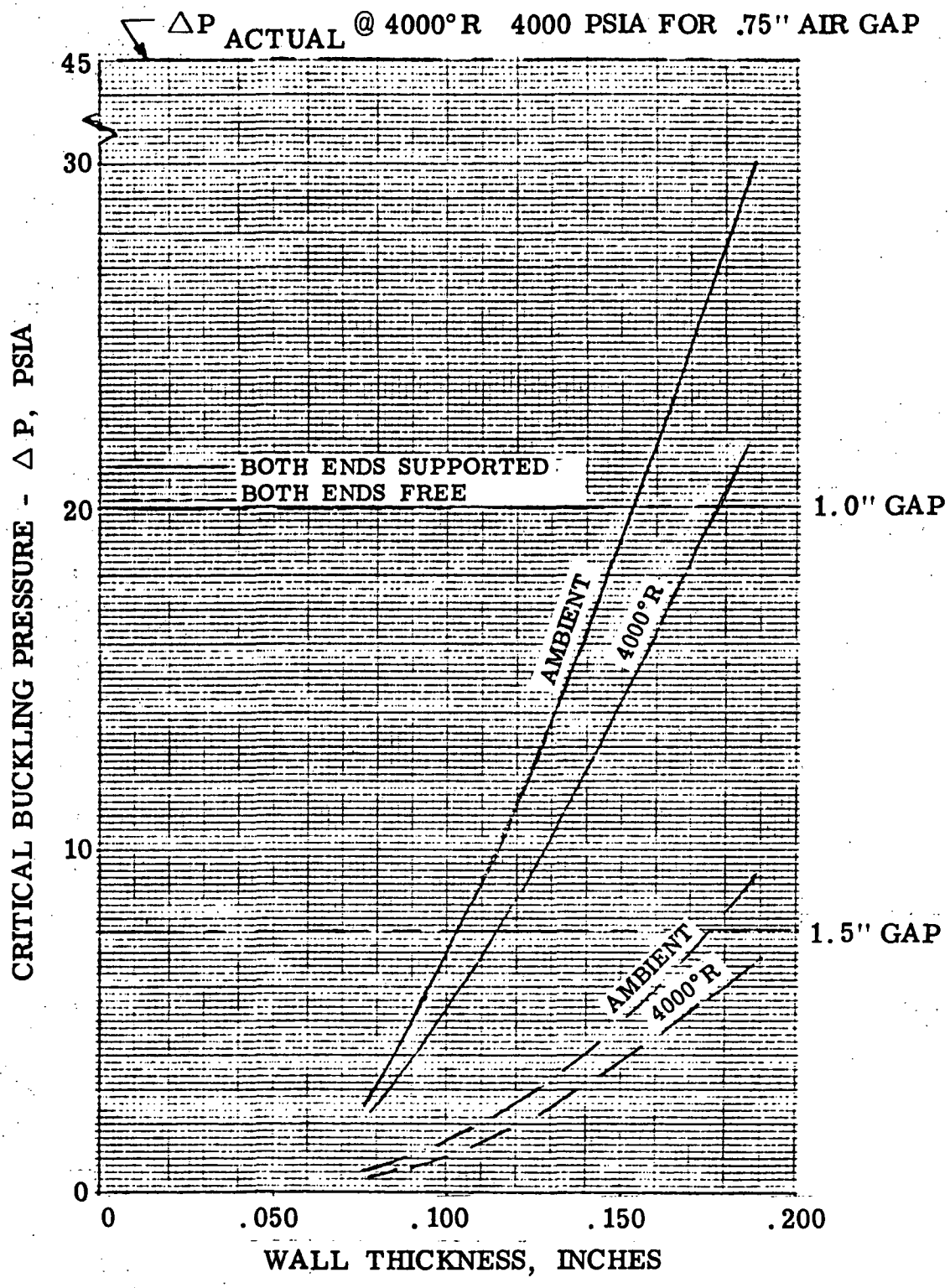

Figure 24. Comparison of Critical Buckling Pressure.

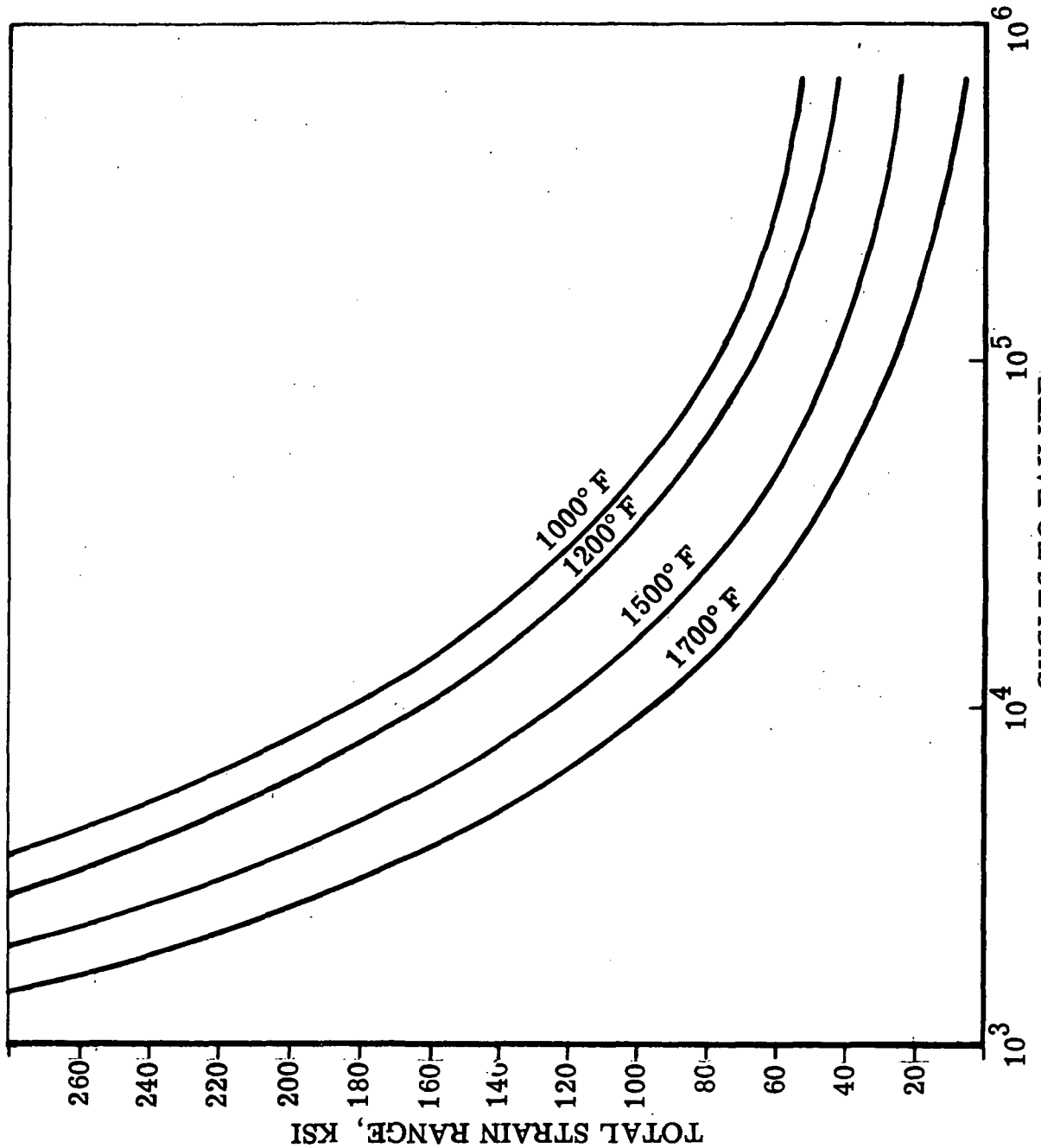

Figure 25. Low Cycle Fatigue Life of Inconel 600.

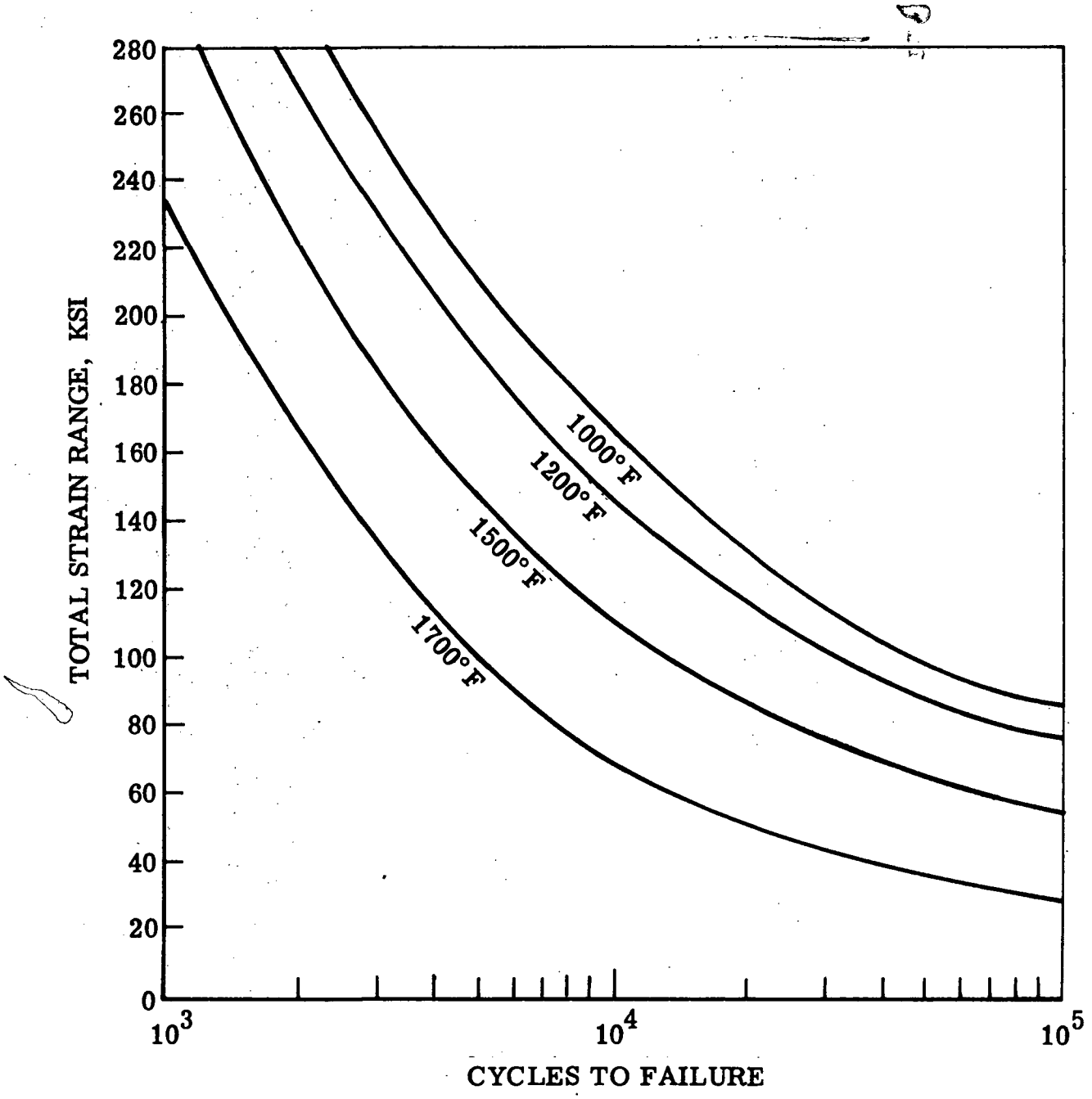

Figure 26. Low Cycle Fatigue Life of Hastelloy X.

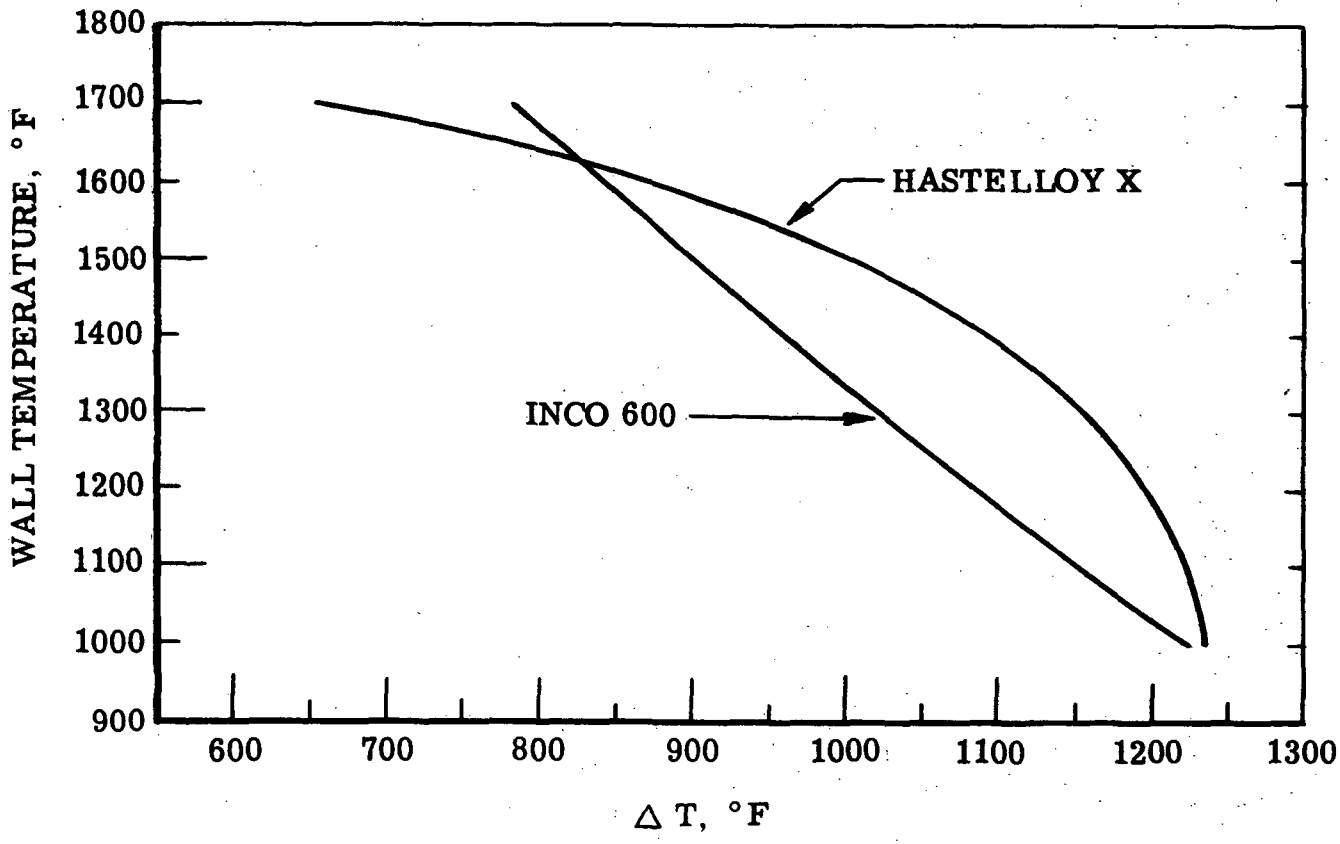

Figure 27. Liner Materials Comparison of Thermal Conditions for 1500 Cycles.

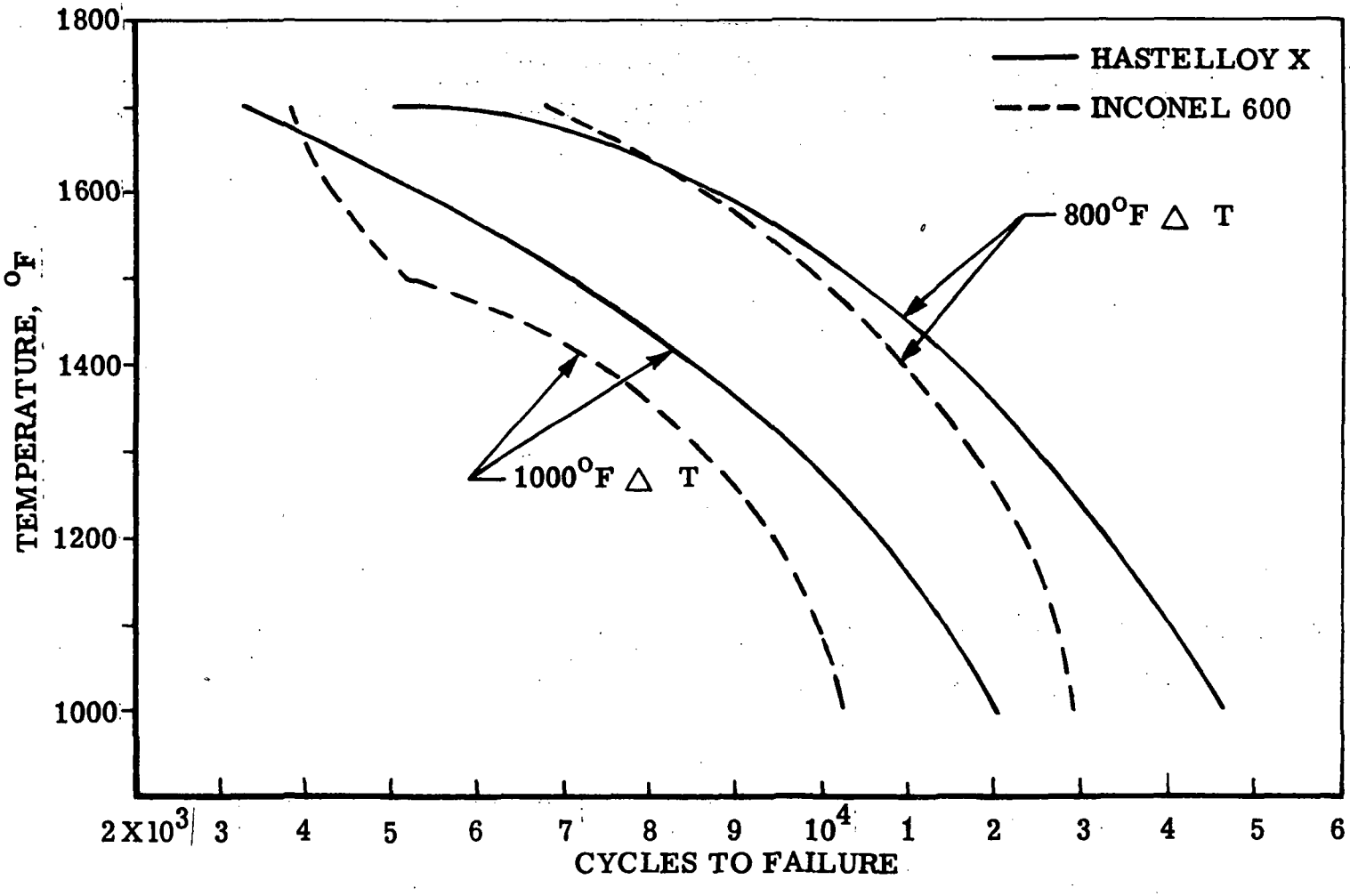

Figure 28. Comparison of Low Cycle Fatigue Life for Two Materials

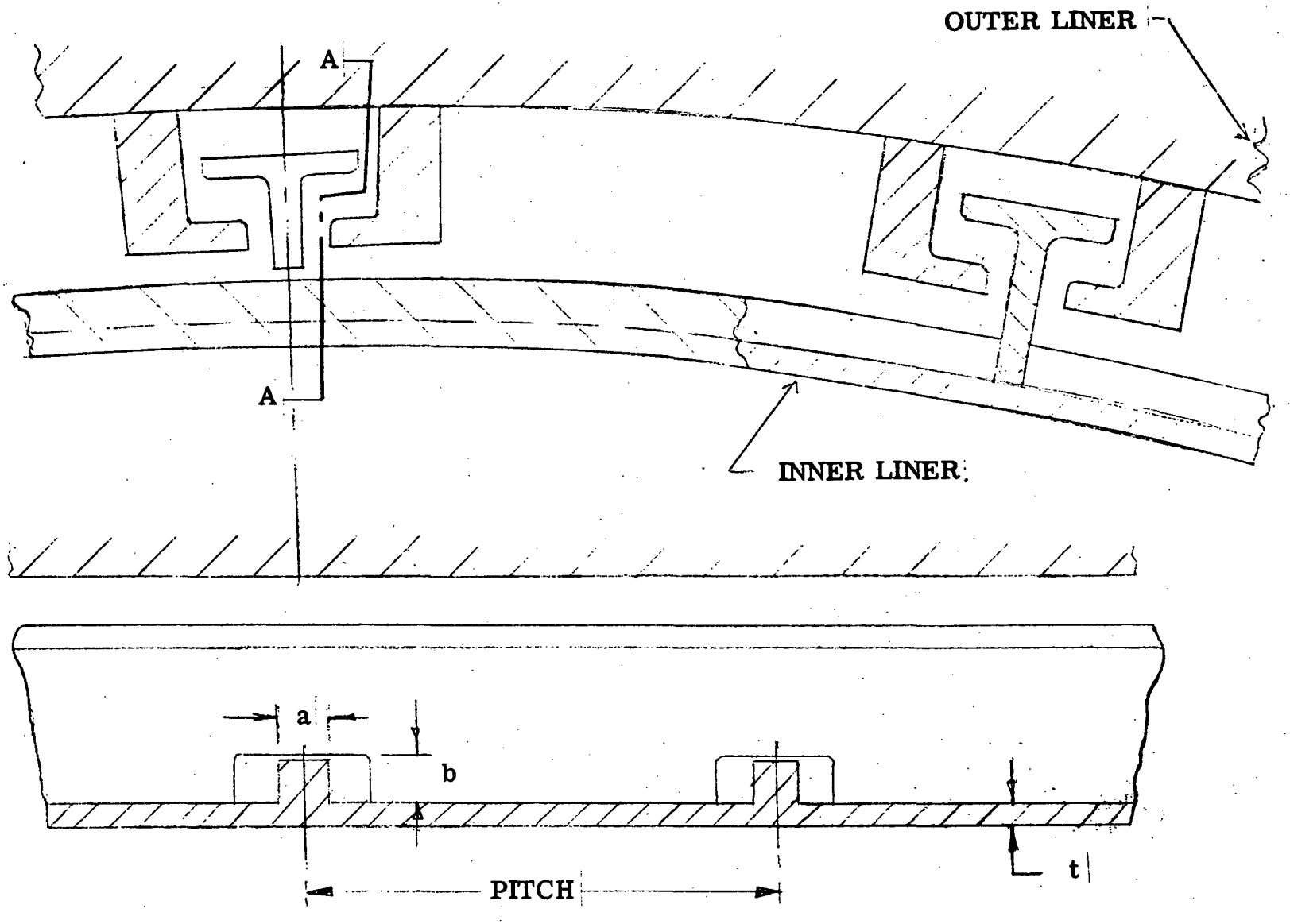

Figure 29. Air-Cooled Ring Stiffened Liner.

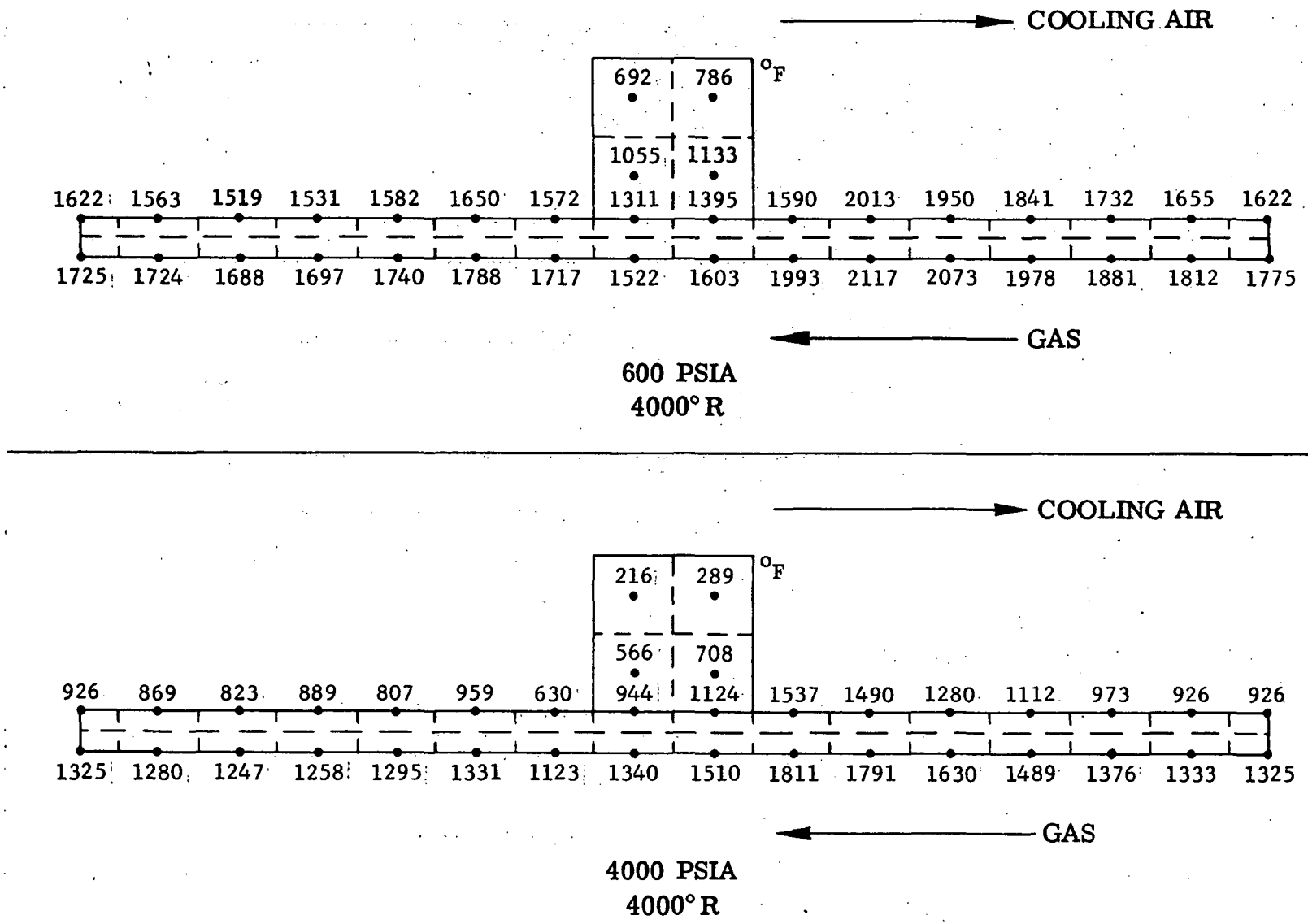

Figure 30. Air-Cooled Ring Stiffened Liner Temperature Distribution at 600 psia and 4000 psia.

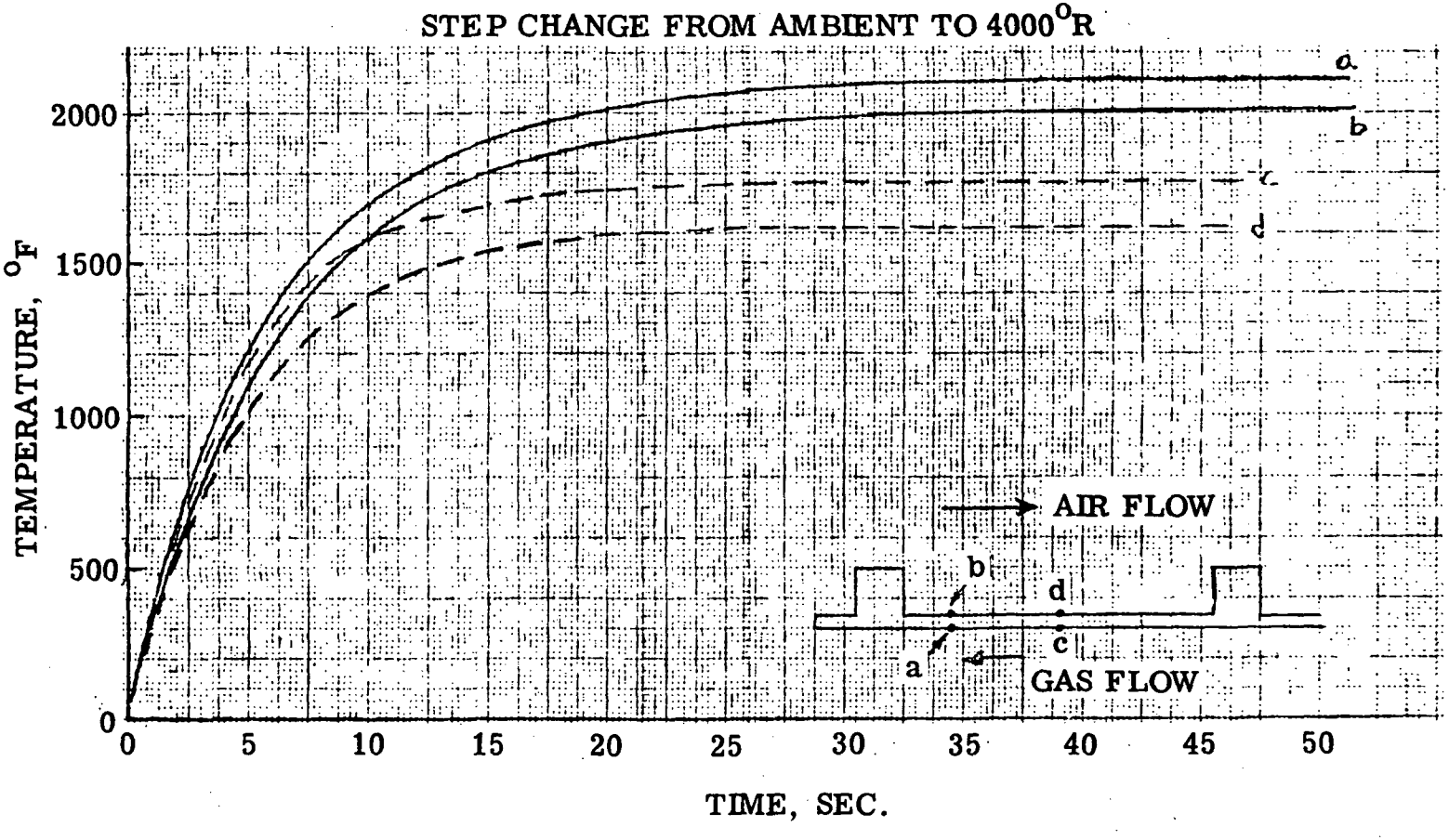

Figure 31. Air-Cooled Ribbed Liner Transient Temperatures at 600 psia.

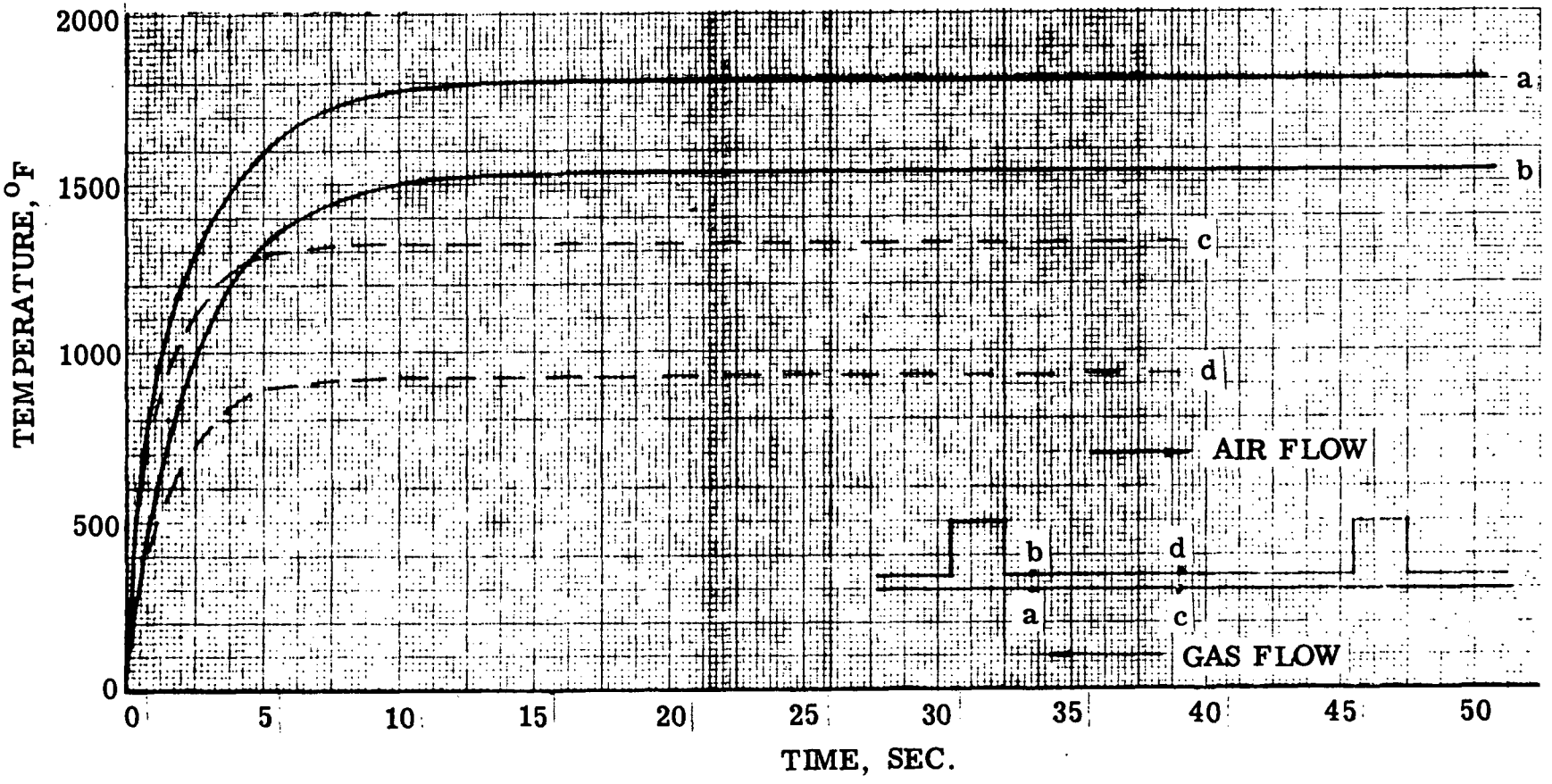

Figure 32. Air-Cooled Ribbed Liner Transient Temperatures at 4000 psia.

Page Intentionally Left Blank

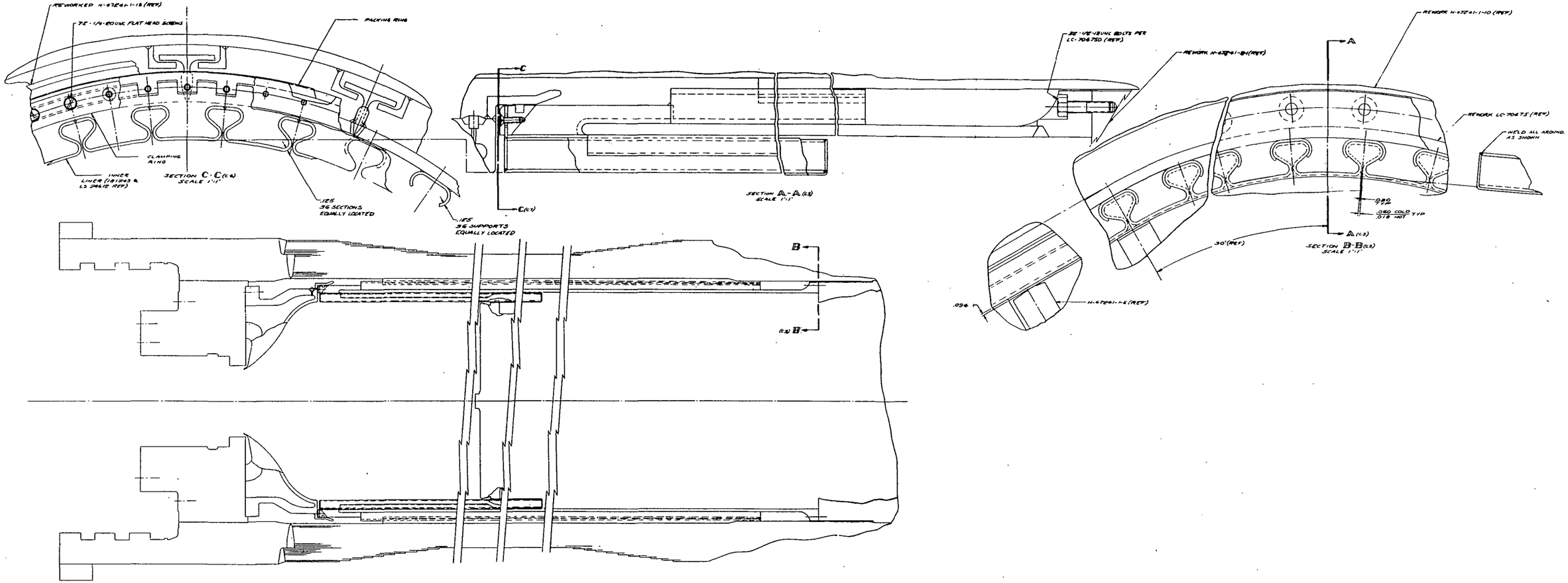

Figure 33. Air-Cooled Omega Segmented Liner

"Page missing from available version"

page 92 missing

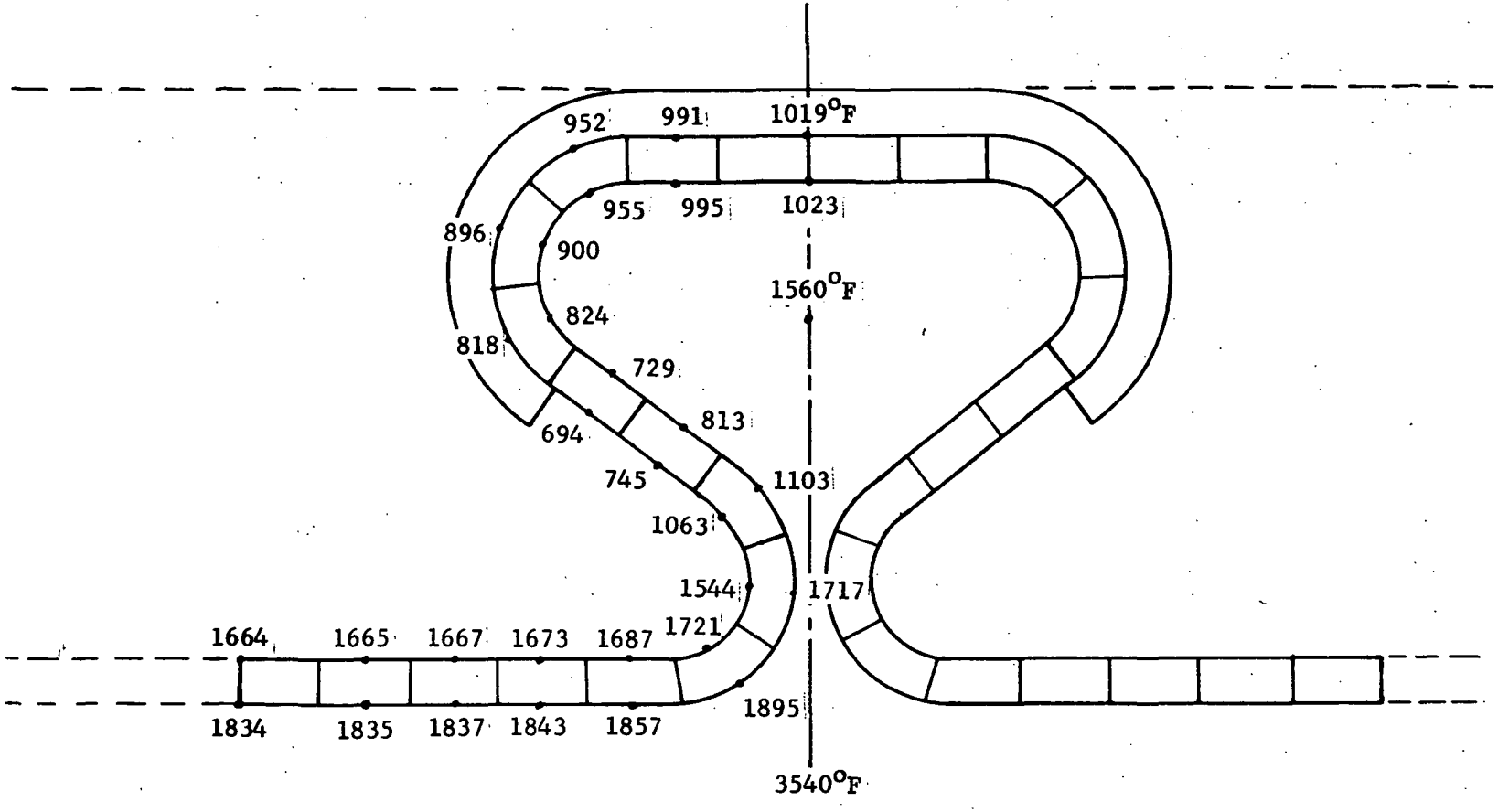

Figure 34. Omega Liner Temperature Distribution at 600 psia.

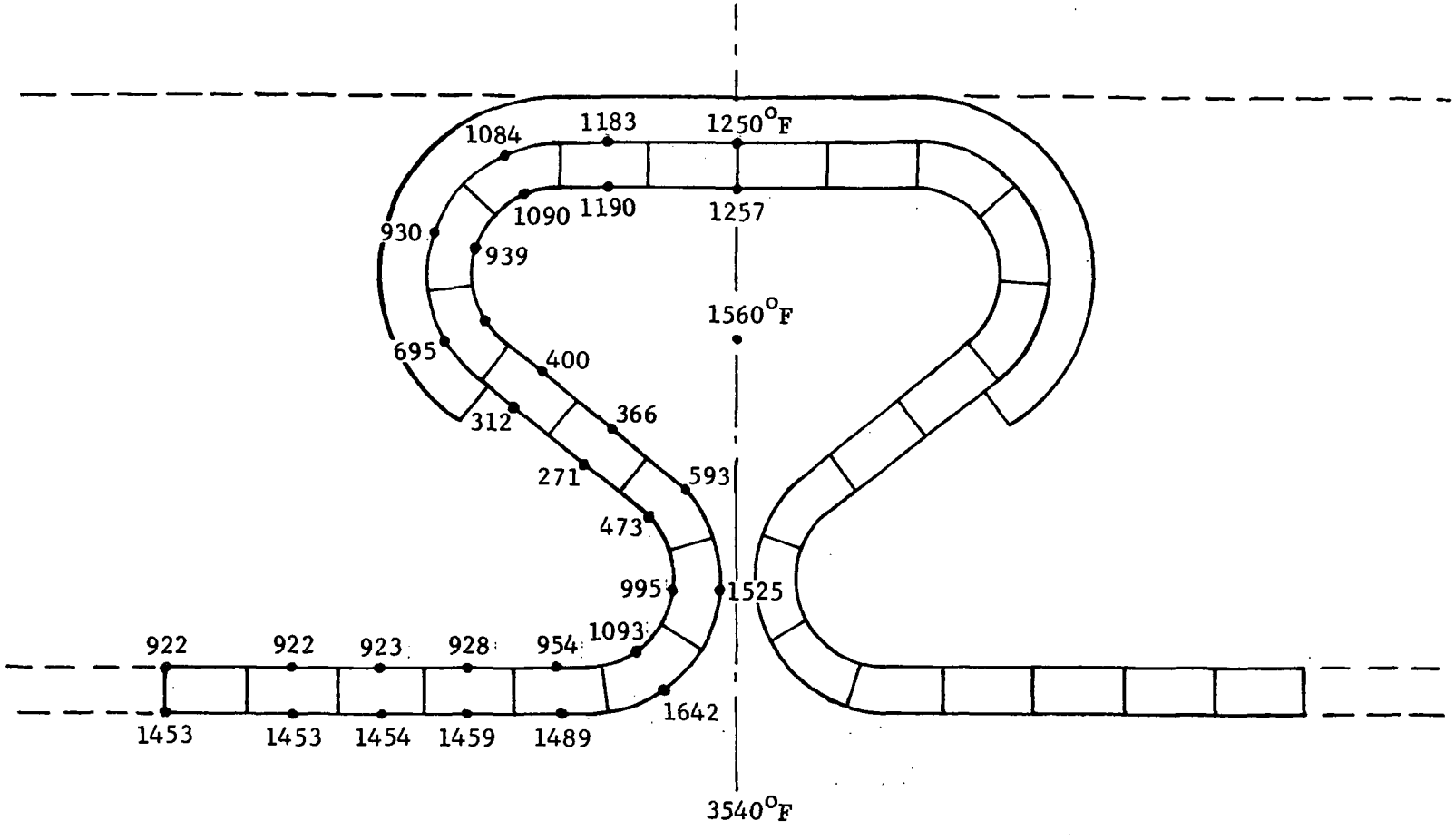

Figure 35. Omega Liner Temperature Distribution at 4000 psia.

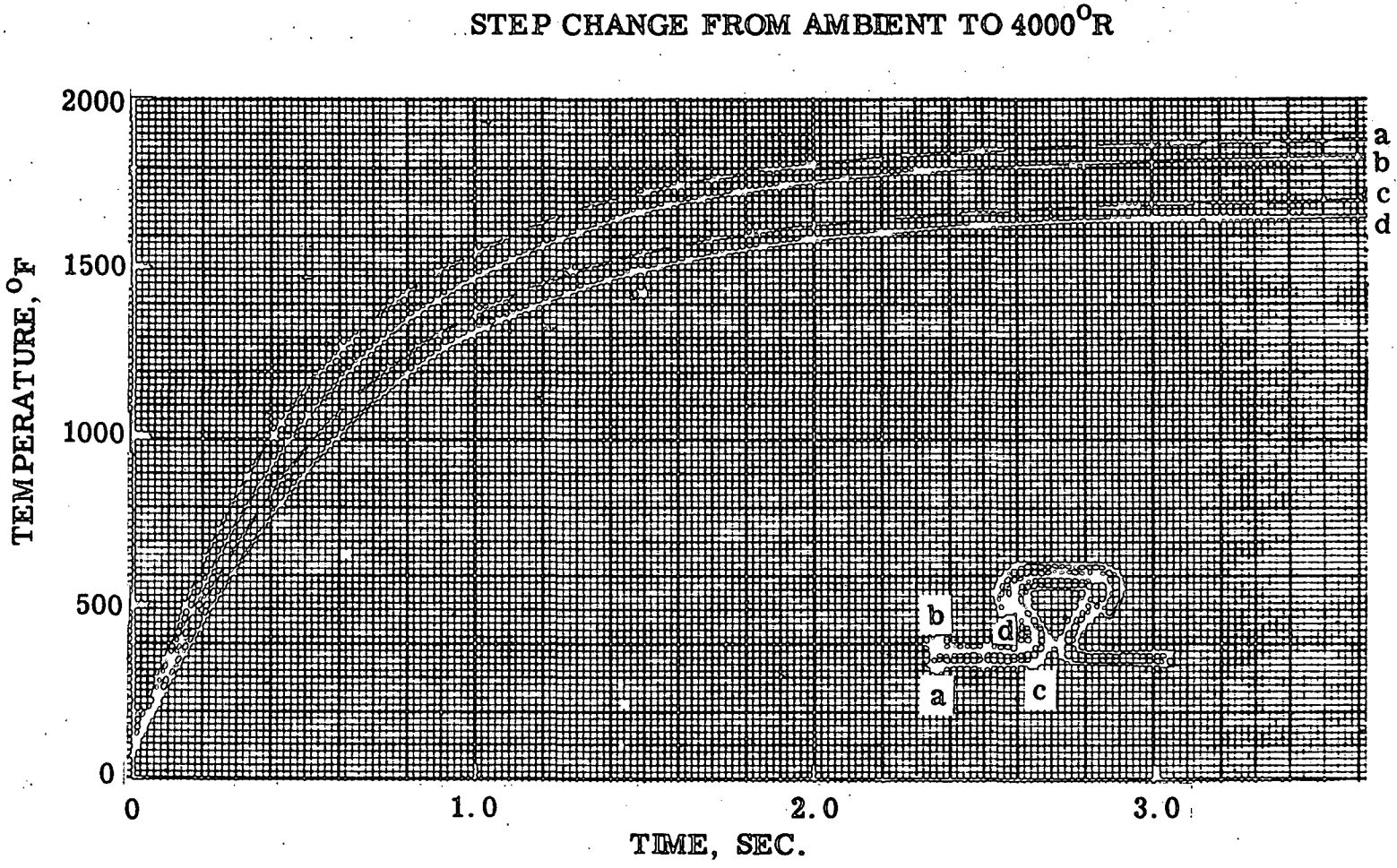

Figure 36. Omega Liner Transient Temperatures at 600 psia.

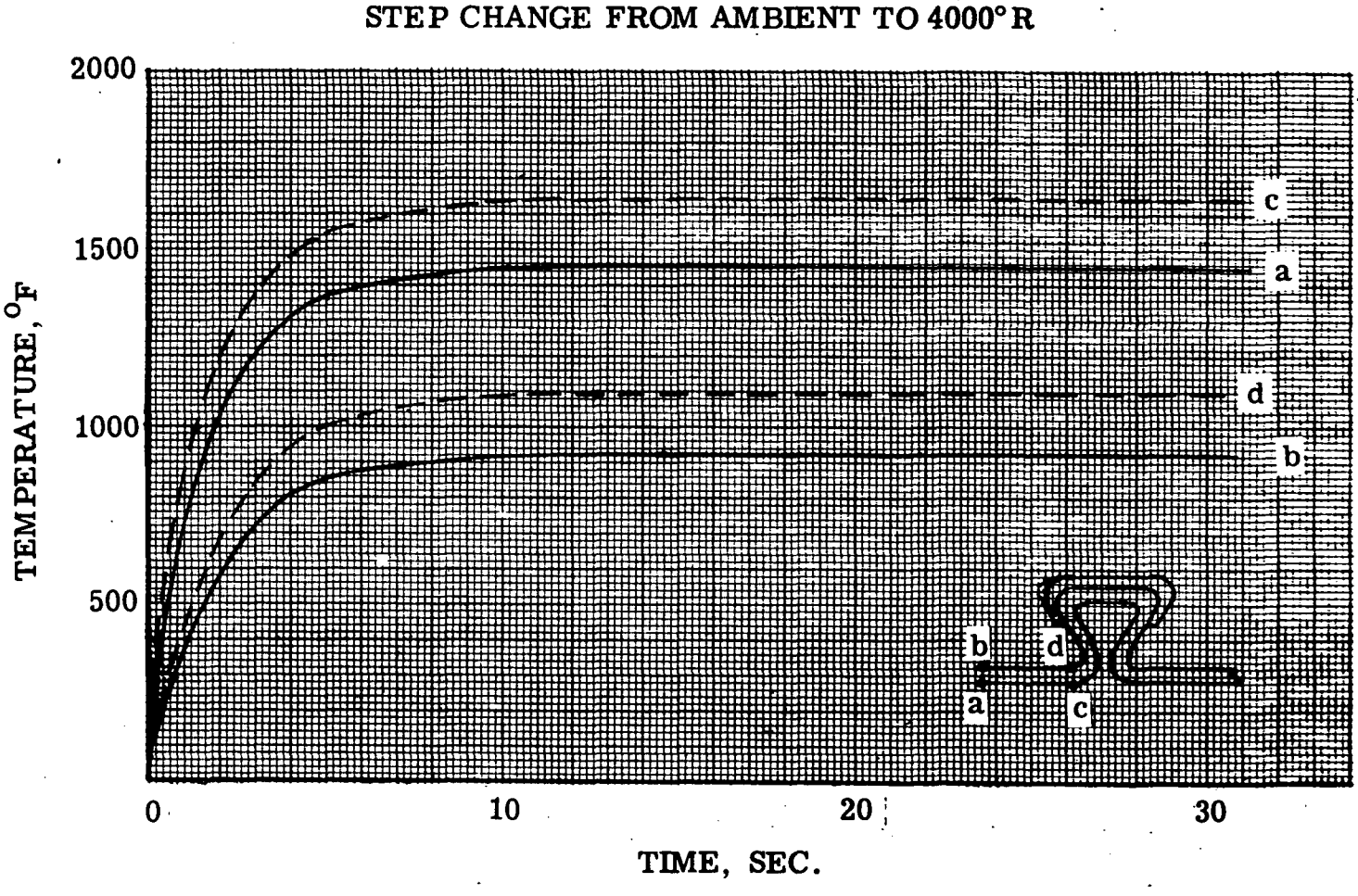

Figure 37. Omega Liner Transient Temperatures at 4000 psia.

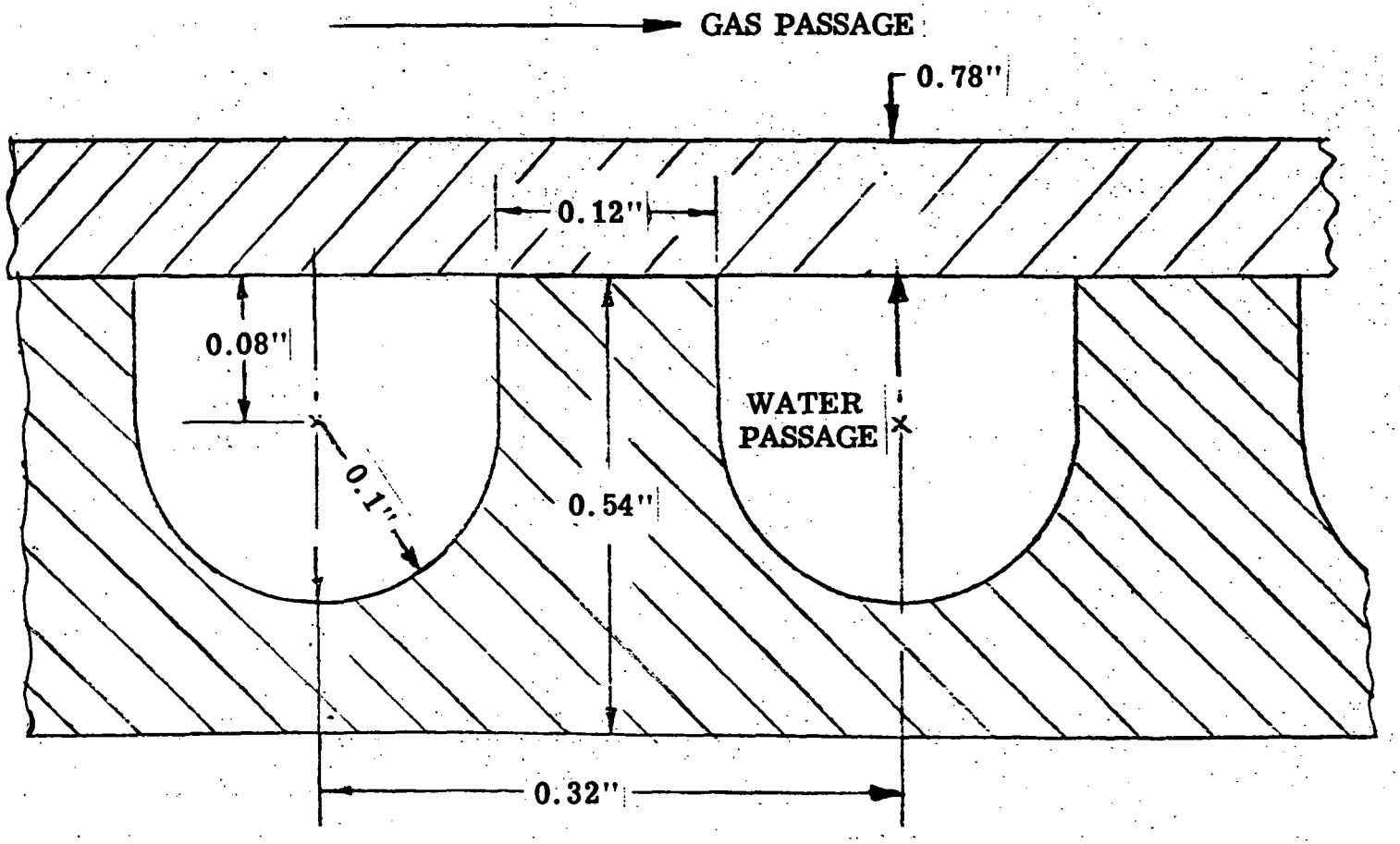

Figure 38. Dimensions of Water-Cooled Liner with Grooved Jacket.

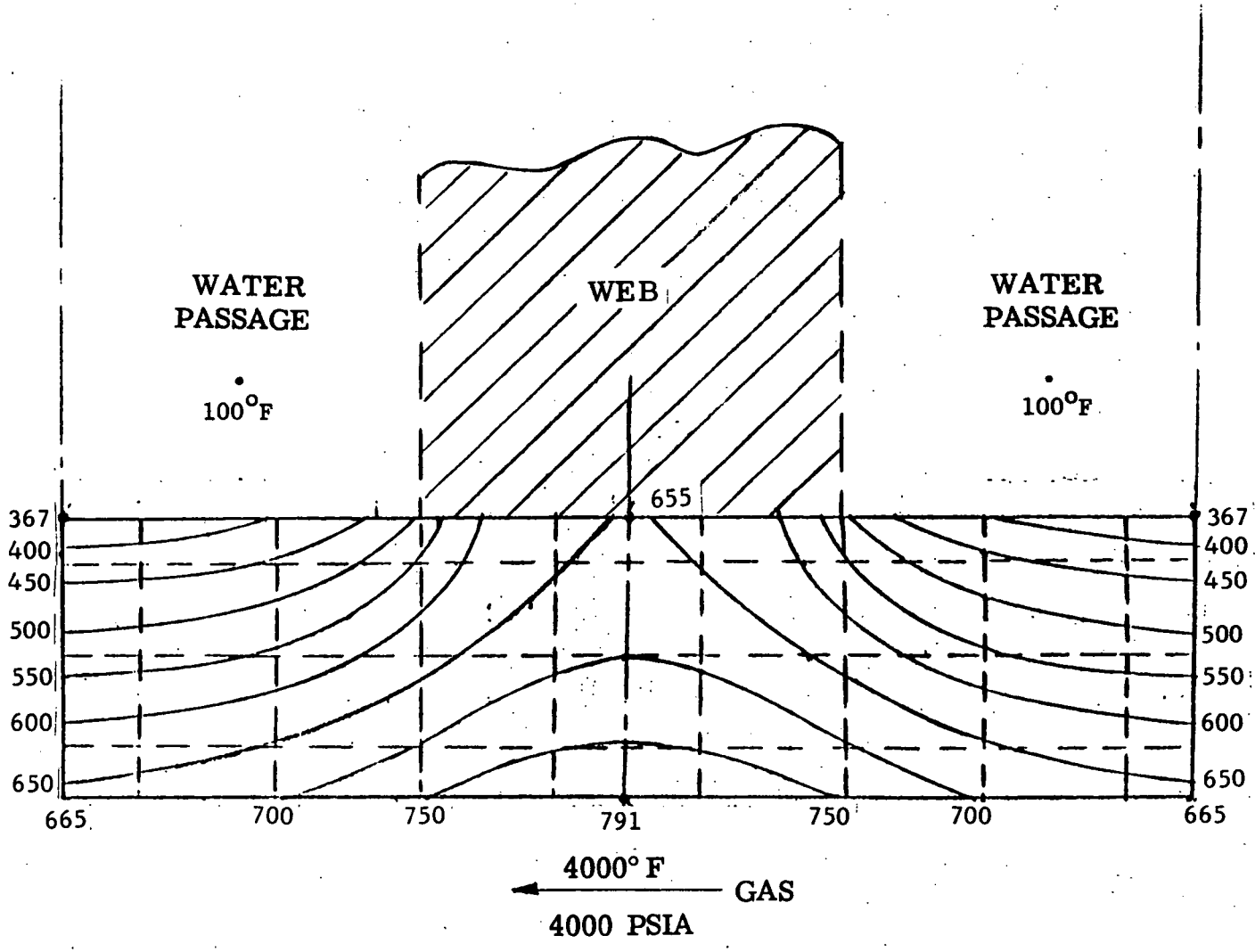

Figure 39. Water-Cooled Shell Liner Temperature Distribution at Water Inlet Manifold

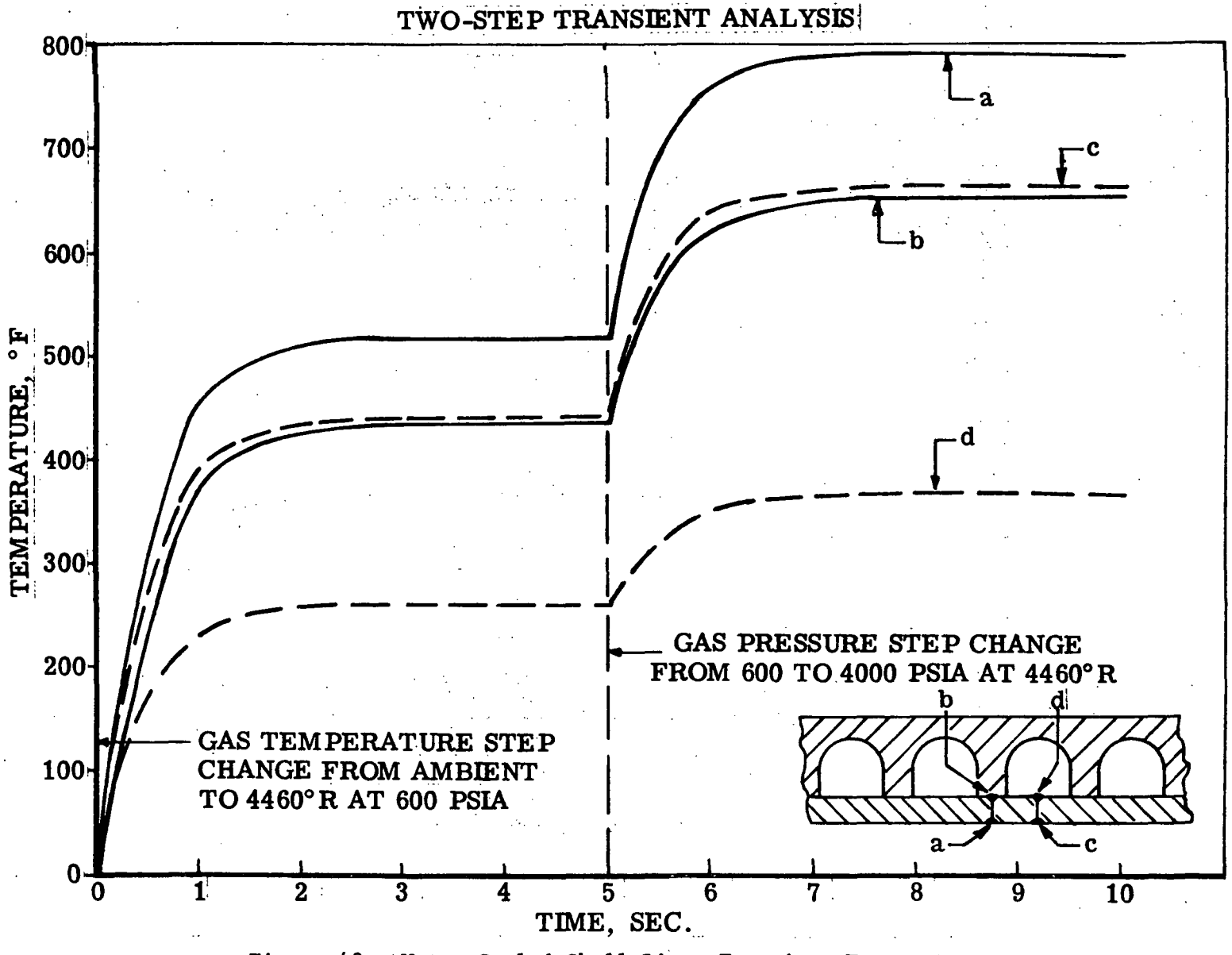

Figure 40. Water-Cooled Shell Liner Transient Temperatures.

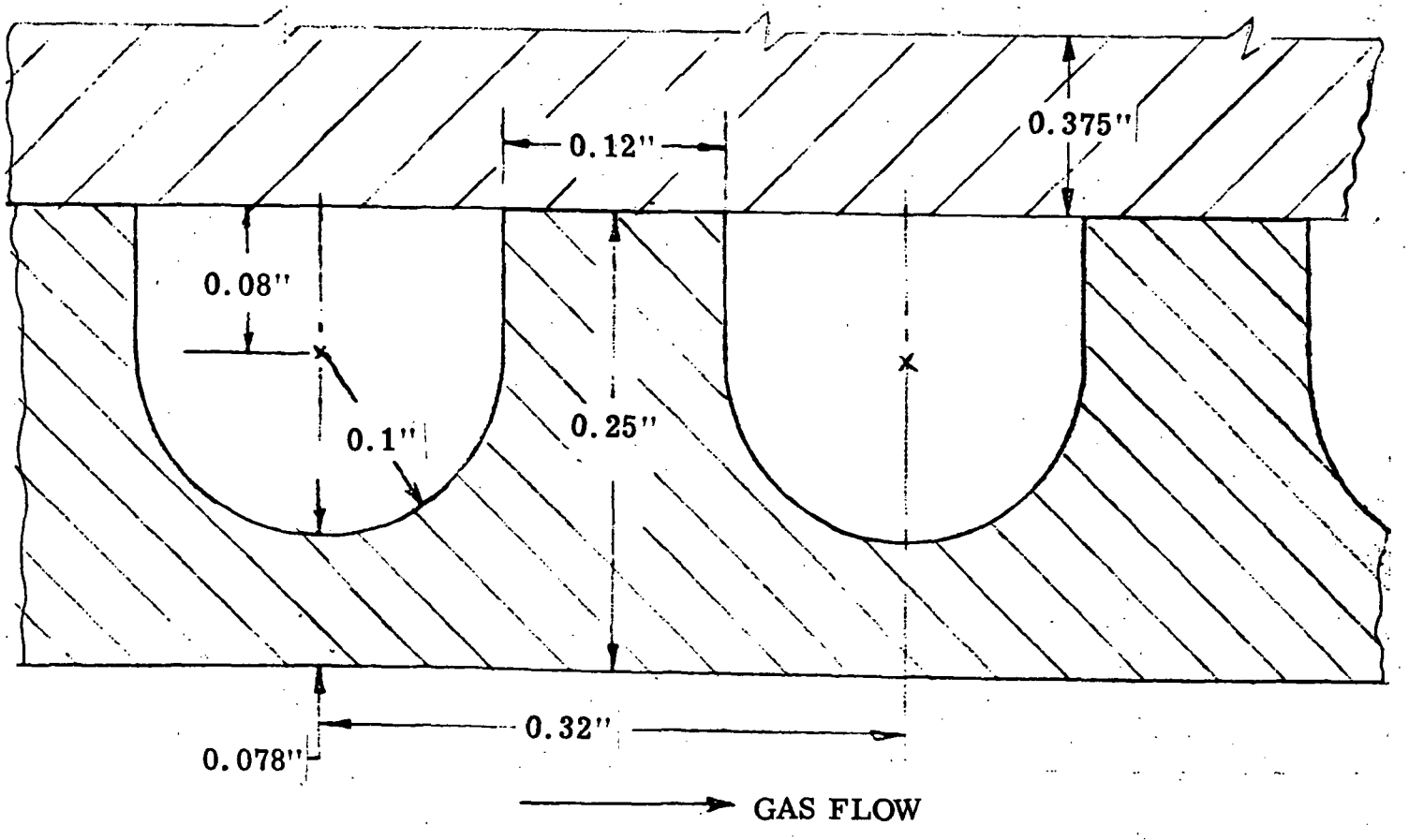

Figure 41. Dimensions of Water-Cooled Liner with Grooved Nickel Shell.

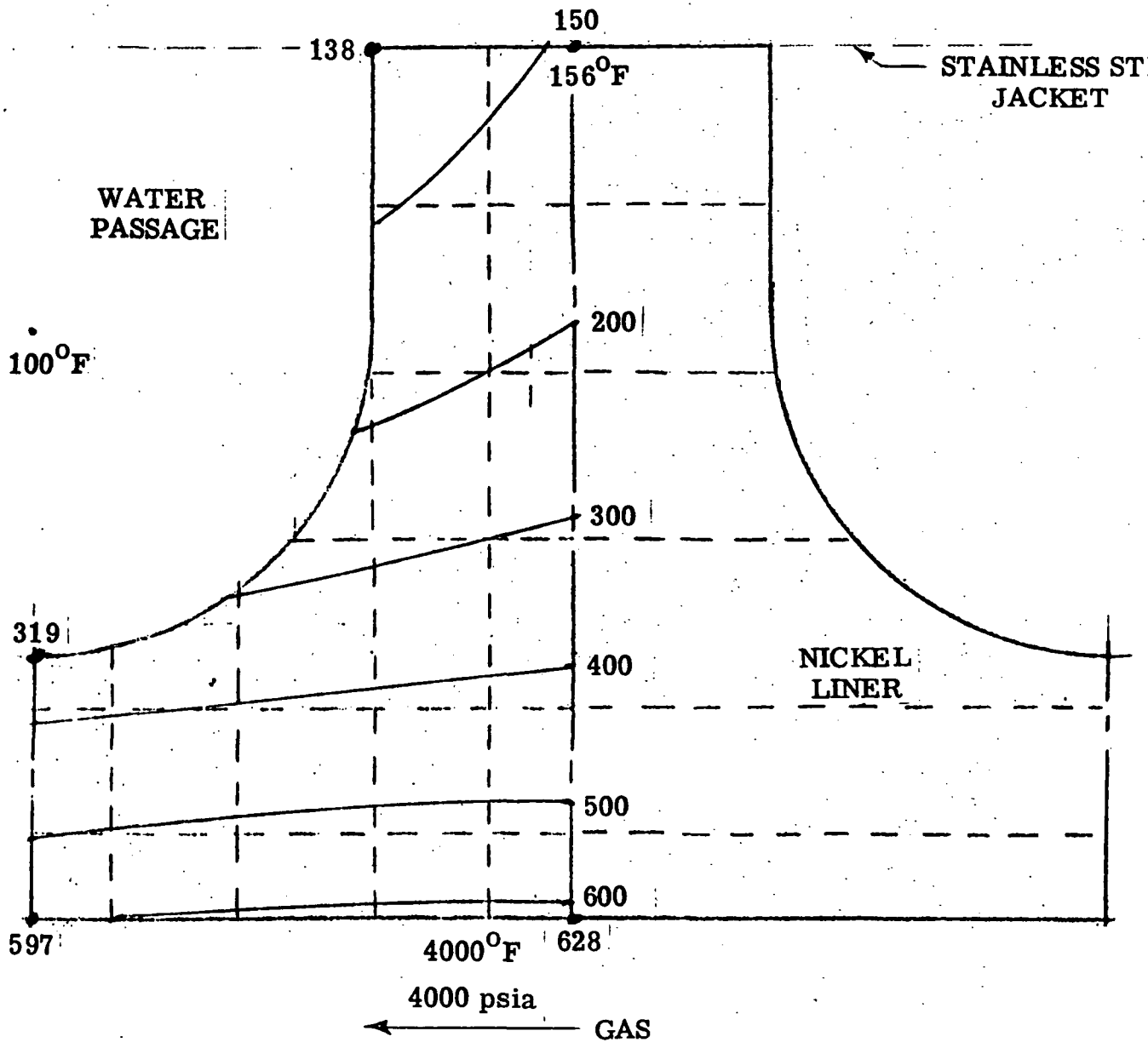

Figure 42. Water-Cooled Liner Temperature Distribution at Water Inlet.

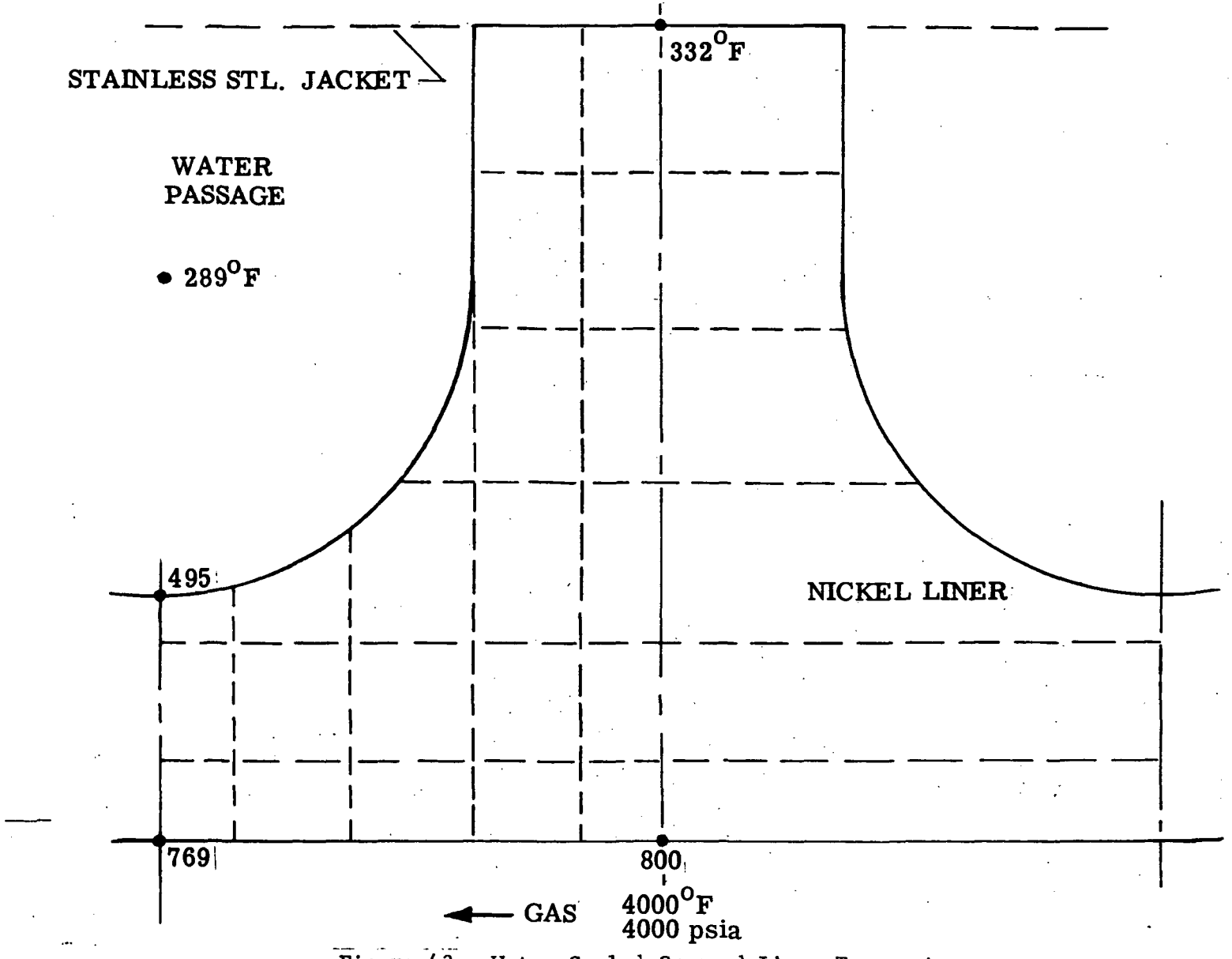

Figure 43. Water-Cooled Grooved Liner Temperature Distribution at Water Outlet.

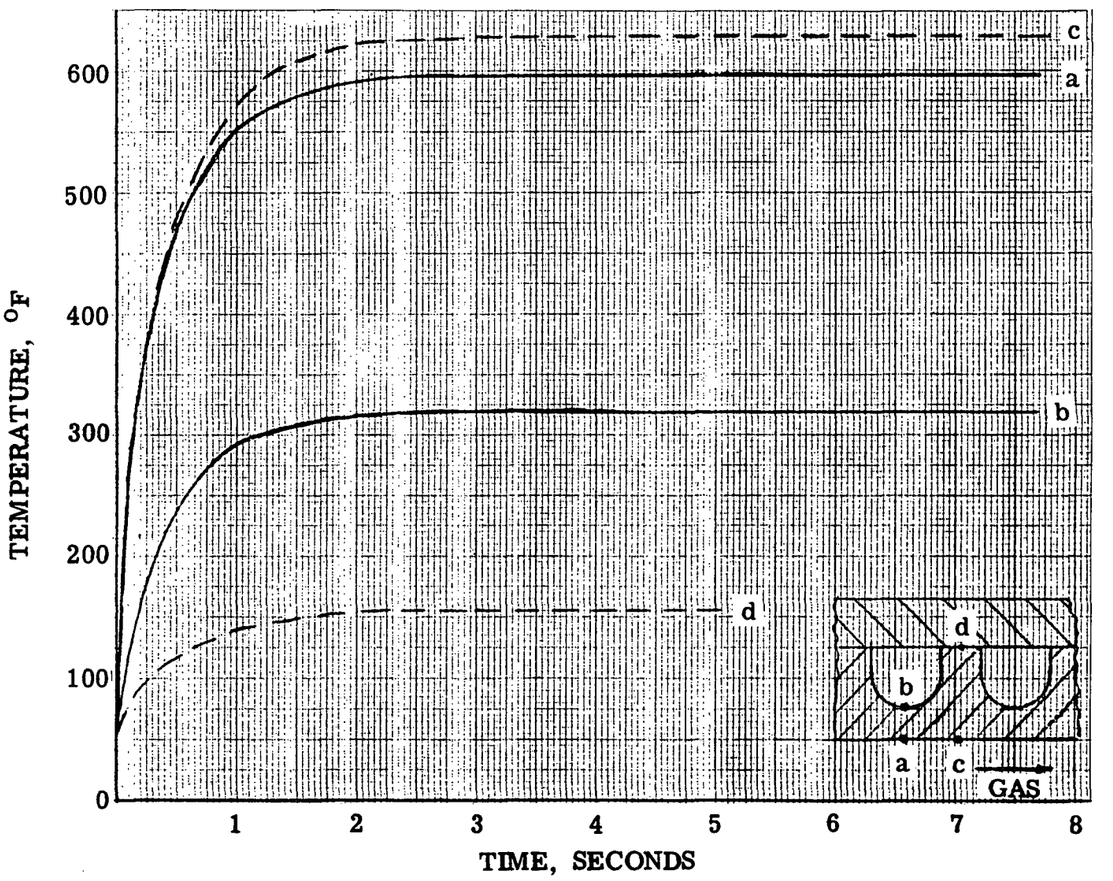

Figure 44. Water-Cooled Grooved Liner Transient Temperature at 4000 Psia

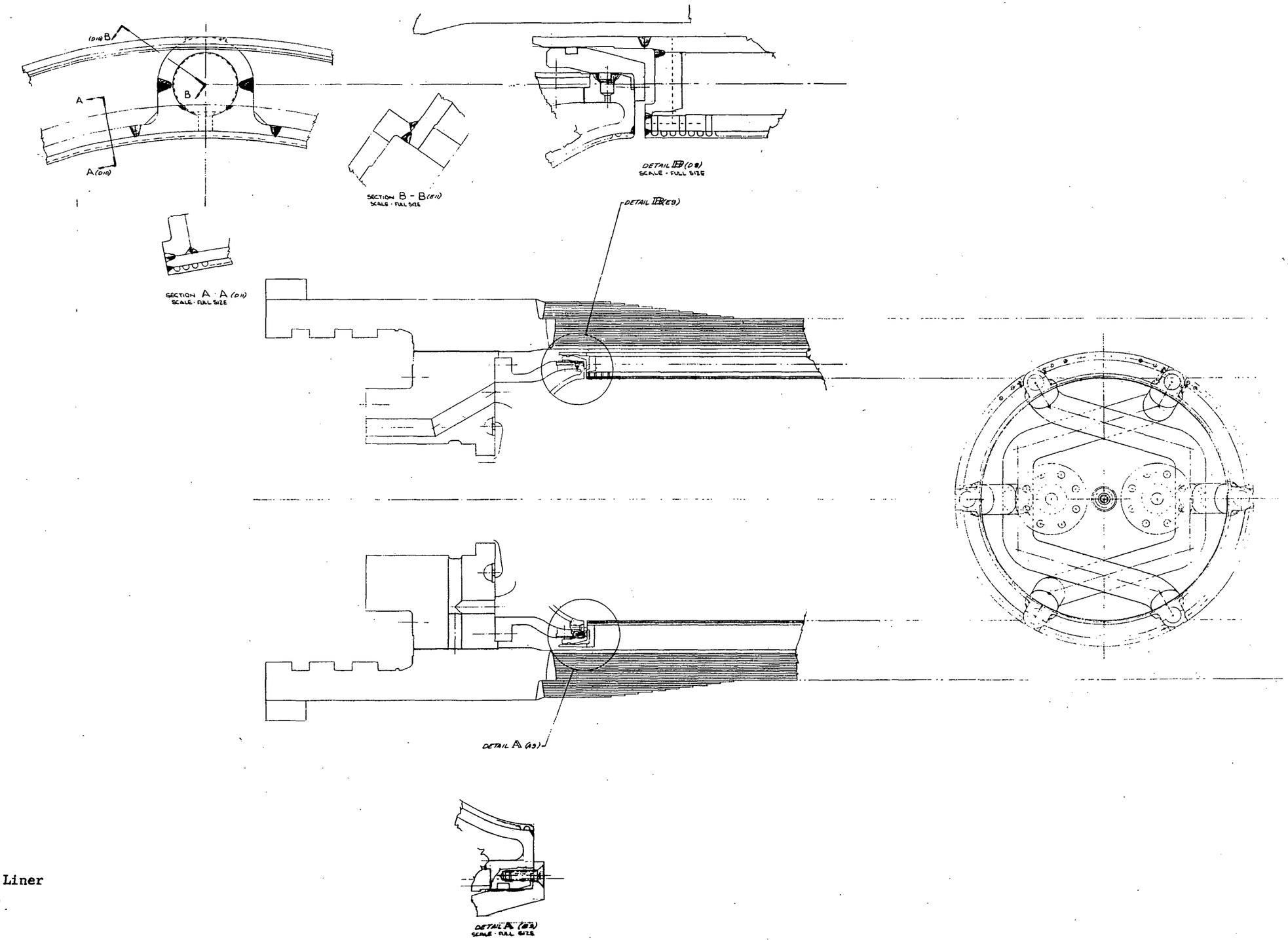

Figure 45. Water-Cooled Shell Liner Design Arrangement. (Sheet 1 of 2)

73-027

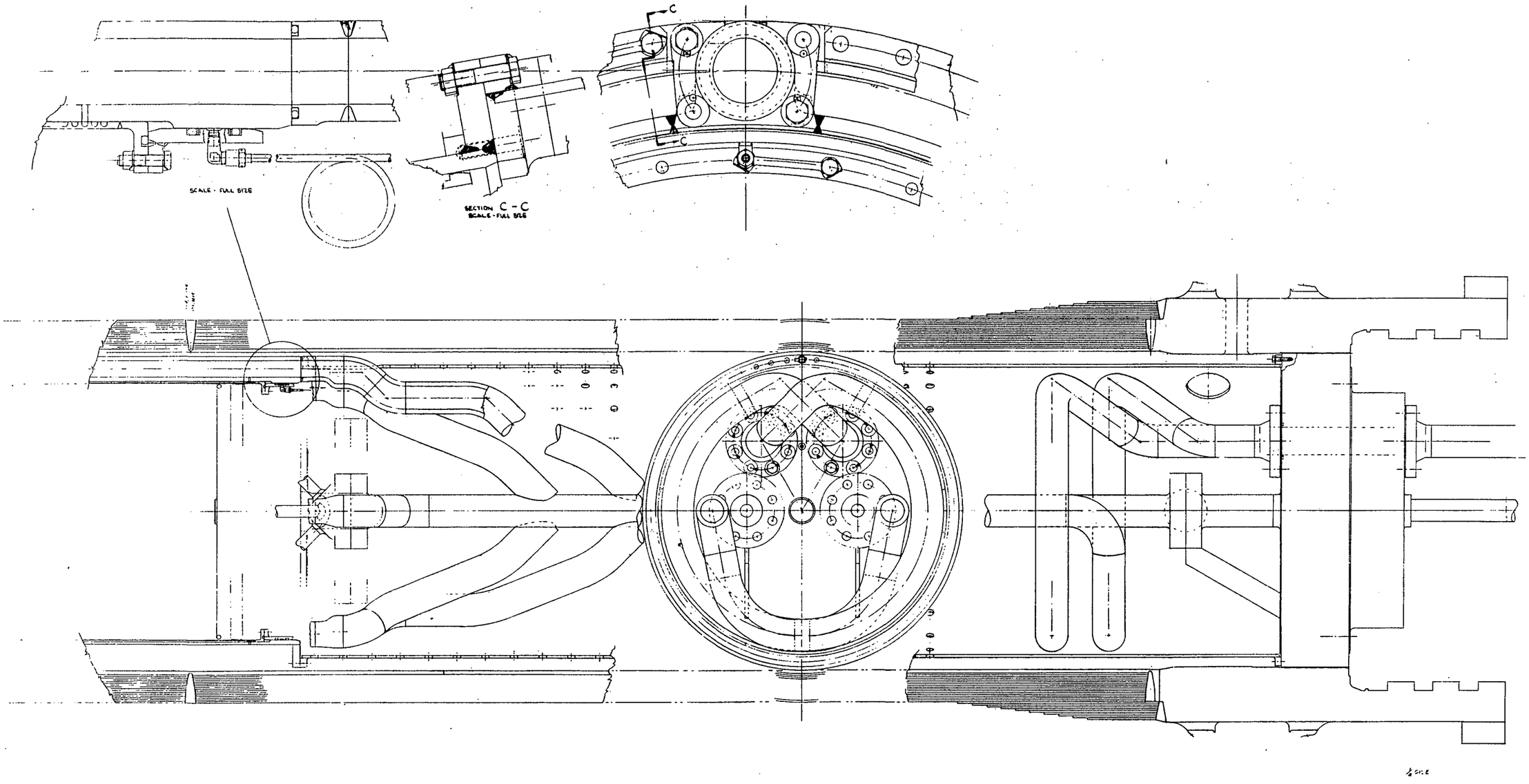

Figure 45. Water-Cooled Shell Liner Design Arrangement. (Sheet 2 of 2)

Page Intentionally Left Blank

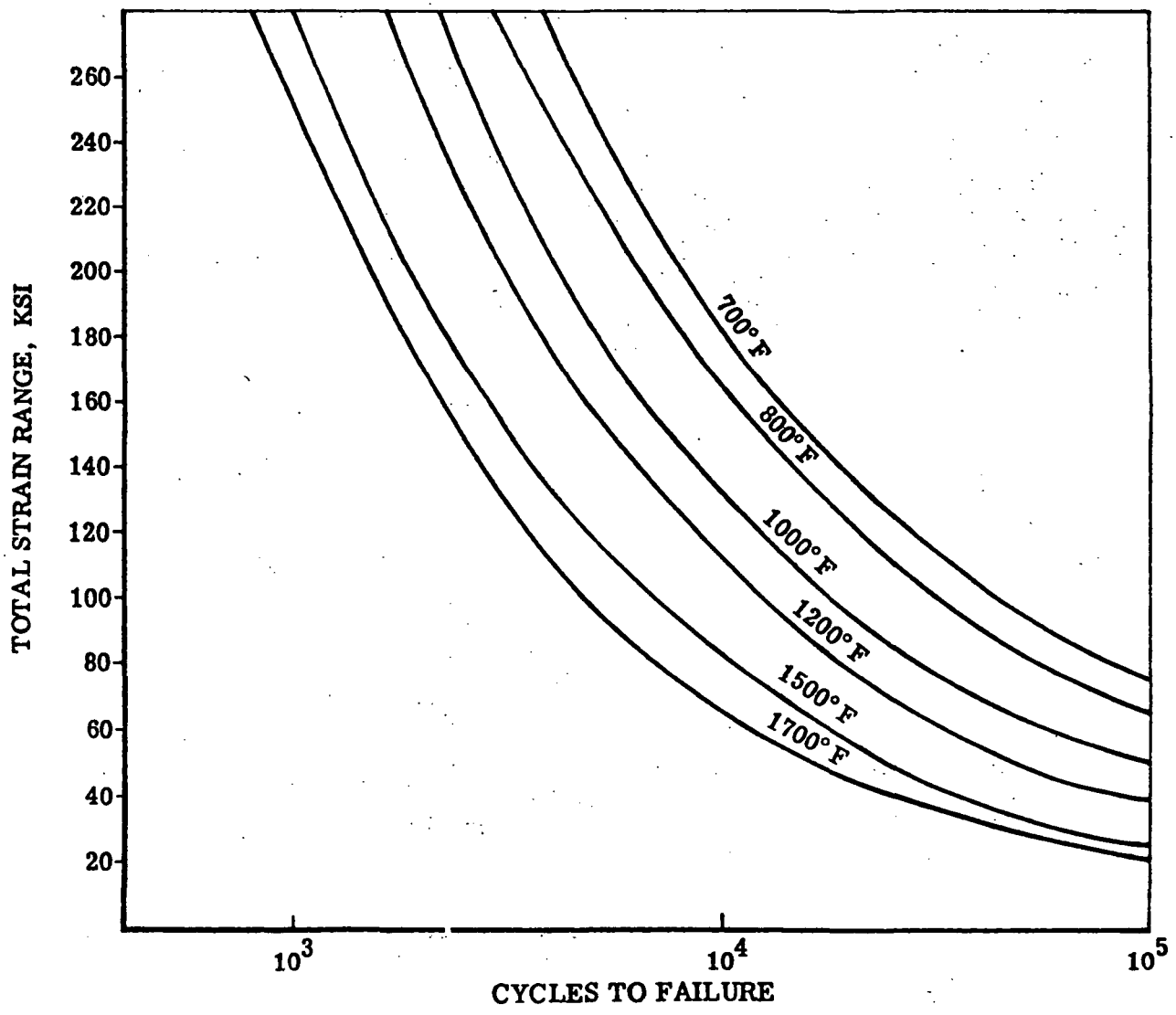

Figure 46. Low Cycle Fatigue Life of Nickel A.

Page Intentionally Left Blank

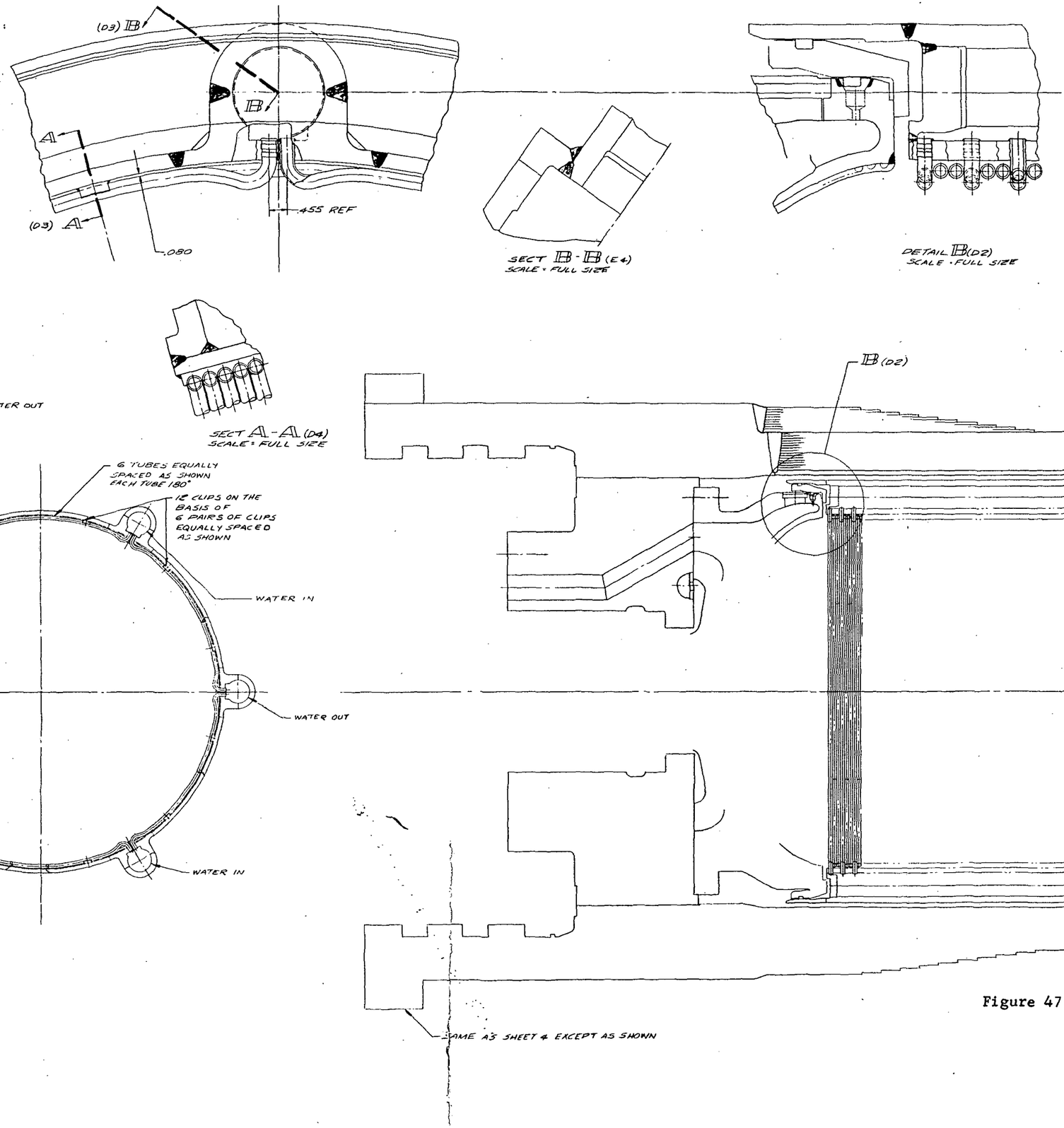

Figure 47. Water-Cooled Nickel Tube Liner Design Arrangement.

Page Intentionally Left Blank

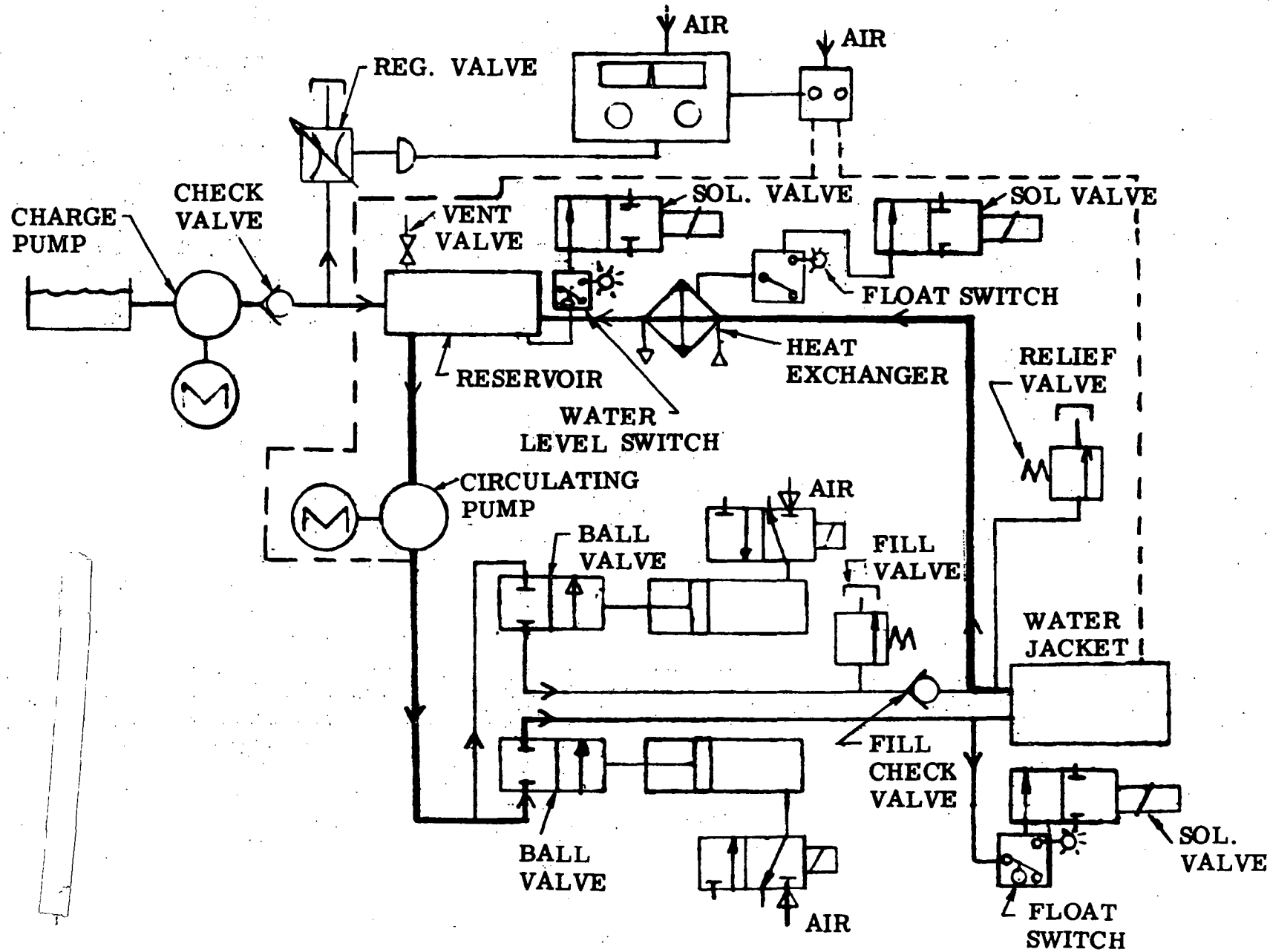

Figure 48. Water Cooling System I.

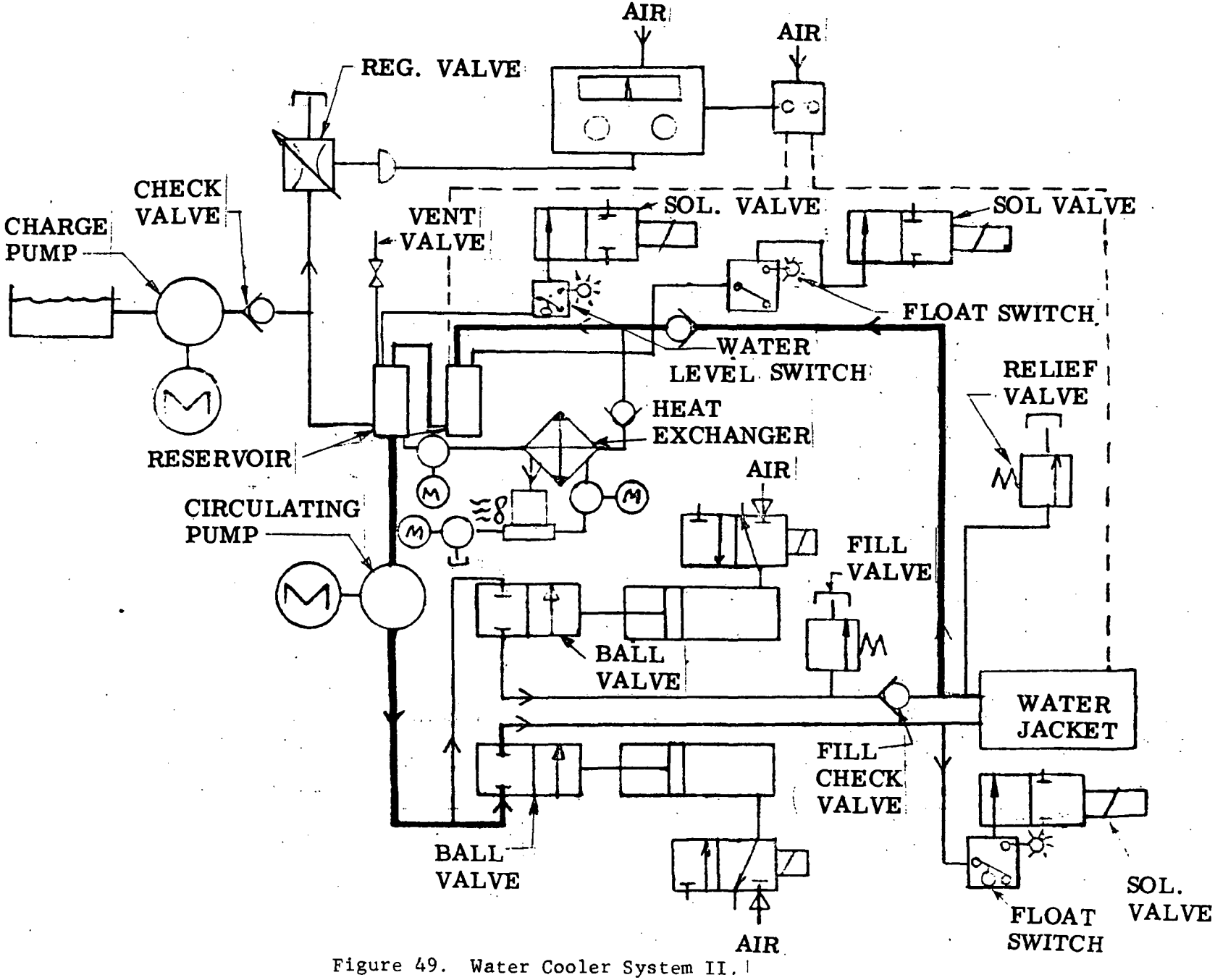

Figure 49. Water Cooler System II.

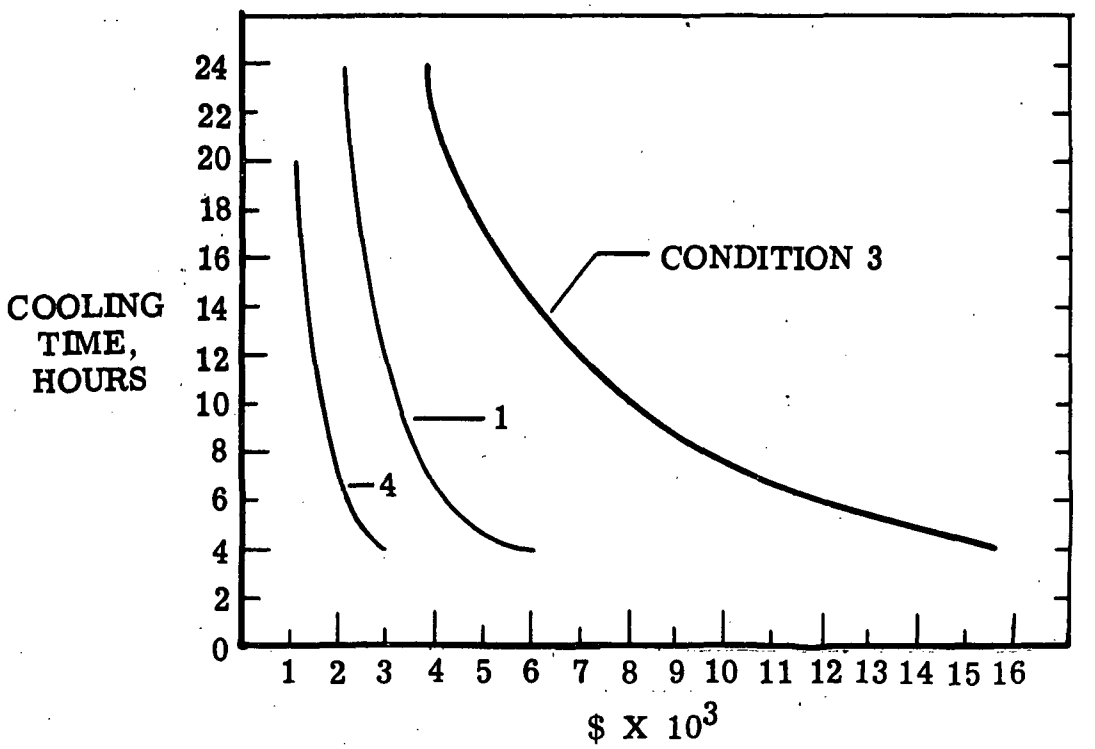

Figure 50. Heat Exchanger and Raw Water Loop Costs.

"Page missing from available version"

PAGE 114

APPENDIX A

Combustor Operating Conditions

The general arrangement of the 8-Foot High Temperature Structures Tunnel is shown in Figure A-1 and details of the combustor section in Figure A-2. The operating envelope and characteristics of the combustor facility are presented in Figures A-3 and A-4. The operating mode of the combustor is described in Reference 22 as follows:

A. The mass flow of combustion air (W_c) for the tunnel operating range is given in Figure 1.

B. The mass flow of the fuel (W_F) is approximately

$$W_F = 236 \frac{W_C}{T_T}$$

C. For tunnel starting, cold air at a minimum temperature (T_T) of 450° R is introduced into the combustor at a maximum rate of change (dW_C/dt) of 250 lb/sec^2 until a predetermined total pressure (P_T) is established within the combustor; this pressure level is limited to 2000 psia. At this predetermined pressure level, primary ignition of the fuel burner occurs and the temperature of the gas downstream of the burner increases to the desired operating value within one to three seconds. Next, the desired operating pressure is obtained by either lowering or increasing the flow into the combustor at a maximum rate of change (dW_C/dt) of ± 150 lb/sec^2 until the steady-state operating condition is achieved. Maximum operating pressure is 4000 psi.

D. For tunnel stopping, the fuel is cut off instantaneously and the temperature of the exhaust gas drops to the incoming air temperature within two seconds. While this is happening, the pressure within the combustor is automatically lowered to 1000 psia if operating above that level. The tunnel may continue to operate without combustion for as long as 60 seconds to permit cooldown of various components.

E. Items C and D above constitute one tunnel run or one thermal cycle of the combustor.

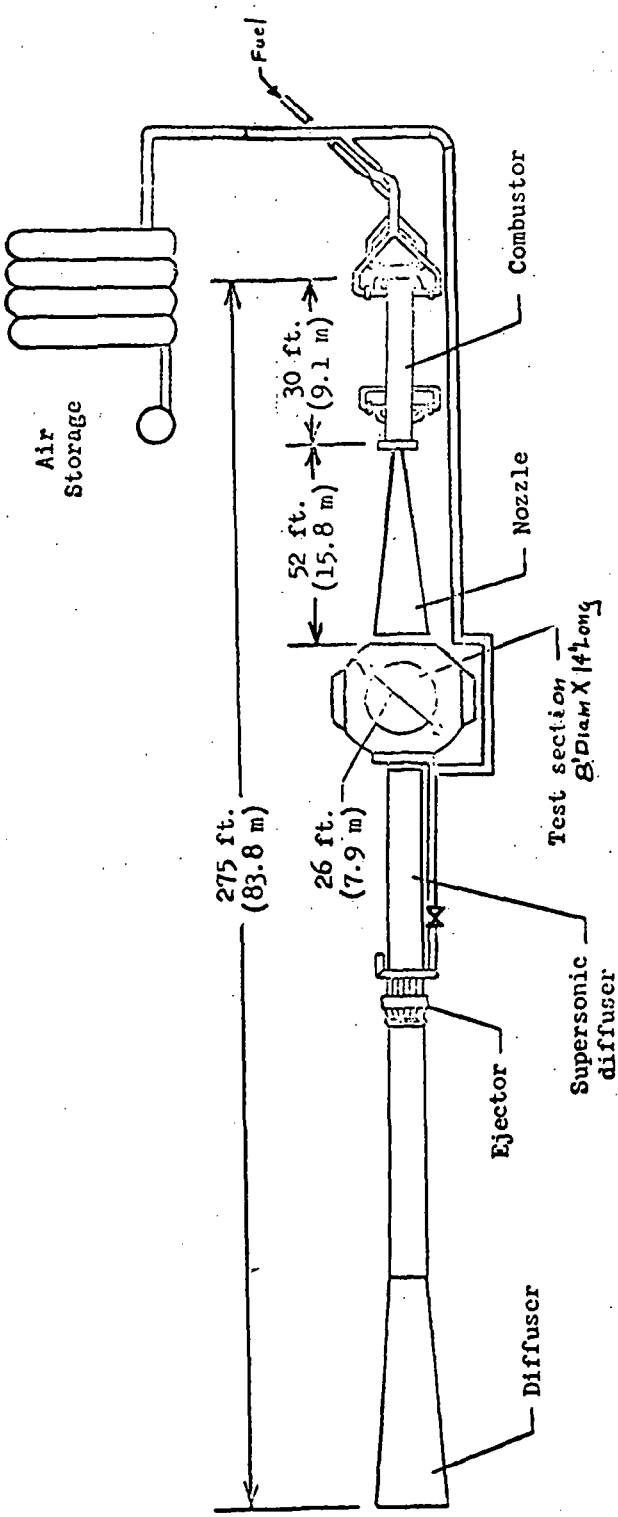

Figure A-1. Sketch of the 8-Foot High Temperature Structures Tunnel.

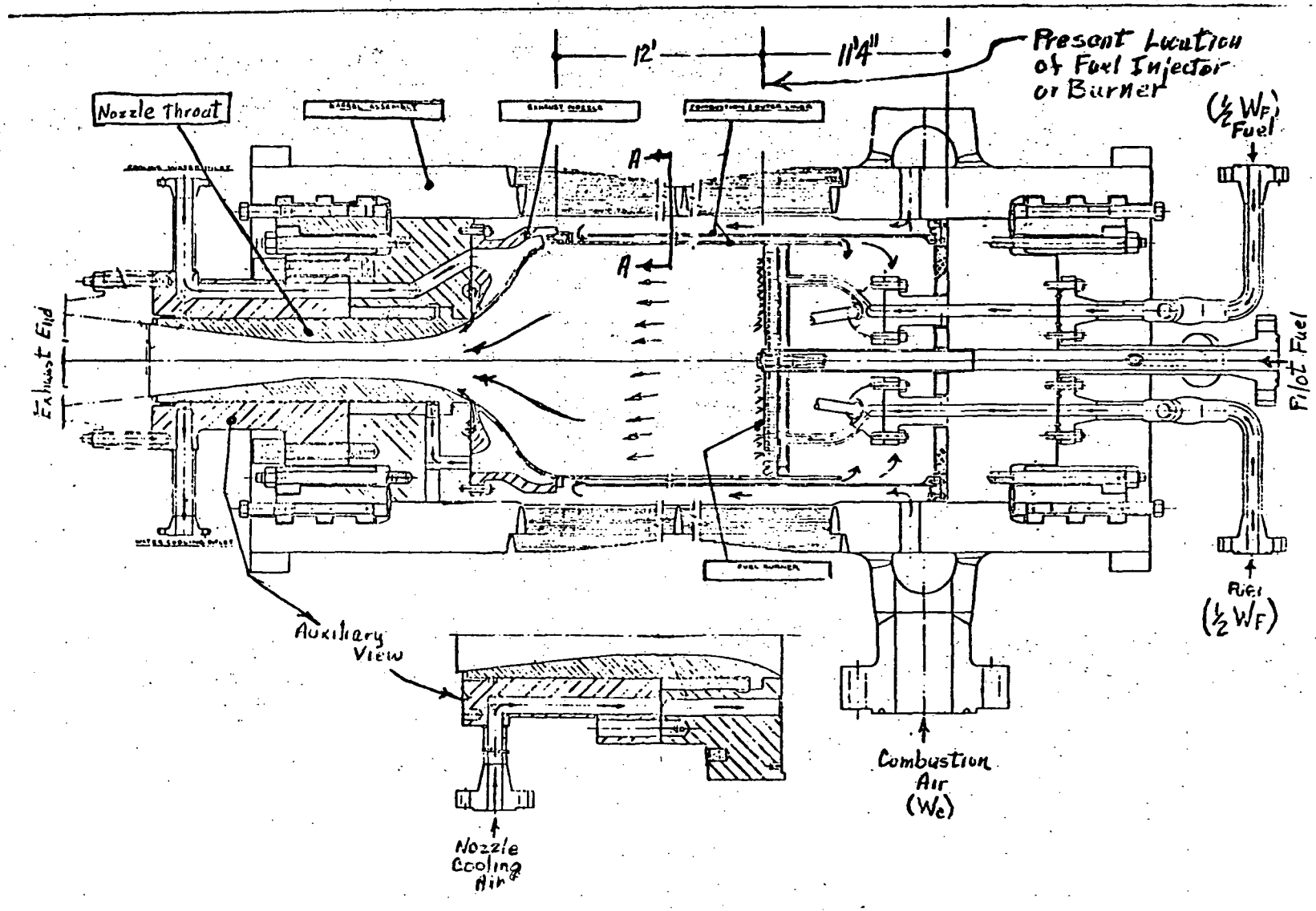

Figure A-2. Layout of High Pressure Combustor.

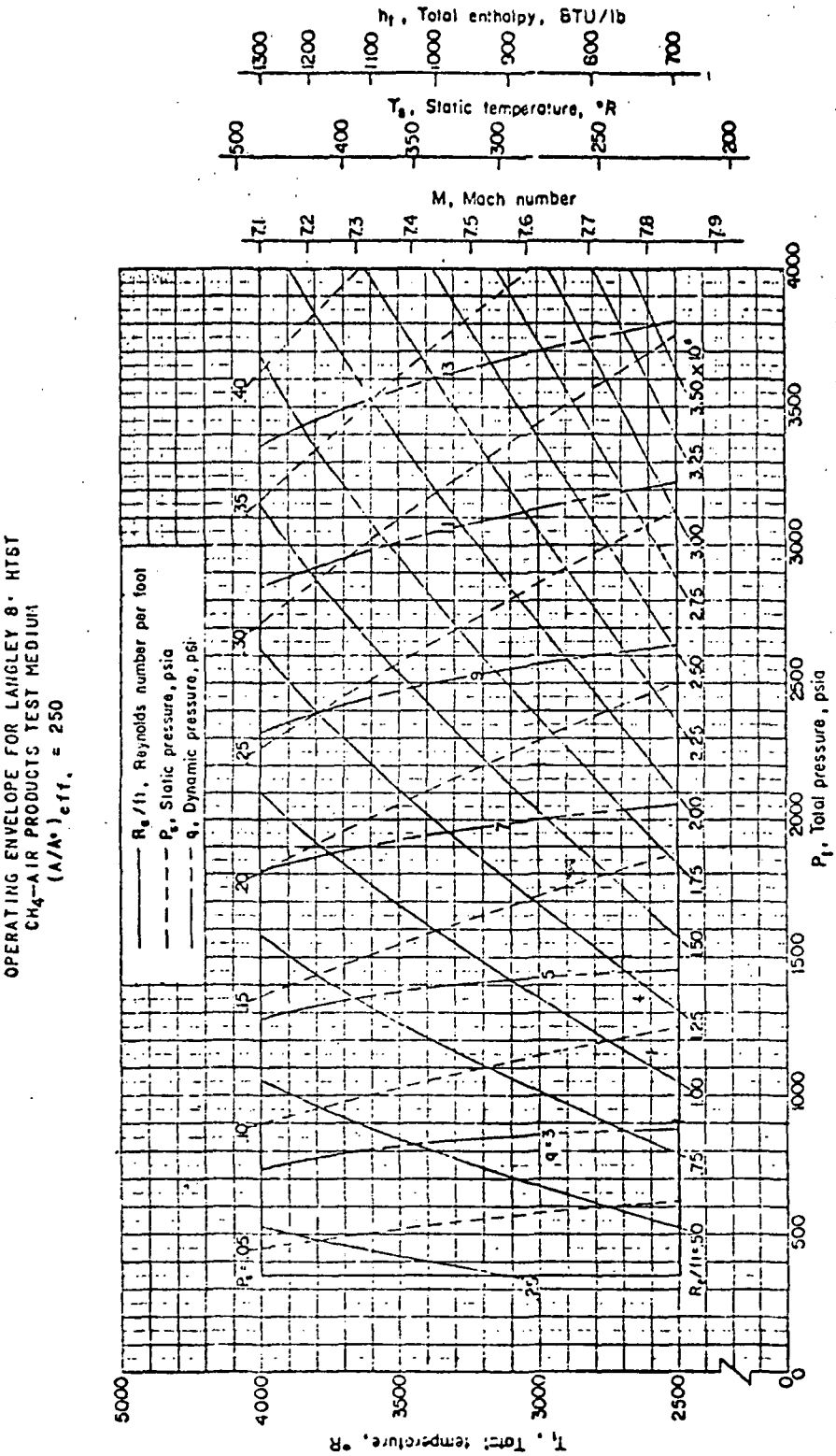

Figure A-3. Operating Envelope for Langley 8 Ft. HTST.

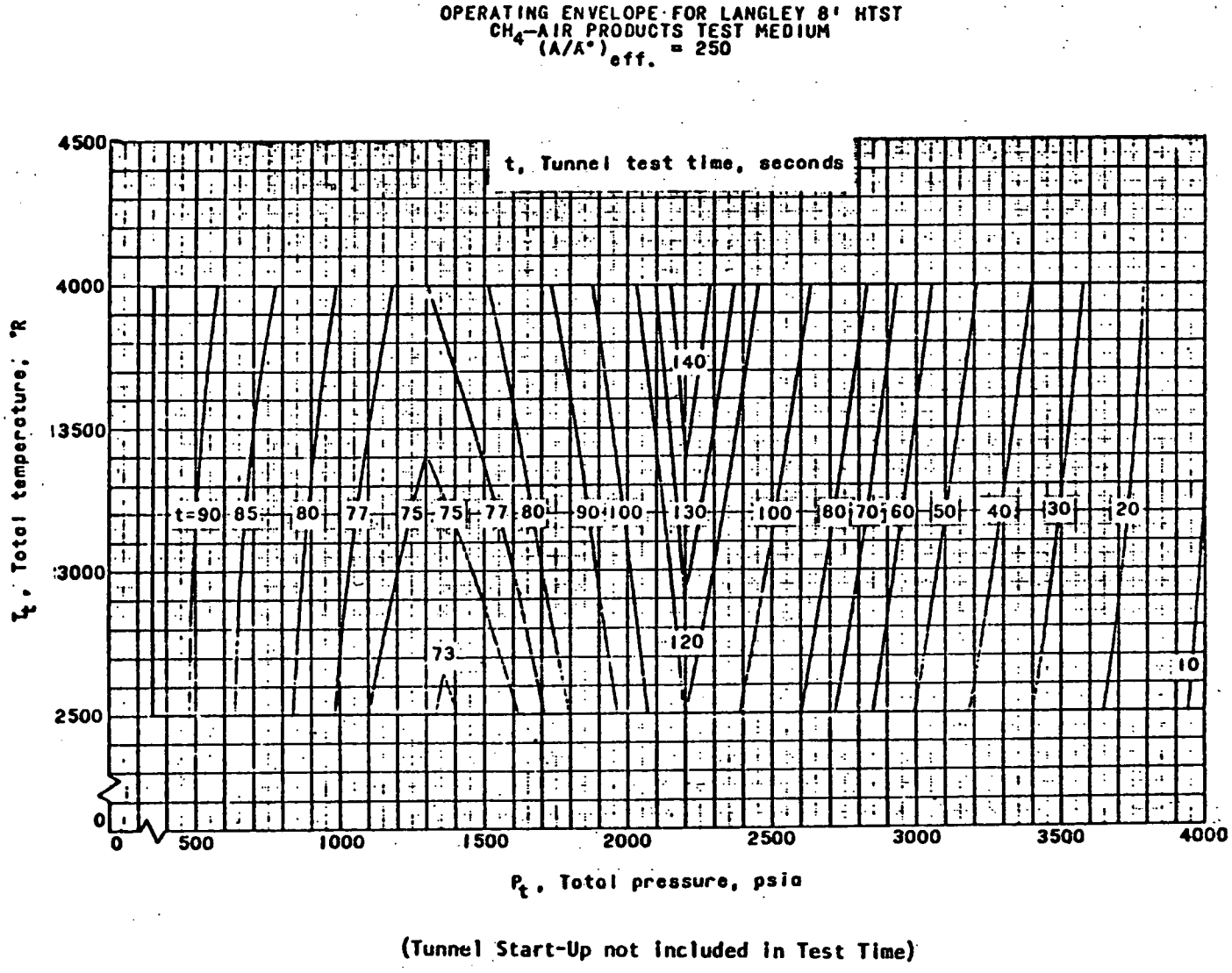

Figure A-4. Operating Envelope for Langley 8 Ft. HTST.

"Page missing from available version"

PAGE 120

APPENDIX B

Vibration Survey (Preliminary)

A preliminary survey of the vibration characteristics of the 8-Foot HTST combustor was conducted during the design study after it was recognized from the metallurgical failure analysis that vibratory fatigue (rather than low cycle fatigue) was responsible for the combustor cracks.

Dynamic instrumentation was applied to the combustion chamber of the 8-Foot HTST. Figure B-1 shows the location of the six strain gages on the inner liner and the four gages on the outer liner. The gages were used to measure the vibratory stress in a circumferential direction during a normal hot run of the facility. In addition to the strain gages, a dynamic pressure pickup was attached to one of the fuel inlet tubes just upstream of the fuel spray rings. A microphone pickup was attached to the outside wall at the aft-end of the combustor pressure vessel in the general plane of the tunnel nozzle. Data was recorded on magnetic tape.

Figure B-2 is a sketch of the inner liner vibratory stress as a function of time. Two incidents of peak stress are observed; one peak occurs at/or just after the lite-off and a second peak occurs 4 to 5 seconds after shut-down (possibly during the fuel system purge operation). There are two distinct major frequency components, 31 cps and 81 cps. The 81 cps component is only evident after the fuel is shut off. The 31 cps component starts just before lite-off and continues throughout the run.

The magnitude of the stress is shown as total stress range (vibratory stress is one-half the value shown) on Figure B-3. The high stress recorded on gage No. 3 during the low pressure cold flow test condition may indicate a discrepancy in gage sensitivity and the data is considered questionable. In summary, the stress data revealed the following:

(1) Vibratory stresses on the inner liner are over twice those on the outer liner

(2) Vibratory stress at T-bars is about one-half that for locations between T-bars

(3) Stress magnitudes in general are more uniform on the outer liner than on the inner liner

(4) Vibratory stresses are of sufficient amplitude to introduce a potential fatigue failure when steady-state stresses, temperature and stress concentration factors are taken into consideration

Examination of signals from all six strain gages on the inner liner revealed that the stresses are in phase for the 31 cps component. This indicates that at a given instant of time, the gages at all locations show a tension stress. The strain gages No. 9 and 10 on the outer liner revealed the signals are in phase with each other but out-of-phase with 11 and 12. Thus, at a given instant of time, the gage No. 9 and 10 show a tension stress while No. 11 and 12 show a compression stress.

The 31 cps frequency that is observed on the liners is close to a natural frequency of both liners. The inner liner has a 6-node mode at 33.6 cps and the outer liner has a 4-node mode at 31.4 cps. Figure B-4 shows the respective mode shapes for the two liners at these frequencies. The mode shape and the strain gage signals were analyzed to determine which was vibrating at its natural frequency. If the locations of the strain gages on the inner liner are placed anywhere along the mode shape of that inner liner, it can be seen that all six gages cannot have the same phase. Since the gage signals were in phase during the tunnel operation, it may be concluded that the inner liner is not vibrating at its natural frequency. For the outer liner, the gage locations and phase relationships do conform to the 4-mode natural frequency of the liner. Based on the frequency and phase relationship, it may be concluded that the outer liner is vibrating at its natural frequency.

In order to identify the source of 31 cps excitation, Figure B-5 was constructed. Two types of natural frequencies are considered. The natural frequency of a closed organ pipe was considered as one type of aerodynamic excitation. For the organ pipe, the higher modes of vibration are direct multiples of the fundamental. The fourth mode is four times the fundamental. If a cylinder response is considered as the form of mechanical excitation, the relationship between the frequency of the fundamental mode and higher modes is given by

$$\frac{\text{Higher Mode}}{\text{Fundamental Mode}} = \frac{n\,(n^2 - 1)}{\sqrt{1 + n^2}}$$

where n is half the number of modes which is 2 for the fundamental and increases by 1 for each higher mode. Thus, the fourth mode is 8.8 times the fundamental mode.

The results of an electronic wave analysis performed on the strain gage signals recorded during the hot flow test are presented in Figure B-6. For each parameter measured, the 31 cps component was the major response. The higher responses are predominantly direct multiples of the 31 cps frequency. This suggests that the major excitation source is of an aerodynamic nature.

It is also noted that an organ pipe natural frequency will vary as the temperature of the media changes. The frequency noted during the tunnel test was always 31 cps. It was first observed when the combustor gas temperature was about 500° F and prior to the final gas temperature of 2840° F.

The 81 cps frequency observed after shutdown was primarily evident on the inner liner and most pronounced near one of the spray bar pads. For these reasons it is felt that stress is due to vibratory motion of the fuel spray bar assembly which has radial clearance under hot conditions. This stress burst takes place just about the time the fuel line is purged with high pressure nitrogen.

Based on the results of this preliminary analysis, the following recommendations are made:

(1) Provide additional strain gage instrumentation on the inner and outer liner to better define the dynamic interaction between the two liners

(2) Analyze and instrument the air and fuel piping system to determine source of excitation

(3) Determine the fuel spray bar natural frequency

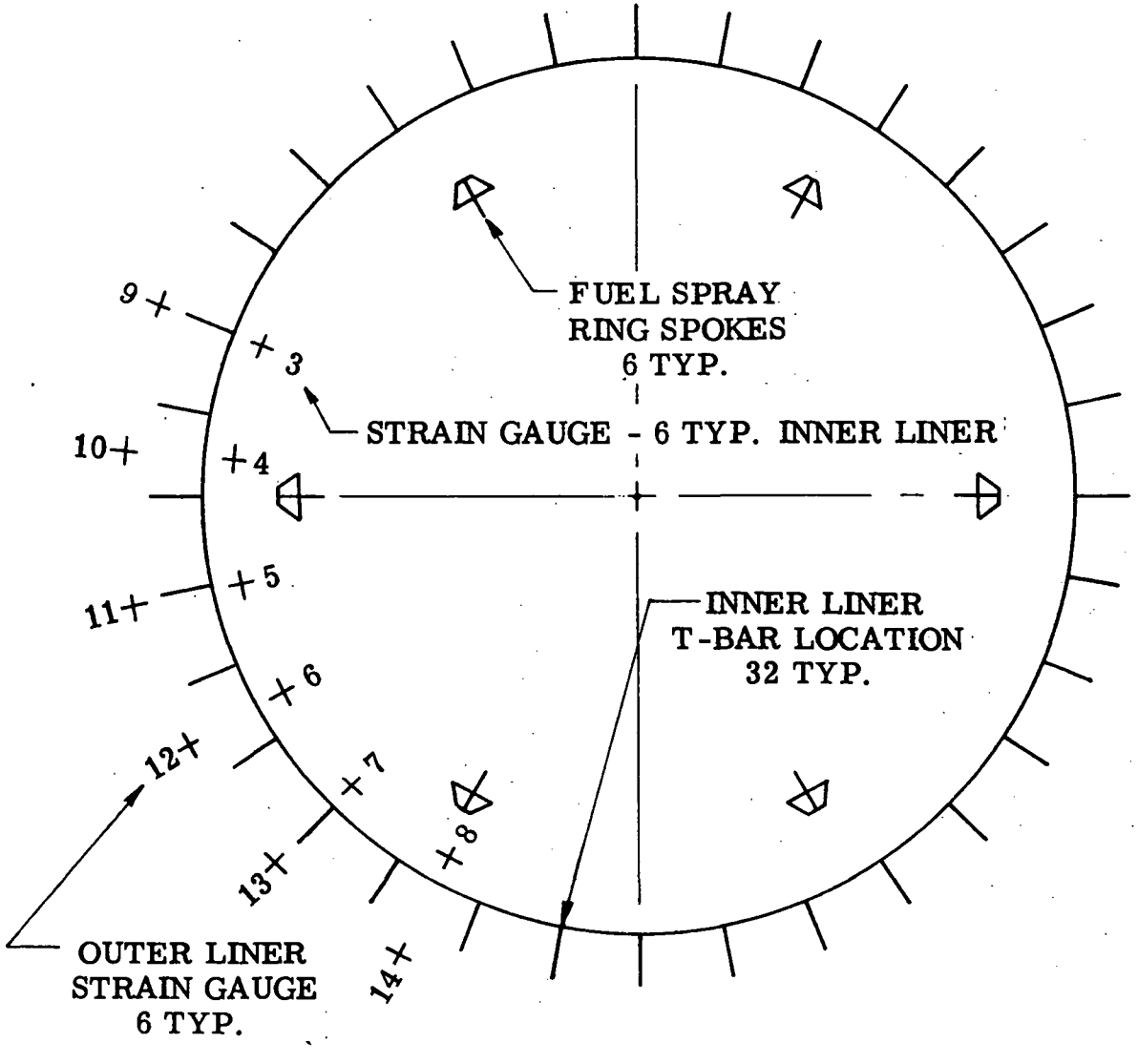

Figure B-1. Strain Gauge Locations

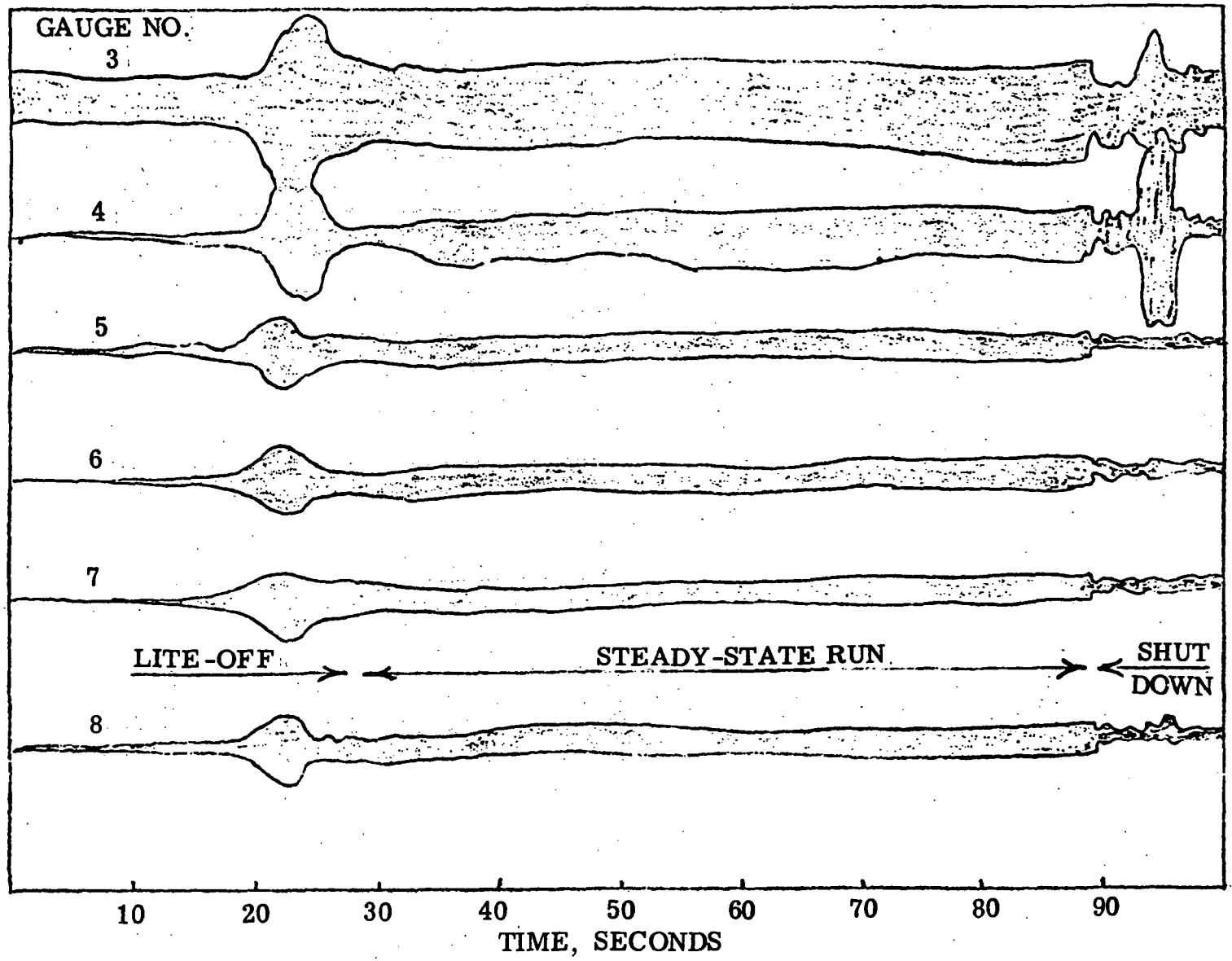

Figure B-2. Inner Liner Vibratory Stresses.

INNER LINER

	STRESS, PSI						TIME SEC.
STRAIN GAUGE LOCATION	3	4	5	6	7	8	
MID PT. BETWEEN START & LIGHT-UP	6,750	350	430	250	280	180	12
MAX. STRESS DUE TO LIGHT-UP	26,250	20,190	14,190	25,530	14,190	22,260	24
AFTER LIGHT-UP	11,250	2,880	5,110	7,000	8,510	6,040	26
MID PT. BETWEEN LIGHT-UP - FUEL OFF	13,110	9,370	4,540	7,000	6,810	7,640	59
MAX. STRESS DUE TO FUEL OFF	11,250	25,370	3,410	4,900	3,410	6,360	97

OUTER LINER

	STRESS, PSI					TIME SEC.
STRAIN GAUGE LOCATION	9	10	11	12	13	
MID PT. BETWEEN START & LIGHT-UP	320	360	320	290	N.G.	12
MAX. STRESS DUE TO LIGHT-UP	6,000	10,410	9,360	8,400	N.G.	24
AFTER LIGHT-UP	2,250	1,870	2,920	2,680	N.G.	26
MID PT. BETWEEN LIGHT-UP - FUEL OFF	2,020	2,340	3,250	2,300	N.G.	59
MAX. STRESS DUE TO FUEL OFF	2,700	OUT	1,560	2,010	N.G.	97

Figure B-3. Vibration Survey Measured Total Stress Range

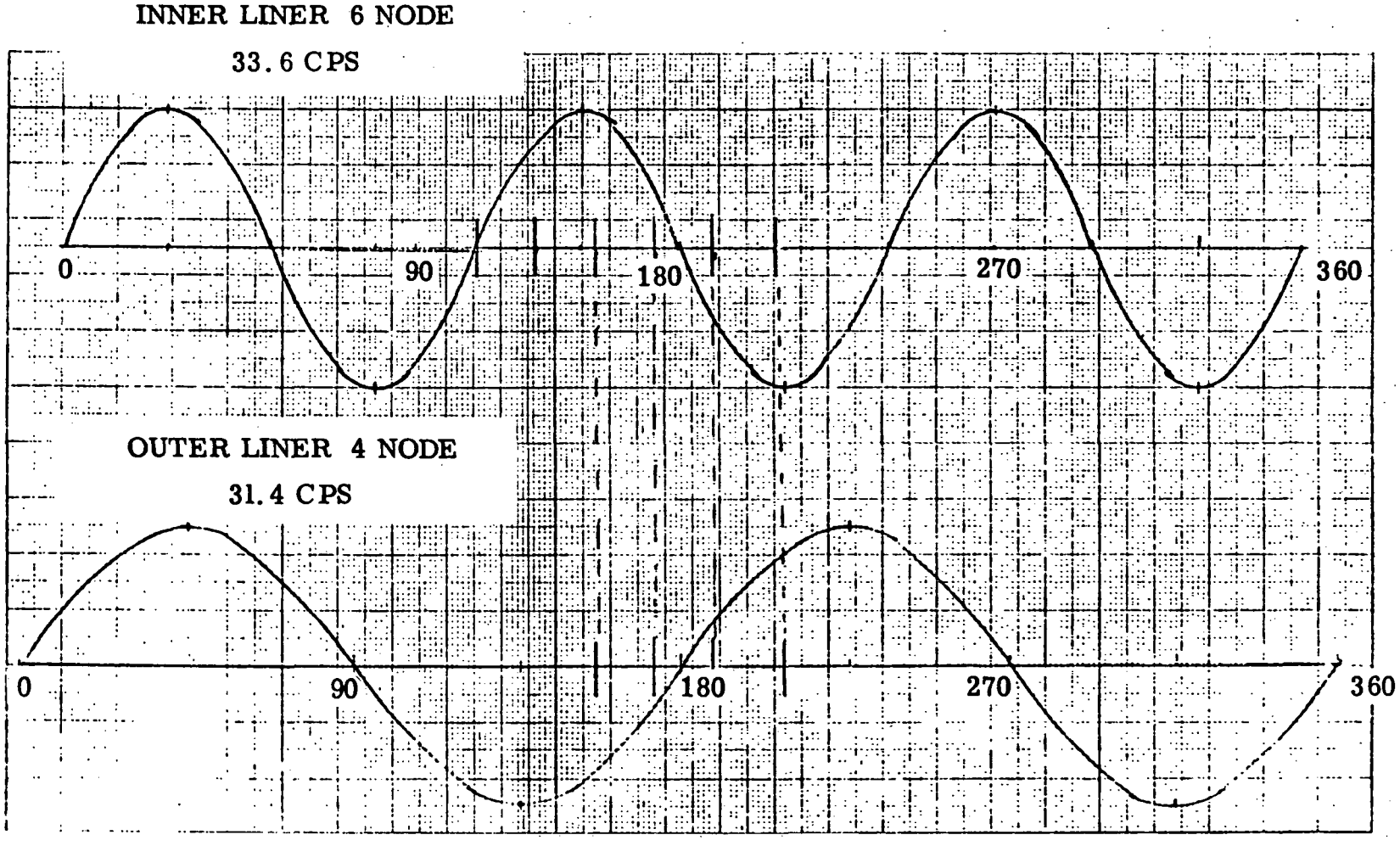

Figure B-4. Mode Phase Relationship of Inner & Outer Liners.

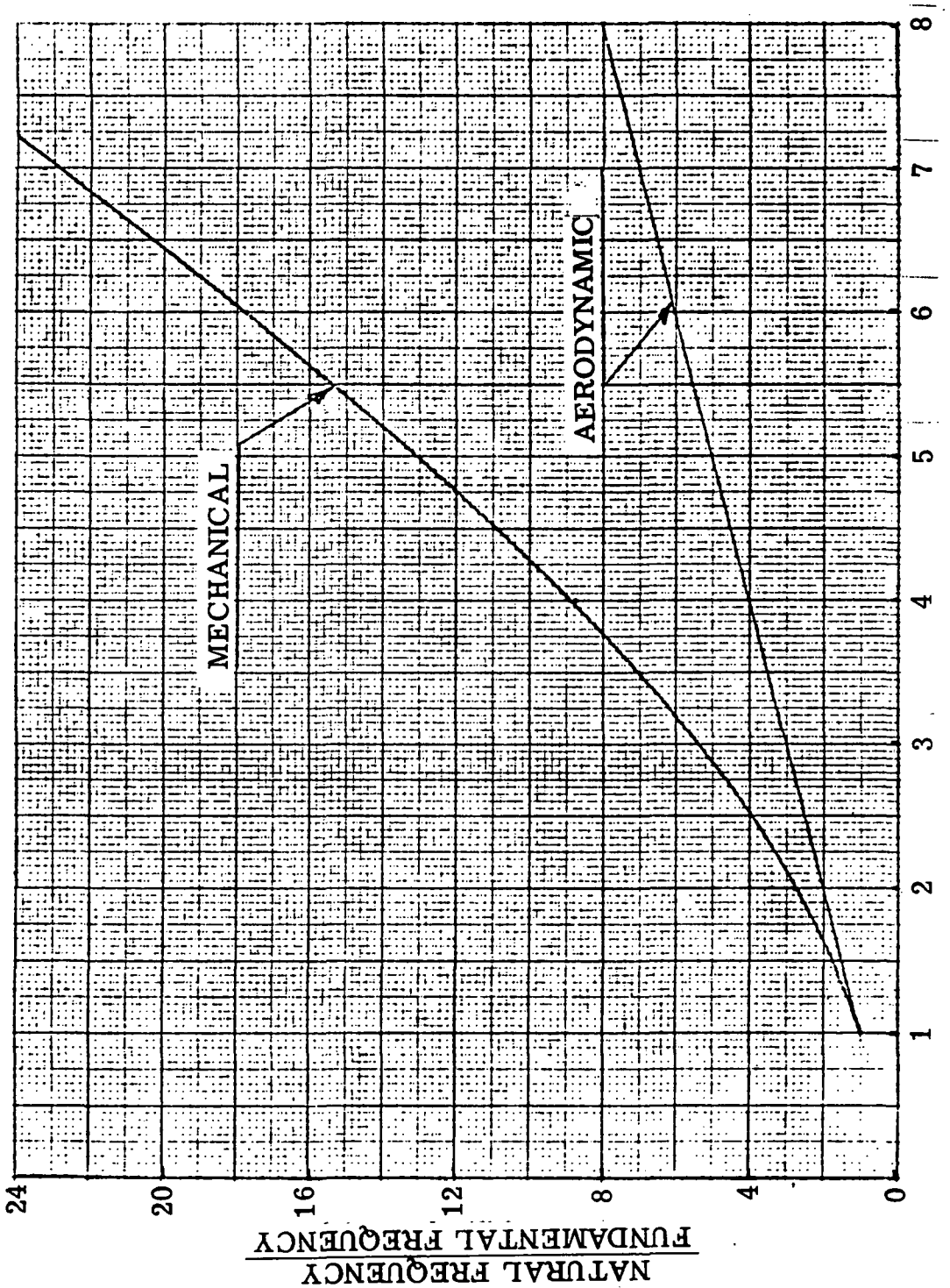

Figure B-5. Vibration Response.

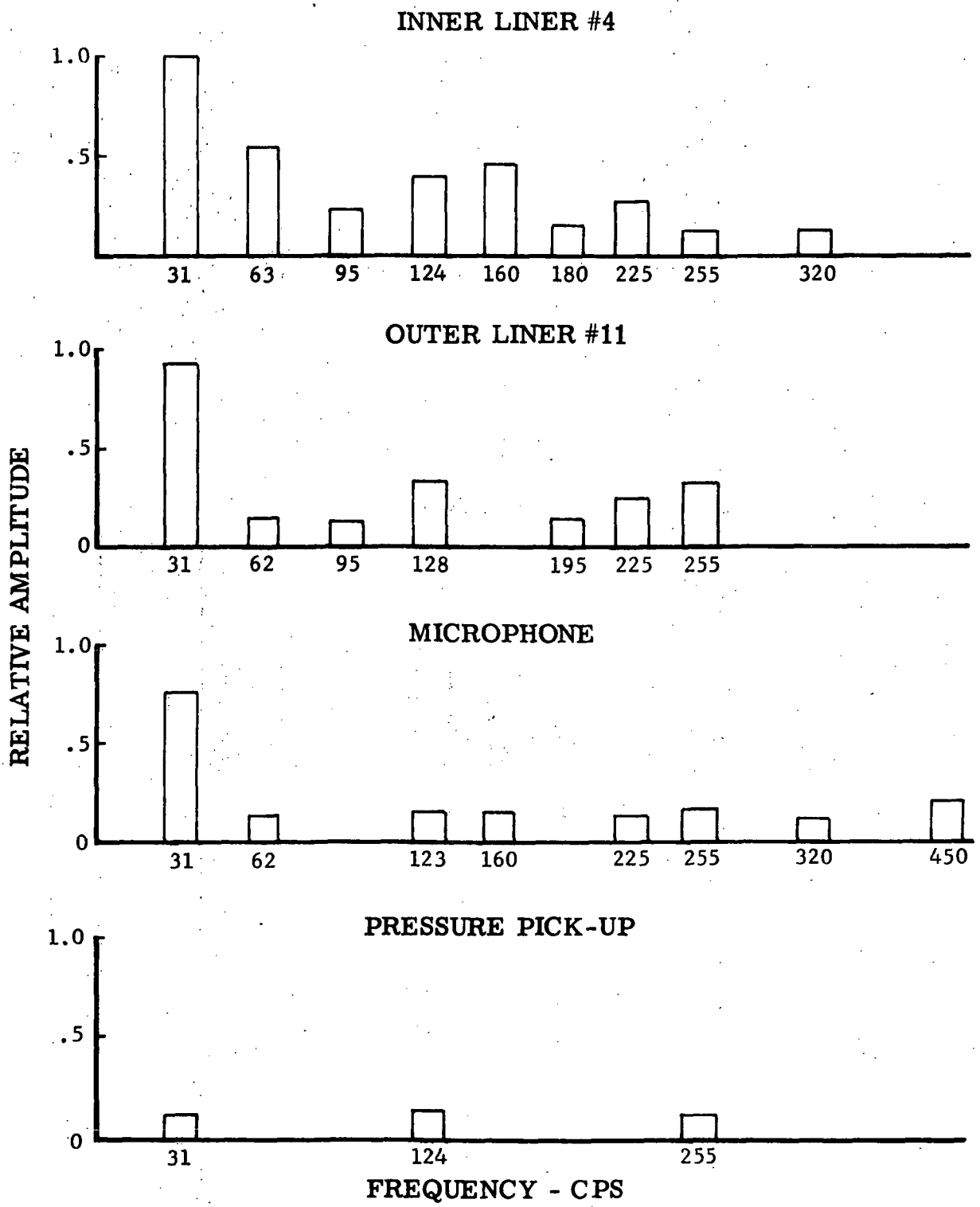

Figure B-6. Wave Analysis Frequency Content.

DISTRIBUTION LIST

1. NASA Langley Research Center
   Hampton, Virginia 23365
   Attention: Report & Manuscript Control Office, Mail Stop 180A — 1
   Raymond L. Zavasky, Mail Stop 115 — 1
   John R. Karns, Mail Stop 208 — 20

2. NASA Ames Research Center
   Moffett Field, California 94035
   Attention: Library, Mail Stop 202-3 — 1

3. NASA Flight Research Center
   P.O. Box 273
   Edwards, California 93523
   Attention: Library — 1

4. NASA Goddard Space Flight Center
   Greenbelt, Maryland 20771
   Attention: Library — 1

5. NASA Lyndon B. Johnson Space Center
   2101 Webster Seabrook Road
   Houston, Texas 77058
   Attention: Library, Code JM6 — 1

6. NASA Marshall Space Flight Center
   Huntsville, Alabama 35812
   Attention: Library — 1

7. Jet Propulsion Laboratory
   4800 Oak Grove Drive
   Pasadena, California 91103
   Attention: Library, Mail 111-113 — 1

8. NASA Lewis Research Center
   21000 Brookpark Road
   Cleveland, Ohio 44135
   Attention: Library, Mail Stop 60-3 — 1

9. NASA John F. Kennedy Space Center
   Kennedy Space Center, Florida 32899
   Attention: Library, IS-DOC-1L — 1

10. National Aeronautics & Space Administration
    Washington, D.C. 20546
    Attention: KSS-10/Library — 1

11. NASA Scientific & Technical Information Facility
    P.O. Box 33
    College Park, Maryland 20740 — 9 plus reproducible

Top

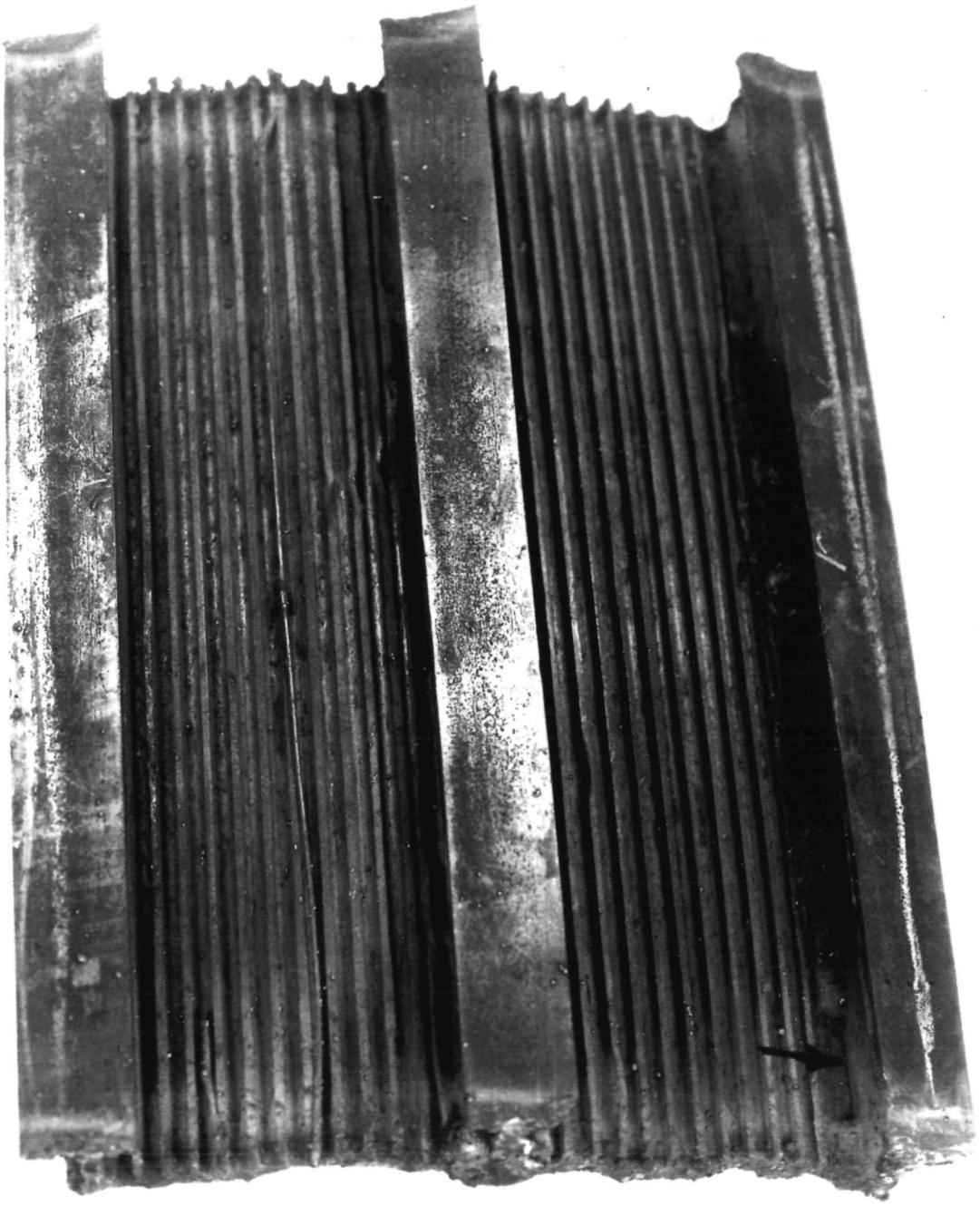

fig. 3

Top

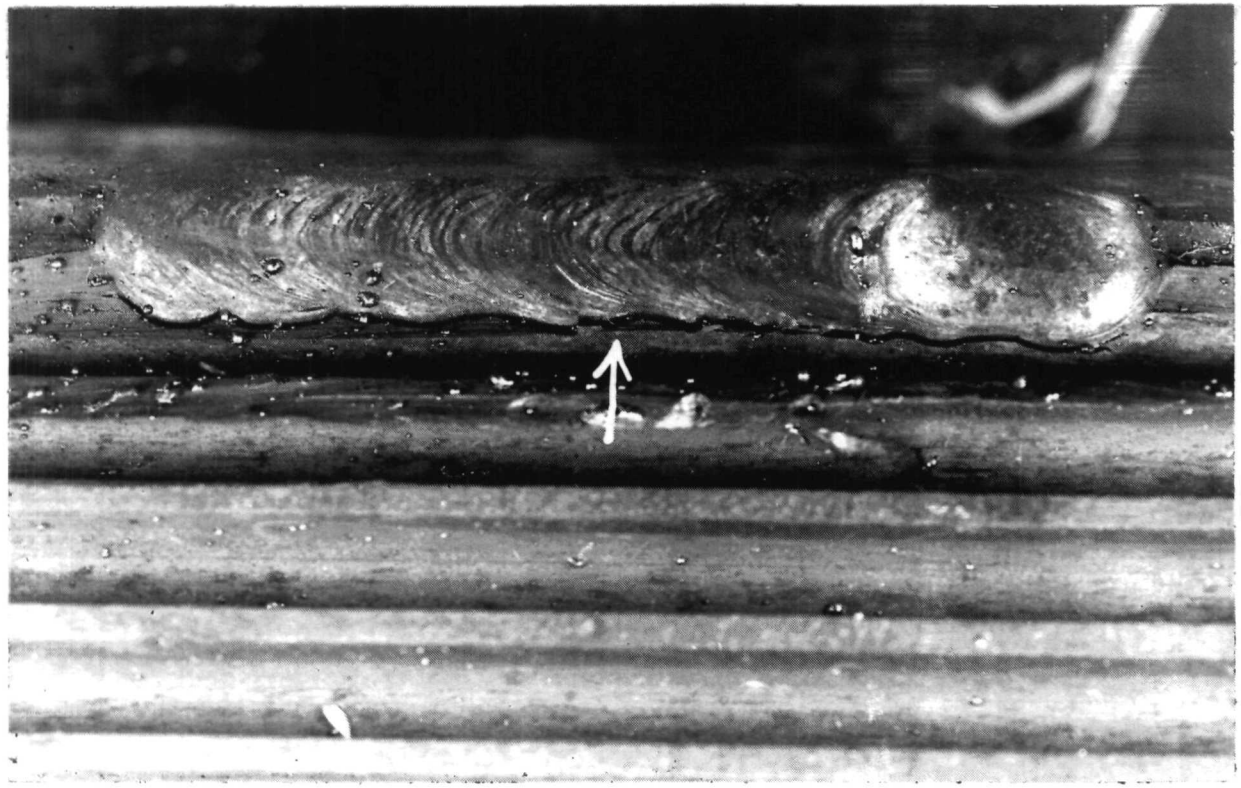

fig 4.

Same size

top

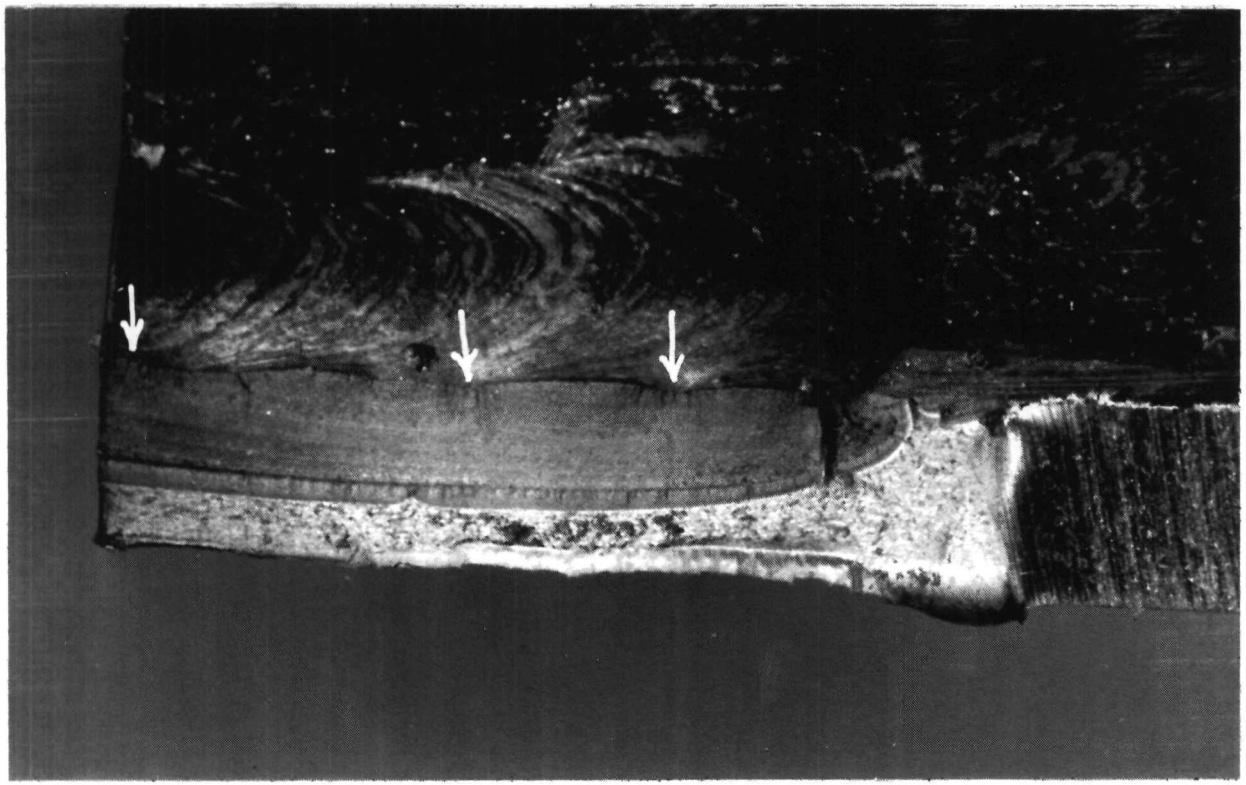

fig 5.

Same size

Top

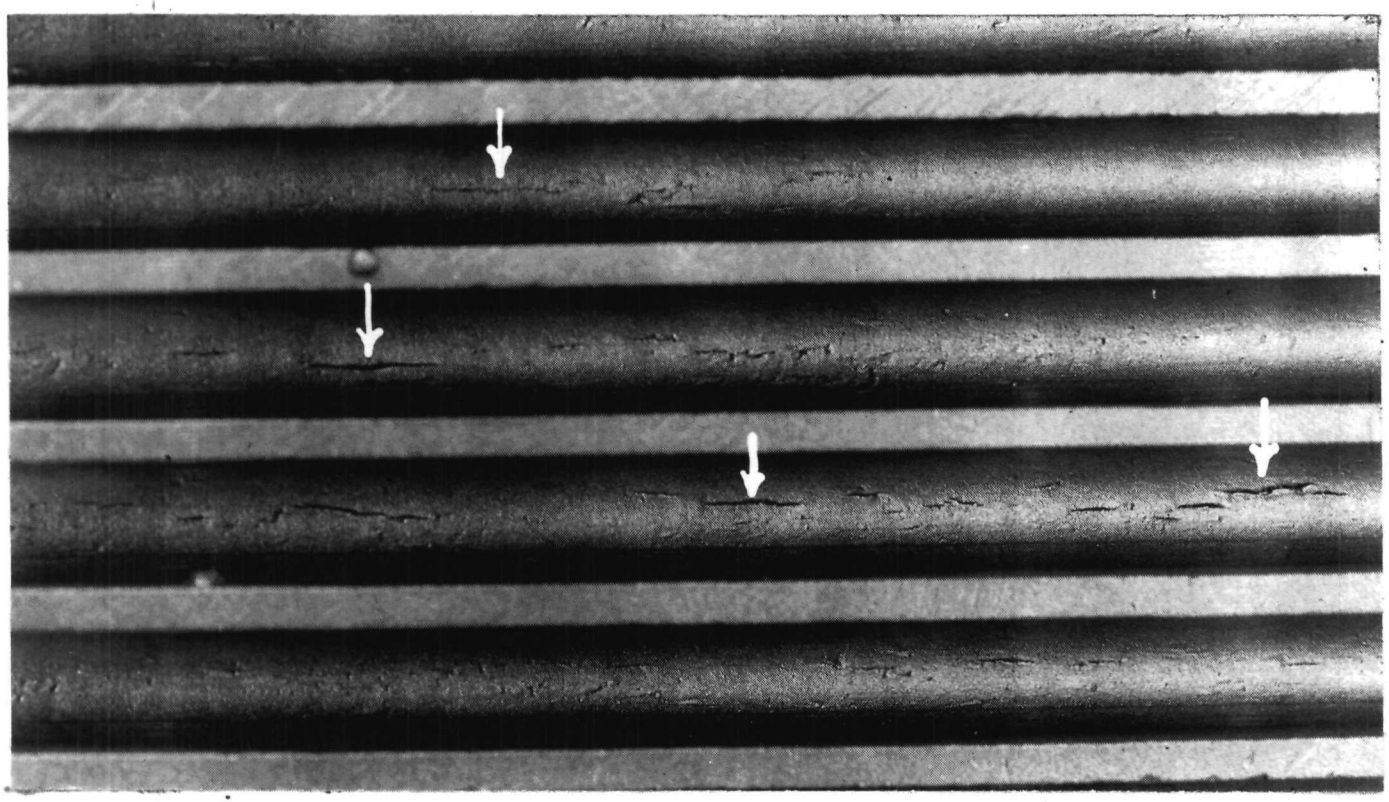

fig 6.

Same 512

top

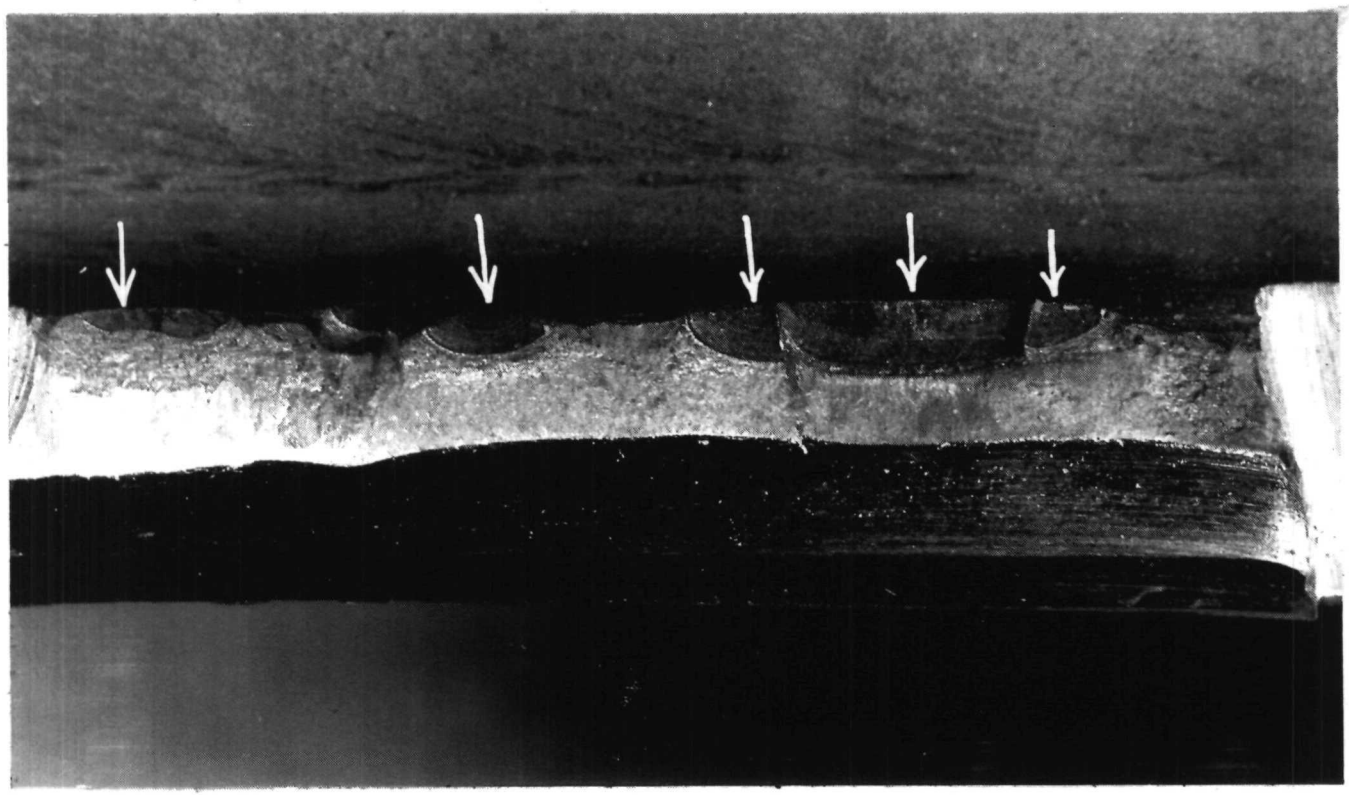

fig 7.

Same size

Top

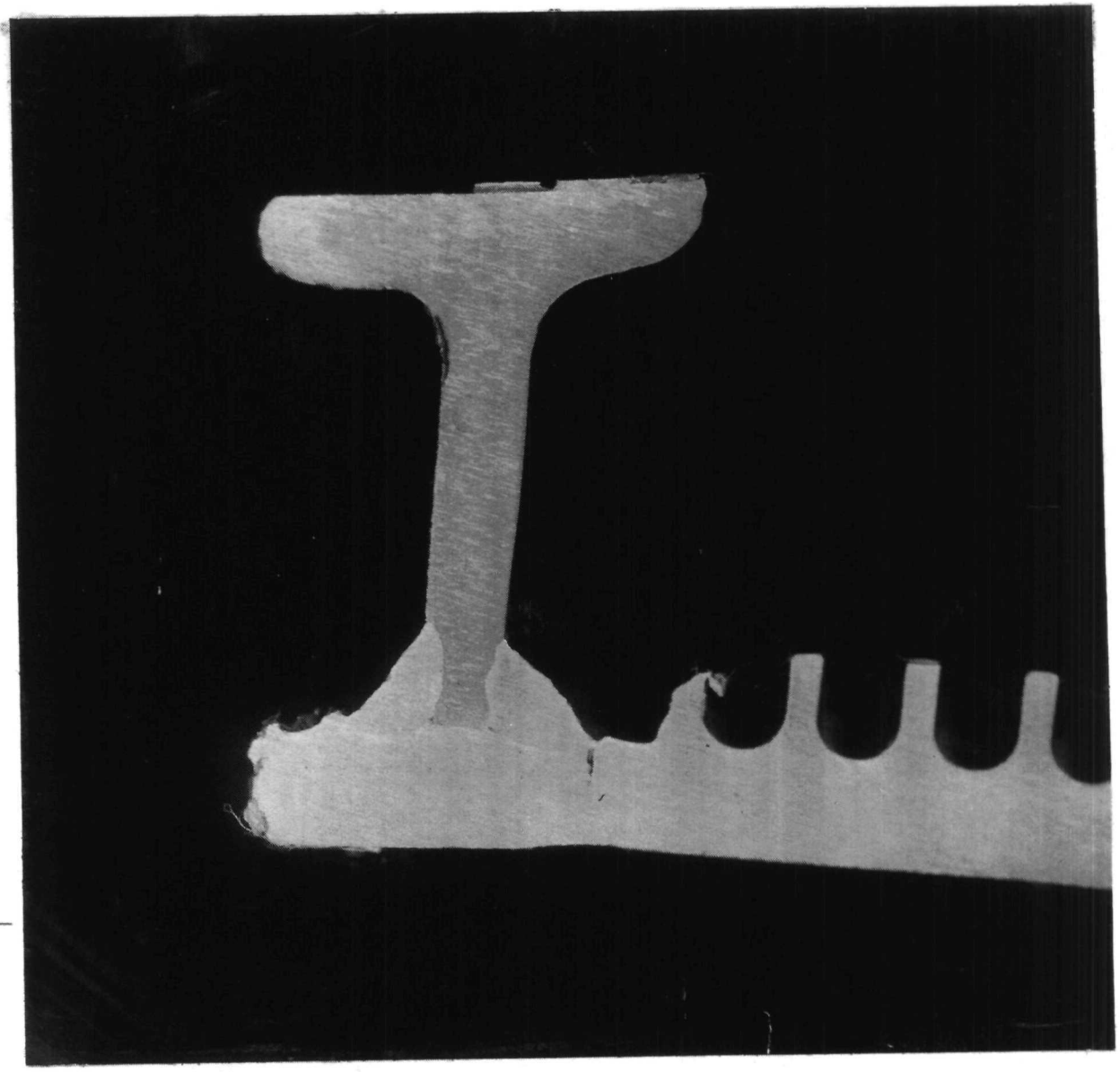

Fig. 8.

TOP

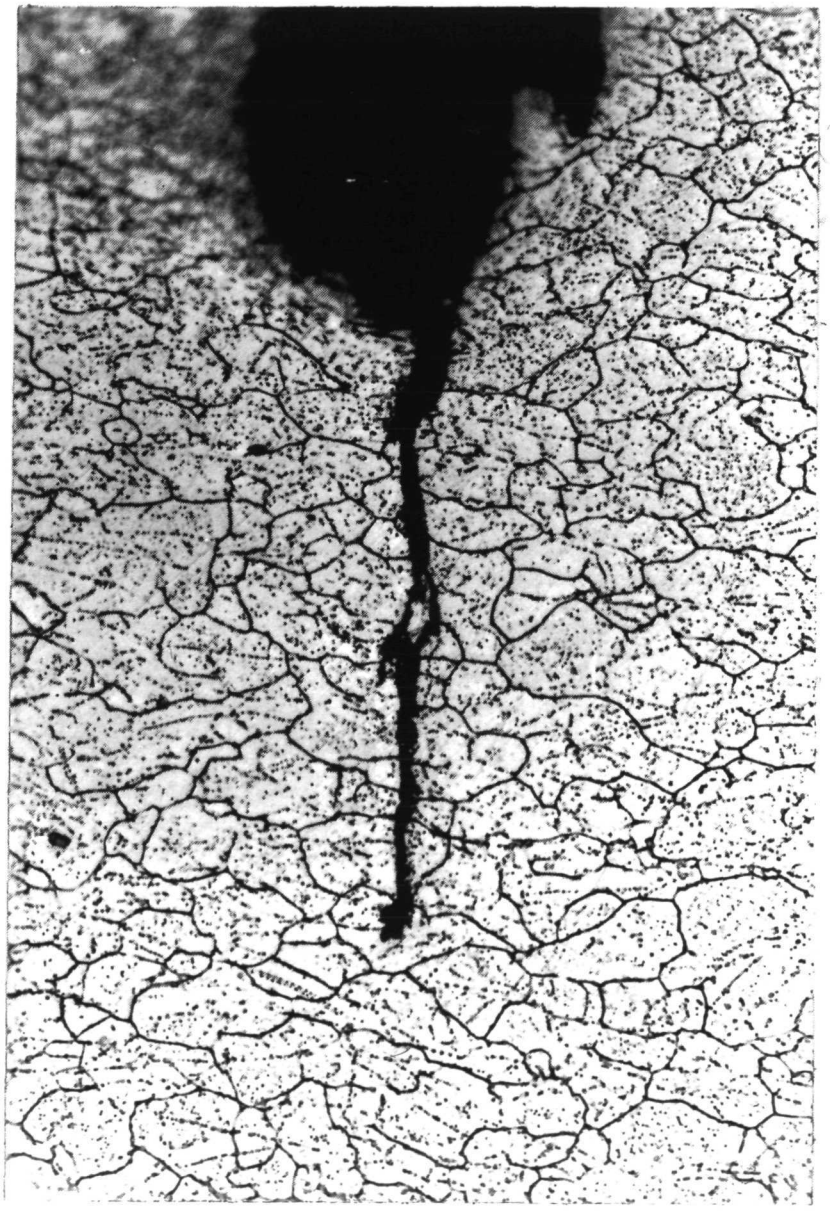

fig. 9.

top

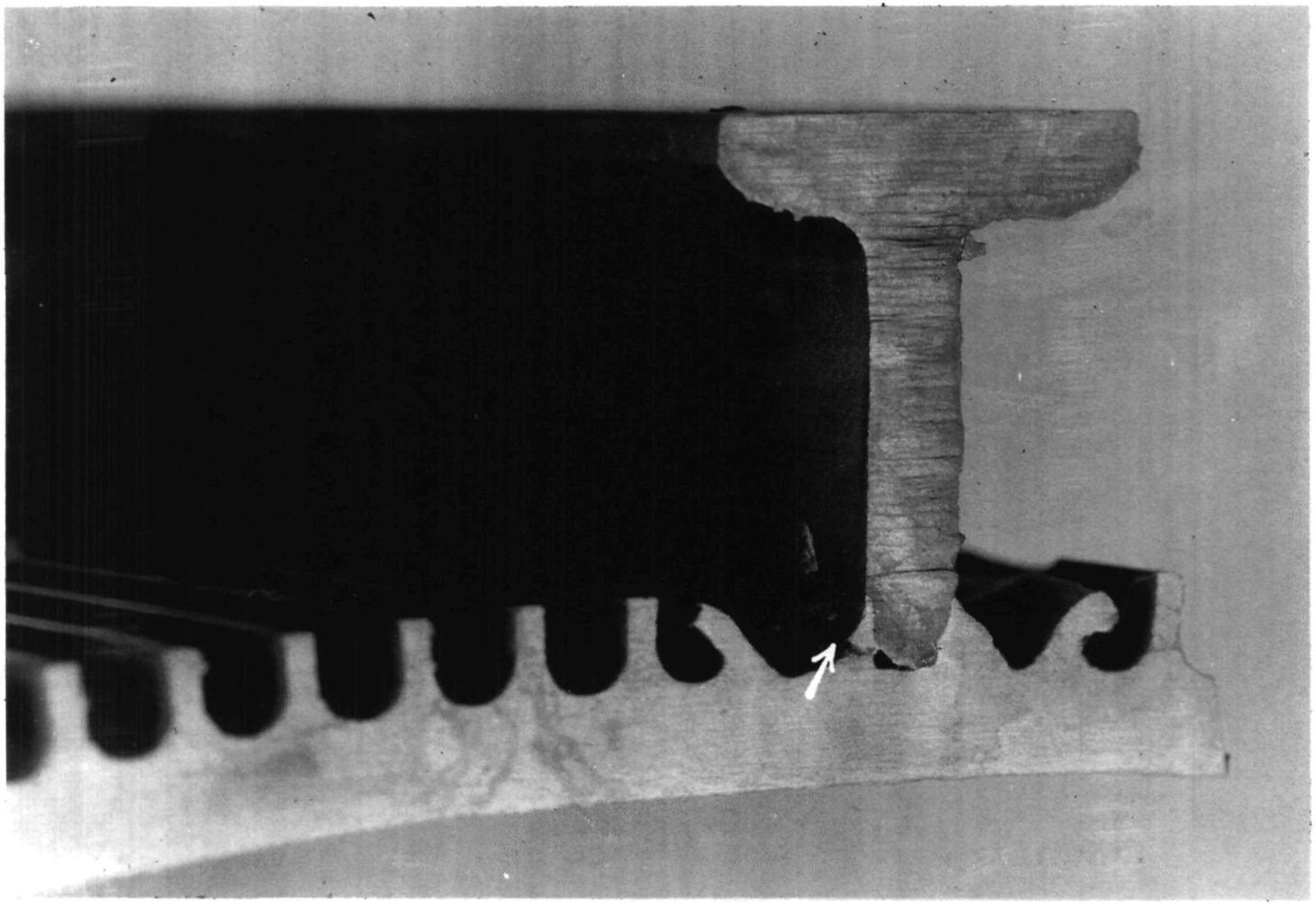

fig. 10.

Same size